

NOTE TO USERS

This reproduction is the best copy available.

UMI[®]

USING MICROEARTHQUAKES AS PROBES OF LARGER
EARTHQUAKE RUPTURE

A DISSERTATION
SUBMITTED TO THE DEPARTMENT OF GEOPHYSICS
AND THE COMMITTEE ON GRADUATE STUDIES
OF STANFORD UNIVERSITY
IN PARTIAL FULFILLMENT OF THE REQUIREMENTS
FOR THE DEGREE OF
DOCTOR OF PHILOSOPHY

Justin L. Rubinstein

March 2006

UMI Number: 3209015

INFORMATION TO USERS

The quality of this reproduction is dependent upon the quality of the copy submitted. Broken or indistinct print, colored or poor quality illustrations and photographs, print bleed-through, substandard margins, and improper alignment can adversely affect reproduction.

In the unlikely event that the author did not send a complete manuscript and there are missing pages, these will be noted. Also, if unauthorized copyright material had to be removed, a note will indicate the deletion.

UMI[®]

UMI Microform 3209015


Copyright 2006 by ProQuest Information and Learning Company.

All rights reserved. This microform edition is protected against unauthorized copying under Title 17, United States Code.

ProQuest Information and Learning Company
300 North Zeeb Road
P.O. Box 1346
Ann Arbor, MI 48106-1346

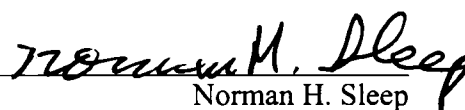
© Copyright by Justin L. Rubinstein 2006
All Rights Reserved

I certify that I have read this dissertation and that in my opinion it is fully adequate, in scope and quality, as a dissertation for the degree of Doctor of Philosophy.



Gregory C. Berroza (Principal Adviser)

I certify that I have read this dissertation and that in my opinion it is fully adequate, in scope and quality, as a dissertation for the degree of Doctor of Philosophy.



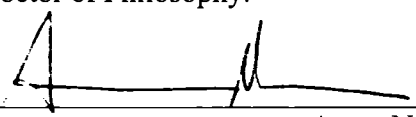
Norman H. Sleep

I certify that I have read this dissertation and that in my opinion it is fully adequate, in scope and quality, as a dissertation for the degree of Doctor of Philosophy.



Paul Segall

I certify that I have read this dissertation and that in my opinion it is fully adequate, in scope and quality, as a dissertation for the degree of Doctor of Philosophy.



Amos Nur

Approved for the University Committee on Graduate Studies.

Abstract

Although they garner very little attention from the public, microearthquakes are an extraordinarily valuable tool that seismologists use to understand better the physics underpinning faulting and earthquake rupture. Microearthquakes may not influence fault behavior on a large scale, but their ubiquitous nature has allowed me to determine precisely the time-dependent behavior of earth materials and to compute detailed descriptions of wave propagation, tasks which have significantly improved our understanding of fault slip and earthquake strong ground motion.

The majority of this dissertation is dedicated to understanding nonlinear strong ground motion. To this end, I identify reductions in the near-surface seismic velocity coincident with four moderate and large earthquakes. Applying moving-window cross correlation on multiple repeating earthquake sequences allows me to identify these time dependent changes in seismic velocity. There are multiple lines of evidence that suggest that velocity reductions are evidence of nonlinear strong ground motion induced damage. First, velocity always decreases following earthquakes, which suggests a damage mechanism. The size of the velocity reductions that I observe are correlated with the strength of shaking for the earthquake that caused them, indicating a cause and effect relationship between strong ground motion and velocity reductions. For multiple earthquakes, I also identify a correlation between the size of velocity reductions and site conditions. This is expected; soft rocks are easier to damage with strong ground motion than hard rocks. The healing behavior of these velocity reductions also parallels the behavior of velocity reductions observed in laboratory studies of the recovery of materials from transient nonlinear strain.

In the final chapter of this dissertation, I develop a new earthquake location technique. This method takes advantage of the expected similarity of the waveforms of nearby earthquakes to determine wave propagation parameters for many windows of time in a seismogram. This allows me to locate earthquakes that were sparsely recorded. I apply this technique to three medium magnitude earthquakes on the Calaveras Fault near streaks of seismicity. The new locations of these events suggest that streaks represent seismicity induced by the interaction between zones of a fault that accommodate slip differently, i.e., aseismically and seismically.

Acknowledgements

First, I would like to thank my advisor Greg Beroza. In my opinion, Greg has been a model advisor. He is always available to talk and is very patient with the constant stream of questions I have. He has always been a source of new and creative ways to approach problems. I appreciate that he has let me find my own research path, allowing me to grow into my own scientist. He has also been very tolerant of my shenanigans, be it traveling the world or spending the majority of my time working from home. Most importantly, though Greg has always been amazingly supportive of me and has done everything he can to help me with my work. In particular, I recall the week before AGU 2004. Greg worked late into the night a number of days in a row to provide me with a supplementary dataset in case my processing did not work out. That he was willing to set his own life aside so that I would have something to fall back on meant a lot to me.

I also thank my committee members Amos Nur, Paul Segall, Norm Sleep, and Götz Bokelmann who all provided something different for me. Amos has always brought me back to the big picture questions, which I find far too easy to forget. Paul's careful and thoughtful approach to science has brought a bit of pause and patience to my approach to science, which at times can be a bit hasty. Paul was also my co-advisor when I arrived, and is the person that most convinced me that I should come to Stanford. I thank him for this as well. Norm has always been an energetic contributor to my research; I appreciate his enthusiasm for my work and his creative approach to science. Götz, prior to his departure for France, was an enthusiastic collaborator and was always available to talk.

Thanks to Naoki Uchida, my primary collaborator for Chapter 5. Uchida-san has been incredibly efficient at getting work done, yet is patient with regular delays on my

end. He is always surprising me with new datasets that allow for new insight into our results. I also appreciate that he has been very accommodating to my near constant requests for obscure datasets.

I also would like to thank Jack Boatwright, Bill Ellsworth, and Paul Johnson for their continuing interest in my work. Their enthusiasm for my research has been a great source of motivation.

I would like to thank all the members of the seismo group who have taught me a lot and were always a pleasure to share space and time with: David Schaff, Martin Mai, Patti Guatteri, Xyoli Pérez-Campos, Eva Zanzerkia, David Shelly, Seok Goo Song, and Anu Venkataraman. In particular, I would like to thank David Schaff, Anu, Patti, and Seok Goo. David's Ph.D. research was the foundation for much of my thesis, and so without him I probably would have found a very different research path. David has always been willing to help out and answer any questions I had. Conversations with both Patti and Anu have been extraordinarily enjoyable and ranged from science to personal life. I've found their insights on the working world (both industry and academic) particularly helpful in determining my own path. I thank Seok Goo for peppering me with questions in his first few years at Stanford. His questions regularly forced me to think about things in a new way, and I often found myself learning, while trying to answer his questions. He has also become a great resource for help with statistics.

During my time at Stanford, I have had the great pleasure of meeting an incredible number of people who have become colleagues, friends, and confidants. My many friends from high school and college are still a great source of support. It would be near impossible to thank all of my friends individually, but I would like to acknowledge a select few. I thank Naomi for being both a great friend and an extraordinarily supportive colleague. Marco has been a great friend; I have immensely enjoyed talking over evenings of food and wine that are well beyond the means of graduate students. I thank Al for being a great officemate, roommate, and neighbor and keeping me on my toes with his witty banter. I thank Brody for supporting me no matter what. I also thank Bryan Kerr, a good friend from UCLA who convinced me to follow his footsteps to Stanford.

My first three years at Stanford were supported by the Wells Family Stanford Graduate Fellowship. Part of my final year was supported by the William K. Whiteford Fellowship. My research was largely supported by USGS grants 02HQGR0039, 03HQGR0073, and 05HQGR0007.

My family has been a tower of strength supporting me. I thank them for all their support and love over the past 5 years.

Contents

ABSTRACT.....	IV
ACKNOWLEDGEMENTS	VI
CONTENTS	IX
LIST OF TABLES	XII
LIST OF FIGURES	XIII
1. INTRODUCTION.....	1
2. EVIDENCE FOR WIDESPREAD NONLINEAR STRONG GROUND MOTION IN THE M_w6.9 LOMA PRIETA EARTHQUAKE.....	6
ABSTRACT.....	6
2.1 INTRODUCTION	7
2.2 DATA.....	8
2.3 METHOD.....	10
2.3.1 Data Processing.....	10
2.3.2 Modeling the Delays	14
2.4 RESULTS.....	17
2.5 CONSTRAINING THE SOURCE REGION OF THE DELAYS	21
2.5.1 Path Effects.....	23
2.5.2 Site Effects.....	23
2.6 FACTORS THAT INFLUENCE THE VELOCITY REDUCTIONS	25
2.6.1 Static Stress	25
2.6.2 Strong Ground Motion	26
2.6.3 Lithology	27
2.7 PHYSICAL MODEL	29
2.7.1 Fault Zone Damage	30
2.7.2 Widespread Damage Resulting From Strong Shaking	30
2.7.3 Supporting Evidence from Hydrology.....	32
2.7.4 Other Evidence for Nonlinearity during Strong Ground Motion	33
2.8 CONCLUSIONS.....	34
ACKNOWLEDGEMENTS:.....	34
REFERENCES	36
APPENDIX 1	42

3. NONLINEAR STRONG GROUND MOTION IN THE M_L 5.4 CHITTENDEN EARTHQUAKE: EVIDENCE THAT PREEXISTING DAMAGE INCREASES SUSCEPTIBILITY TO FURTHER DAMAGE 43

ABSTRACT..... 43
3.1 INTRODUCTION 44
3.2 DATA AND METHODS 44
3.3 RESULTS..... 47
 3.3.1 Observations 47
 3.3.2 Factors that Influence the Magnitude of Delays..... 48
 3.3.3 Limitations and Outliers 51
3.4 SUMMARY 52
ACKNOWLEDGEMENTS..... 53
REFERENCES 54

4. DEPTH CONSTRAINTS ON NONLINEAR STRONG GROUND MOTION FROM THE 2004 PARKFIELD EARTHQUAKE..... 55

ABSTRACT..... 55
4.1 INTRODUCTION 56
4.2 DATA..... 57
4.3 METHOD..... 57
4.4 OBSERVATIONS..... 60
 4.4.1 Surface Stations 60
 4.4.2 Borehole Stations 61
4.5 DISCUSSION 61
 4.5.1 Physical Model and Interpretation 62
 4.5.2 Outliers? 63
4.6 CONCLUSIONS 64
ACKNOWLEDGEMENTS..... 65
REFERENCES 66

5. SEISMIC VELOCITY REDUCTIONS CAUSED BY THE 2003 TOKACHI-OKI EARTHQUAKE..... 69

ABSTRACT..... 69
5.1 INTRODUCTION 70
5.2 DATA..... 70
5.3 METHOD..... 73
5.4 OBSERVATIONS..... 77
5.5 CONSTRAINING THE SOURCE REGION OF THE DELAYS 83
 5.5.1 Site Effects..... 83
 5.5.2 Path Effects..... 84
5.6 PHYSICAL MECHANISM FOR SEISMIC VELOCITY REDUCTIONS..... 86
 5.6.1 Site Effects..... 87
 5.6.2 Path Effects..... 89
 5.6.3 Fluids?..... 91
5.7 SUMMARY 92
5.8 ACKNOWLEDGEMENTS 92
REFERENCES 93

6. FULL WAVEFORM EARTHQUAKE LOCATION: APPLICATION TO SEISMIC STREAKS ON THE CALAVERAS FAULT, CALIFORNIA 96

ABSTRACT..... 96
6.1 INTRODUCTION 97
6.2 GEOLOGIC SETTING AND MOTIVATION..... 99
6.3 METHOD 100
 6.3.1 Precise Determination of Slowness Parameters 103
 6.3.2 Precise Determination of Earthquake Locations 106
 6.3.3 Error Analysis 110
6.4 INTERPRETATION..... 115
6.5 LOCATING EARTHQUAKES WITHOUT DIRECT ARRIVALS..... 117
6.6 CONCLUSIONS 119
ACKNOWLEDGEMENTS..... 119
REFERENCES 120

List of Tables

Table 2.1: Station Parameters and Observations.....	22
Table 2.2: Explanation of Rock Types.....	42
Table 5.1: Timing of Repeating Earthquake Sequences Used.....	72
Table 6.1: List of earthquakes relocated by each station.....	103
Table 6.2: Centroid offsets determined by new array location method.....	111
Table 6.3: Error estimates for each earthquake centroid.....	114
Table 6.4: Centroid offsets determined using coda only.....	117

List of Figures

Figure 2.1: Map of the study region.....	10
Figure 2.2: Example repeating earthquake sequence.....	11
Figure 2.3: Example of moving window correlation technique and its results.....	13
Figure 2.4: Raw <i>S</i> delays plotted over <i>S</i> delay model for JRR and JEC.....	15
Figure 2.5a-f: Delay observations of multiplet 13 at 6 NCSN stations	17
Figure 2.5g: <i>S</i> delays of multiplet 13 at 6 NCSN stations.....	18
Figure 2.5h: <i>S</i> delay as a function of the logarithm of time since Loma Prieta for multiplet 13 at 6 NCSN stations.....	19
Figure 2.5i-n: <i>S</i> delay model as a function of time for 6 NCSN stations.....	20
Figure 2.6: Loma Prieta induced <i>S</i> delays plotted against Loma Prieta earthquake parameters	21
Figure 2.7: Loma Prieta induced <i>S</i> delay plotted versus site amplification	24
Figure 2.8: Loma Prieta induced <i>S</i> delay plotted against site conditions and strong ground motion parameters.....	28
Figure 3.1: Map of the study region.....	45
Figure 3.2: Example of moving window correlation technique and its results	47
Figure 3.3: Raw <i>S</i> delays plotted over <i>S</i> delay model for HGW and JRG.....	48
Figure 3.4: <i>S</i> delay plotted as a function of the logarithm of time after the Chittenden Earthquake.....	49
Figure 3.5: Chittenden induced <i>S</i> delays plotted against distance to the Chittenden earthquake and <i>S</i> delay caused by Loma Prieta.....	50
Figure 4.1: Map of the study region.....	58
Figure 4.2: Example of moving window correlation technique and its results	59
Figure 4.3: Delay as a function of time for surface station PMM and borehole station EAD.....	60
Figure 4.4: <i>S</i> delay versus strong ground motion of the Parkfield earthquake	61
Figure 5.1: Map of the study region.....	71
Figure 5.2: Example of moving window correlation and delay fitting techniques.....	74
Figure 5.3: Delay plotted versus time for multiplet 3 at MMRH and HBTH	77
Figure 5.4: Delay plotted versus time for multiplet 1 at AKK and AYWH.	78

Figure 5.5: Delay plotted as a function of time for events 2 and 3 of multiplet 4 at Hi-Net station SKNH.	79
Figure 5.6: Maps showing slowness change for each multiplet at each station.	80
Figure 5.7: Average Tokachi-Oki induced slowness change at each station overlying a topographic map of Hokkaido	81
Figure 5.8: Tokachi-Oki induced slowness changes versus station elevation.....	82
Figure 5.9: Tokachi-Oki induced slowness changes versus site amplification	84
Figure 5.10: The effect of path on Tokachi-Oki induced slowness increases.	86
Figure 5.11: Tokachi-Oki induced slowness change versus PGA.....	88
Figure 5.12: Tokachi-Oki induced slowness change versus sensor depth.	90
Figure 6.1: Map of the study region.....	100
Figure 6.2: Cross section of the seismicity and earthquakes studied.....	101
Figure 6.3: Schematic representation of source array analysis	102
Figure 6.4: Waveforms showing the results of source array analysis.....	106
Figure 6.5: Power of the source-array stack \tilde{S}_{acd} for window 2 of medium magnitude earthquake 1, for station CYB.....	108
Figure 6.6: Optimal propagation azimuth and angle from the vertical for all 20 time windows at station HPL for medium magnitude earthquake 1	110
Figure 6.7: Location of earthquake #3 as determined by a stack of all stations and a stack of station BSC.	112
Figure 6.8: Relocations of the 3 medium magnitude earthquakes.....	113
Figure 6.9: Location of earthquake #3 using determined by using only the coda for a stack of all stations and a stack of station BSC.	118

Chapter 1

Introduction

Earthquakes are one of the most devastating natural hazards in terms of both the human and financial costs associated with them. Recently, we have seen that earthquakes are particularly dangerous, as they can trigger other natural disasters including tsunamis (the 2004 Sumatra-Andaman Islands earthquake) and landslides (the 2001 El Salvador earthquake) in addition to the hazards of strong shaking. The role of an earthquake seismologist is to use modern techniques and instrumentation to understand the physics governing earthquake rupture and fault slip, with an ultimate goal of reducing the hazards posed to humans. As a result, seismologists often focus on large earthquakes and their implications. This gives seismologists a very limited dataset as large, damaging earthquakes are relatively infrequent. In this study I take advantage of much more frequent microearthquakes to learn about larger earthquakes and fault mechanics.

Recent advances in earthquake location techniques have been a significant boon for microearthquake studies. The use of cross-correlation measurements to determine relative arrivals of different earthquakes have vastly improved the precision to which earthquakes are located. Double-difference techniques that minimize the influence of unknown structure have refined earthquake locations further. Using these techniques in combination has revealed previously unseen seismic phenomena including streaks and allowed for the easy identification of repeating earthquakes. These two phenomena are the focus of the research contained in this thesis.

The main thrust of this thesis has been in using repeating microearthquakes to observe and understand time dependent changes in seismic velocity. For years

seismologists have searched for the time dependence of wave propagation parameters in hopes of identifying precursory changes in earth properties before large earthquakes. Such studies have not yet been successful in identifying any predictive phenomena. A number of recent studies, including this one, have been able to identify reductions in seismic velocity following large earthquakes (Poupinet *et al.*, 1984; Li *et al.*, 1998, 2003, *submitted*; Nishimura *et al.*, 2000; Schaff and Beroza, 2004; Peng and Ben-Zion, *in press*). The implications of these velocity changes are far reaching in a number of fields including earthquake engineering, earthquake triggering, and fault mechanics.

This thesis contains 5 chapters that use microearthquakes as tools to better understand larger earthquakes and the physics underlying fault slip. Each chapter has been prepared as an individual journal article, so, as a result, they all have their own abstracts, introductions, and conclusions. In chapter 2, I use repeating microearthquakes to identify velocity reductions caused by the 1989 M_w 6.9 Loma Prieta earthquake. Based on an analysis of the strong ground motion parameters and the static stress changes of the Loma Prieta earthquake, I determine that these velocity reductions are the result of the strong shaking of the Loma Prieta earthquake and are evidence of nonlinear strong ground motion. In chapter 3, I further explore the same dataset used in chapter 2, and identify a second decrease in seismic velocity 6 months after Loma Prieta that coincides with the M 5.4 Chittenden earthquake, the largest aftershock of Loma Prieta. I find a correlation between the velocity reductions caused by Chittenden and those caused by Loma Prieta. This implies that the damage induced by the Loma Prieta earthquake made these sites particularly weak and susceptible to damage by the weaker shaking of the Chittenden earthquake. In chapter 4, I take advantage of the surface and borehole networks in the Parkfield region to search for a depth dependence of nonlinear strong ground motion. Following the Parkfield earthquake, I find that the shallow borehole stations detect no change in travel times while the surface stations indicate very large changes. This suggests that nonlinear strong ground motion is generally limited to the very near surface. In chapter 5, I again use repeating earthquakes to search for changes in seismic velocity, this time caused by the Tokachi-Oki earthquake. Here I find evidence of both nonlinear strong ground motion and damage to the fault zone. Finally, in Chapter 6 I develop a new technique of earthquake relocation. This method takes advantage of

the expected similarity of the waveforms for nearby microearthquakes and allows me to determine wave propagation parameters, which I use to relocate other events.

In chapter 2, I offer a new technique in which one can identify the occurrence of nonlinear strong ground motion in a large earthquake. In this chapter, I analyze a catalog of repeating microearthquake sequences located just south of the Loma Prieta rupture zone. Using a moving window cross-correlation technique on the repeating earthquakes, I observe a sudden increase in the S - P time and S coda arrival times coincident with the Loma Prieta earthquake. With increasing time after the Loma Prieta earthquake, the S - P time often recovers back to pre-mainshock levels. I argue that these transient reductions in seismic velocity are evidence of strong motion induced damage at the near surface (nonlinear strong ground motion). This argument is supported by the strong motion data, in that the regions of strongest shaking also were the regions where the S - P time changed the most as a result of Loma Prieta. Further evidence that my observations of velocity reductions are evidence of nonlinear strong ground motion can be found in the healing of the velocity changes, which mimics that of laboratory studies. These observations of nonlinear strong ground motion have large implications earthquake engineering. Most importantly, these observations indicate that nonlinear strong ground motion is more widespread than previously thought. For the Loma Prieta earthquake, I observe velocity reductions at distances greater than 20km from the mainshock. Most engineers only consider nonlinearity when the structures that they are building are going to be subject to the strong shaking of significantly larger earthquakes (Loma Prieta was Mw 6.9), at distances much closer than 20km, and typically only on strata that are particularly weak. The evidence from this study suggests that engineers need to consider nonlinearity in strong ground motion for a much larger range of earthquake scenarios than they currently do.

In chapter 3, I further analyze the dataset from chapter 2 to examine a curiosity in the results from chapter 2. Specifically, I analyze a secondary decrease in the seismic velocity that occurs approximately six months after the Loma Prieta earthquake. I find that this correlates temporally with the M5.4 Chittenden earthquake. Our basic understanding of nonlinear strong ground motion suggests that this is improbable, that the strong motion of a M5.4 earthquake would be strong enough to cause damage. Further

investigation reveals that those stations where significant velocity reductions were observed for the Chittenden earthquake are the same stations where the largest velocity reductions were observed for the Loma Prieta earthquake. Based on this, I argue that the damage imparted by Loma Prieta weakened some sites so significantly that the relatively weak shaking of the Chittenden earthquake, which normally wouldn't be able to damage these sites, was able to damage them. This finding corresponds with laboratory and field data which suggests that strong motion induced damage is largest in soft materials. There are multiple implications of these findings. First, for emergency responders this suggests that earth materials are particularly weak following an earthquake and this should be considered while deciding whether or not to reoccupy buildings. For seismologists, this suggests that materials weakened by strong shaking are particularly sensitive to further damage and failure (i.e. generation of further events). *Vidale and Li (2003)*, suggested this exact scenario, that the strong shaking of earthquake could damage other faults and possibly result in future earthquakes. *Gomberg and Johnson (2005)* and *Johnson and Jia (2005)*, take this a step further and argue that the damage imparted by nonlinear strong ground motion is responsible for the dynamic triggering of earthquakes. Clearly, the influence of strong shaking on earth materials is important for fault physics and seismogenesis.

In chapter 4, I study the influence that the Parkfield earthquake had on seismic velocities in the region. Using the same moving window cross correlation technique as used in chapters 2 and 3, I examine the two repeating earthquake sequences that are the "target events" of the San Andreas Fault Observatory at Depth (SAFOD). From the correlation analysis I identify large increases in the $S-P$ time at the surface stations of the Northern California Seismic Network (NCSN). For the borehole seismometers that are part of the High Resolution Seismic Network (HRSN), I don't see significant changes in $S-P$ time. From this, I conclude that the nonlinear strong ground motion induced velocity reductions are occurring at depths more shallow than the seismometers in the HRSN (100m depth).

In chapter 5, I examine the influence that the M8 2003 Tokachi-Oki earthquake had on seismic velocities in Japan. I again used a moving window cross-correlation analysis to look for velocity changes caused by the earthquake. From this analysis I find

significantly larger velocity reductions in the plains of Hokkaido than in the mountainous regions. This offers further evidence that harder rocks are more resistant to nonlinear strong ground motion than soft rocks, as rocks in the mountains are likely to be harder than those in the plains and plateaus. For this earthquake, I also identified particularly large velocity reductions for paths that crossed the Tokachi-Oki rupture zone. These velocity reductions are a signature of the damage to the fault zone induced by the earthquake rupture, itself.

In chapter 6, I develop a new earthquake location methodology based on array analysis. In this method, I use source arrays of microearthquakes that have been previously well located to determine wave propagation parameters (slowness, azimuth, and angle of incidence) for multiple windows of energy. With this description of wave propagation, I am able to relocate earthquakes that were poorly located due to a lack of data. I also demonstrate that this technique has the power to locate earthquakes using only coda waves and no direct arrivals. With the dataset I examine in this chapter I determine the rupture propagation of 3 medium magnitude earthquakes that nucleate on streaks on the Calaveras fault. These earthquakes tend to rupture into regions devoid of microseismicity, which I believe to be locked. In the region above the upper streak I study, and the region below the lower streak, there is good evidence that much of the slip on the fault is accommodated through ductile (creep) processes. That streaks appear to be located between these regions of differing slip styles suggests that the interplay between creeping locked sections of a fault is what causes streaks to form in the first place.

Chapter 2

Evidence for Widespread Nonlinear Strong Ground Motion in the M_w 6.9 Loma Prieta Earthquake

Abstract

We exploit 55 repeating micro-earthquake sequences on the San Andreas Fault, just south of the rupture zone of the 1989 M_w 6.9 Loma Prieta Earthquake, to search for time dependent properties of the Earth's crust. Using moving window waveform cross-correlation, we identify clear and systematic delays as large as 20ms for the direct S wave and exceeding 50ms in the early S -wave coda following the Loma Prieta mainshock. Others have also identified phase delays (velocity reductions) associated with damaging earthquakes and they have suggested a myriad of possible causal mechanisms. Here, we present new evidence for a mechanism to produce velocity reductions correlated in time and space with an earthquake. A strong correlation between the spatial patterns of S delays and the intensity of strong ground motion in the Loma Prieta Earthquake suggests that physical damage, the formation or growth of cracks during strong ground motion, to the Earth's shallow crust is responsible for the observed velocity reductions. The strong

The material in this chapter has appeared in Rubinstein, J.L. and G.C. Beroza (2004). *Bulletin of the Seismological Society of America*, **94**, 1595-1608.

spatial variability in S delays over short distances and the strong correlation of the magnitude of delays with surface geology indicate that the phase delays accumulate primarily near the receiver. The effect is stronger at stations on young, soft rocks than at stations on old, hard rock. Disproportionately larger S coda delays than P coda delays suggest that the cracks formed by the strong shaking are fluid filled. In the ten years after Loma Prieta, the initial increase in travel times reduces logarithmically with respect to time, often back to the pre-mainshock levels. We attribute this behavior to the same “slow dynamic” healing observed in laboratory studies of the recovery of materials from transient nonlinear strain.

2.1 Introduction

A number of studies have found temporal variations in properties of seismic propagation, including: seismic velocity (e.g., Poupinet *et al.*, 1984; Bokelmann and Harjes, 2000; Rubin 2002; Vidale and Li, 2003, Schaff and Beroza, 2004), coda Q (e.g., Peng *et al.*, 1987; Wang *et al.*, 1989; Su and Aki 1990; Londono 1996), scattering properties of the crust (e.g., Baisch and Bokelmann, 2001) and velocity anisotropy (e.g., Booth *et al.*, 1990; Crampin *et al.*, 1999; Saiga *et al.*, 2003). Some studies have identified subtle, annual cycles in seismic velocity that appear to correlate with the seasons and rainfall (e.g., Rubin, 2002). Evidence for changes in seismic wave propagation have also been associated with volcanic eruptions (e.g., Ratdomopurbo and Poupinet, 1995). The largest documented sudden changes in rock properties, however, appear to be the result of earthquakes. Velocity anomalies as large as six percent have been identified near the rupture zone of recent earthquakes using tomography (Zhao *et al.*, 1996); however, more precise measurements using repeating sources typically find substantially smaller reductions in seismic velocities associated with earthquakes on the order of a few percent (Vidale and Li, 2003; Schaff and Beroza, 2004). Although there is significant variation in the spatial extent and magnitude of velocity reductions associated with earthquakes, a common property of these reported velocity changes is that they are of the same sense: a decrease in velocity at the time of the earthquake.

In this study, we use repeating micro-earthquake sequences to document clear and systematic changes in the S -wave velocity and early S -wave coda that occur at the time of

the Loma Prieta mainshock. In contrast to previous studies, the dense temporal sampling afforded by the micro-earthquakes allows us to determine that their recovery is linear with the logarithm of time. We also find that the effect is greatest in areas where mainshock strong ground motion is strongest and at sites where the surface geology indicates tertiary or younger sedimentary rocks. These observations all point to pervasive damage in the shallow crust during mainshock strong ground motion as the explanation of the velocity reductions that we have identified. This represents new and independent evidence for nonlinearity during earthquake strong ground motion and may help constrain the threshold and extent of nonlinearity in future large earthquakes.

2.2 Data

To improve our understanding of time varying velocity changes, we study repeating micro-earthquakes that occurred on the San Andreas Fault in Northern California. These events were recorded by the Northern California Seismic Network (NCSN) and archived at the Northern California Earthquake Data Center (NCEDC). The NCSN is a network of high gain, short period, vertical component seismometers that record at 100 samples per second. The data is stable over time for frequencies up to approximately 15Hz, but at higher frequencies, time variations in the recording system may affect the data (Ellsworth, *personal communication*). Previous studies of the region have identified changes in absolute timing in the network associated with changes of voltage oscillators (Rubin, 2002). Our technique is not susceptible to either of these problems as we analyze the data in the 1-10 Hz frequency band only and make delay measurements relative to the initial *P*-wave arrival, making them insensitive to absolute time. However, our technique could be susceptible to other changes in the network. We have identified two stations where the polarity of the vertical component reversed twice between 1984 and 1999. We removed these data from our analysis. We have also identified errors, where a single data point was dropped, resulting in spurious delays of 10 milliseconds. The occasional dropping of samples by the NCSN appears to have ended in September of 1990 (D. Neuhauser, *personal communication*). Even though this problem can be repaired, these data do not represent a significant percentage of the total available and we have simply removed them.

Seismic sources that are repeatable (either artificial sources or repeating earthquakes) provide extremely reliable sources for detecting temporal changes in the crust because differences between two seismograms indicate a change in properties of the Earth (e.g., Poupinet *et al.*, 1984). In this study, we exploit the waveform similarity of repeating earthquakes to identify changes in the seismic velocity associated with the Loma Prieta Earthquake. We are able to track the temporal evolution of velocity changes following the earthquake, i.e. the initial co-seismic change followed by post-seismic recovery of the velocity to the background level.

Figure 2.1 shows the location of our catalog of 55 repeating micro-earthquake sequences (multiplets) at the southern end of the rupture zone of the Loma Prieta Earthquake as located by *Schaff* (2001). The magnitude range of these events is $0.5 < M < 3.1$ such that a circular constant stress drop source predicts a source dimension of approximately 10-200 m. Using cross-correlation measurements of the highly similar waveforms, we find that each event within a multiplet is located within meters of the other member events in its sequence. The waveforms for all the events within these sequences are extraordinarily similar. The correlation coefficients of seismograms for two events within a sequence typically are greater than 0.9 (Figure 2.2). The multiplets range in size from doublets that have only two member events to multiplets with as many as 29 member events. The repeating earthquakes we use were provided by D. Schaff and range in time from the onset of digital recording for the NCSN, 1984, through the end of 1999. This provides excellent sampling both before and after the 1989 Loma Prieta Earthquake. Due to the proximity of the multiplet source region to the rupture zone of the Loma Prieta Earthquake, a significant portion of many of the multiplets are aftershocks of the Loma Prieta Earthquake. Because the individual repeating earthquake sequences follow Omori's law of aftershock decay (*Schaff et al.*, 1998), they provide particularly good temporal sampling in the months immediately following Loma Prieta. This is fortunate because, as described below, this is the time period in which the changes we observe are most rapidly varying.

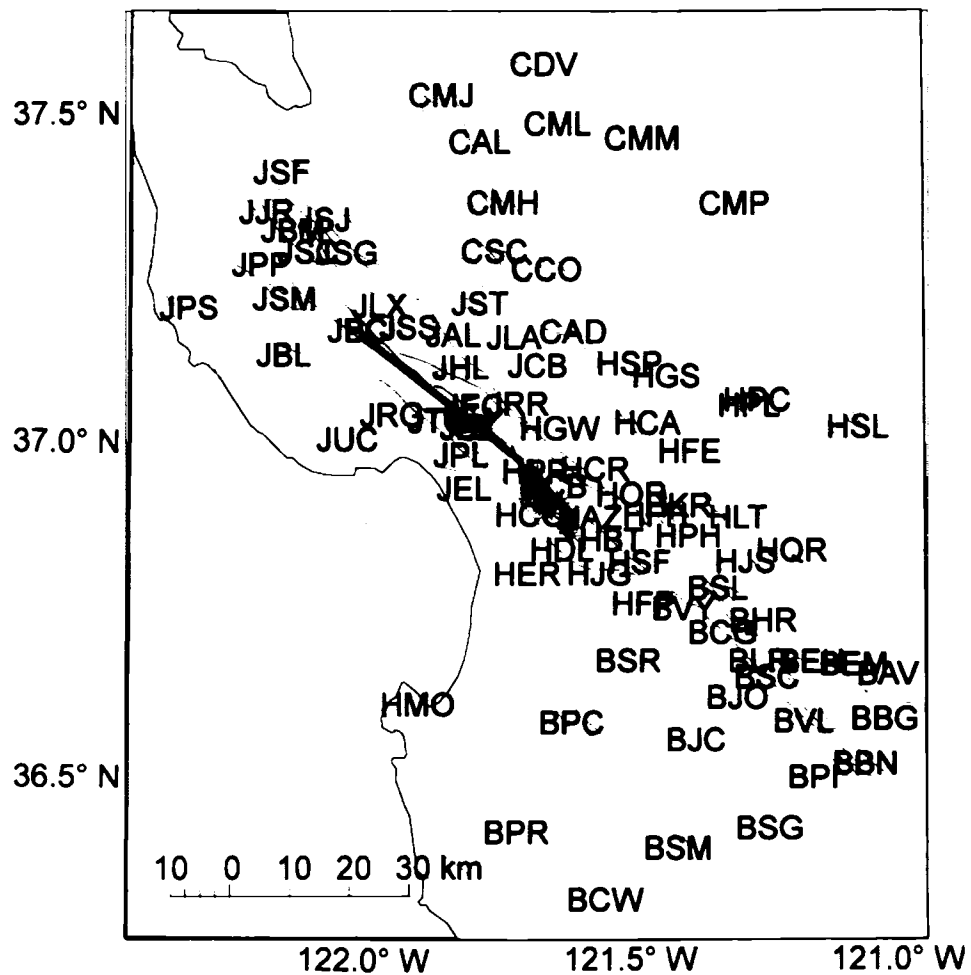


Figure 2.1: Map of the study region showing: Distribution of NCSN stations used in this study, vertical projection of the upper limit of the Loma Prieta rupture (thick solid line), approximate aftershock zone (shaded), epicenters of 55 multiplets (asterisks), and mapped faults (thin, grey lines).

2.3 Method

2.3.1 Data Processing

The first step in our analysis is to filter and align the seismograms. All seismograms are detrended, normalized and zero-phase filtered with a bandpass window of 1 to 10 Hz. Strongly clipped data are also removed.

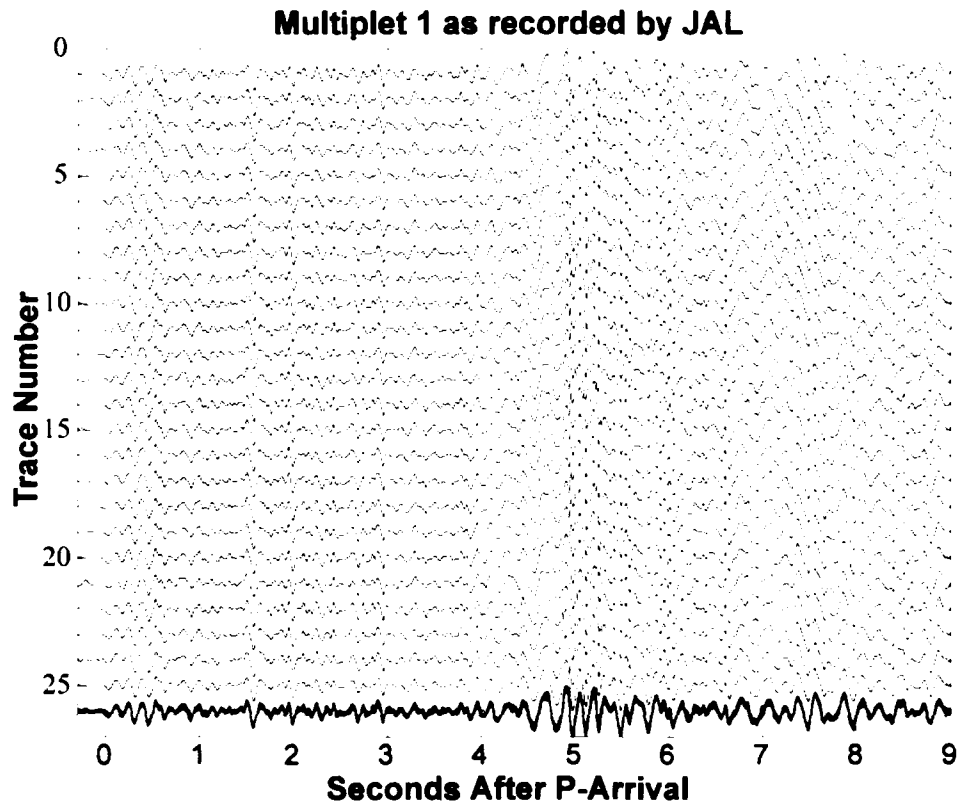


Figure 2.2: Collection of 25 events recorded by JAL for multiplet 1. Bottom trace is a superposition of all the traces, showing the extreme similarity of all the waveforms for this multiplet.

We select a reference earthquake for each multiplet-station pair, to which all the other earthquakes in that multiplet are compared. Because we want to study the effects of the Loma Prieta earthquake, we choose our reference seismogram to be temporally well removed from the Loma Prieta mainshock, either when the crust was in an undamaged state before the Loma Prieta earthquake or in a healed state long afterwards. For multiplet-station pairs that have member events recorded before the Loma Prieta earthquake, the reference event is chosen to be one of the first two or last two events within the sequence. For multiplets with no member events prior to the Loma Prieta earthquake, the reference trace is selected as the last or second to last event within the sequence. Because the reference seismogram affects all the data points for its multiplet, it is very important that it be a clean trace. It is also important that it be highly similar to all the other events within its multiplet. To ensure that the reference seismogram is relatively noise-free and very similar to the other events within its sequence, we select the

reference trace to be the seismogram that has the highest combination of signal to noise ratio and mean coherence to all the other seismograms in that multiplet-receiver pair.

On occasion, the initial, analyst selected P arrival times are significantly off (>0.5 s or 50 samples) due to noise in the record or an emergent onset. To ensure that all further measurements are as precise as possible, the P arrival is manually picked on the reference trace, using all the other events in the sequence, which have been aligned by cross-correlation, as a guide to where the first break is. This alignment helps ensure that the delay measurements are based on the same parts of the seismograms.

Once the reference trace and P -pick for each multiplet-station pair has been selected, we cross-correlate to measure time varying delays in the seismogram using a modification of the method used by *Poupinet et al.* (1984). All events are initially aligned with the manually picked P arrival to single sample precision by cross-correlating 2.56 second long windows centered on the analyst picked P arrival (Figure 2.3a, 2.3b). We obtain subsample precision by fitting a parabola to the peak of the cross-correlation function following the method of *Deichmann and Garcia-Fernandez* (1992). Using the initial P alignments, we then conduct a moving window cross-correlation analysis using windows 128 samples long, stepping forward at increments of 5 samples through nine seconds after the P arrival (Figure 2.3b, 2.3c). Subsample precision of correlation measurements is obtained using the same method as above. All windows are pre-multiplied with a Hanning window to prevent Gibbs' phenomena from causing erroneous results in the correlations (*Arfken and Weber*, 1995).

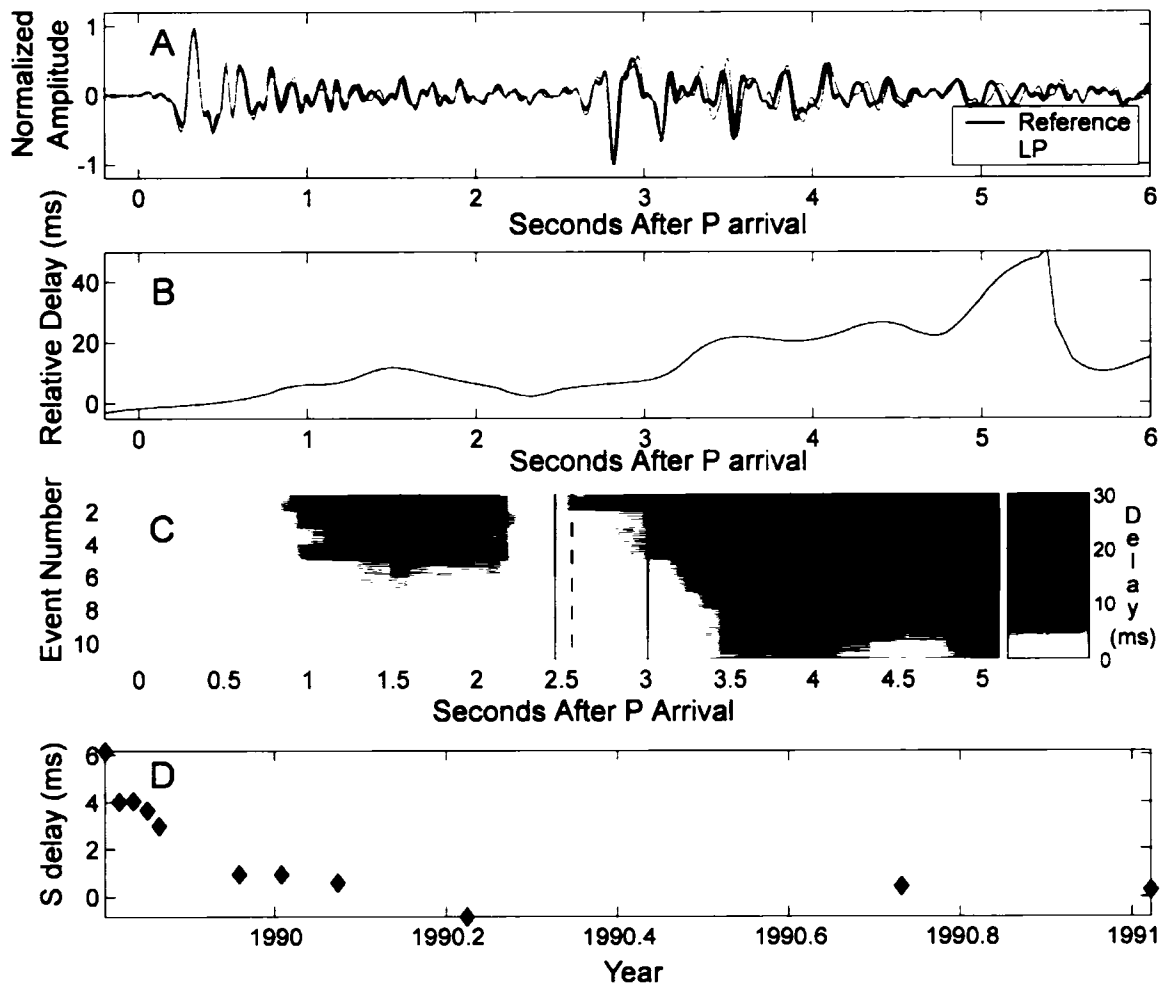


Figure 2.3: (a) Grey seismogram is the first event in repeating earthquake sequence number 17, as recorded by JRR, this event occurred two days after the Loma Prieta Earthquake. The seismogram in black is the reference event for this multiplet for JRR, it is event number 14, and occurred January 8, 1991, slightly more than one year after the Loma Prieta Earthquake. The two seismograms are aligned on the P arrival and then plotted together on the same time axis, where x is seconds after the P arrival. Note the distinct separation between the two traces with time into the trace. (b) Relative delay, as determined by cross correlation between event number 1 and event number 14 for multiplet 17 at JRR. Note that the largest delays are in the S Coda. (c) Relative delays for all of repeating sequence 17 recorded at JRR. Each horizontal line represents a seismogram, with calendar time increasing down the y -axis. Shading represents the relative delay of the seismogram represented by the horizontal stripe with respect to the reference seismogram. Darker shades represent larger delays. Largest delays are in the P and S codas. Also, note that the relative delays decrease as time since Loma Prieta increases. Vertical, dashed, black line represents the theoretical S arrival, and the vertical, solid, black lines represent the extent of the window from which we compute a relative S delay value. (d) This plot shows the relative S delay of each event in repeating earthquake sequence 17, plotted against time, as observed at the station JRR. The relative S delay value is computed as the median of the delay in the window described by the solid, black, vertical lines in Figure 2.3c.

In this paper, we focus on the relative delays expressed in the direct S phase. Although relative delays in the S coda are typically much larger than those for the direct S (Figure 2.3c), these are significantly less consistent from multiplet to multiplet due to strong variation in the nature of the early S -wave coda. Because we use them for alignment, we cannot examine relative delays in the P and early P coda. Some measurements of the relative delay for S cannot be used because for a few multiplet-station pairs the S wave arrives within the initial alignment window. For all other data we compute direct S delay measurements as the median of the delay for windows centered on a time period spanning 0.1s before and 0.45 seconds after the theoretical S arrival time (Figure 2.3c, 2.3d). To ensure the quality of data, we enforce a minimum cross correlation coefficient of 0.8 at the S arrival and a minimum signal to noise ratio of 5:1. We also remove occurrences of cycle skipping by searching for discontinuities in the delay function.

2.3.2 Modeling the Delays

We observe that S wave delays behave consistently for individual stations over many multiplets of varying source locations (Figure 2.4). We verify this by comparing the raw S delay measurements from all the multiplets at one station. If all the multiplets show similar time-varying signatures, then we can conclude that the delays are accumulating near the stations. Figure 2.4 shows that the S delays follow the same trend for all multiplets at stations JEC and JRR. This behavior is common to all stations, which implies that the delays are largely not accumulating near the multiplet source region. Any source dependence can thus be considered a secondary effect and of lesser importance than the site effect. The observation that lags don't vary strongly with source region also indicates that they don't vary with the station-receiver path, at least for the range of paths we have sampled. Therefore, path-induced delays can be treated as constant for all sources at any one receiver. Because there is no strong variation in the source region or path, a station based delay model should capture the general behavior of the data.

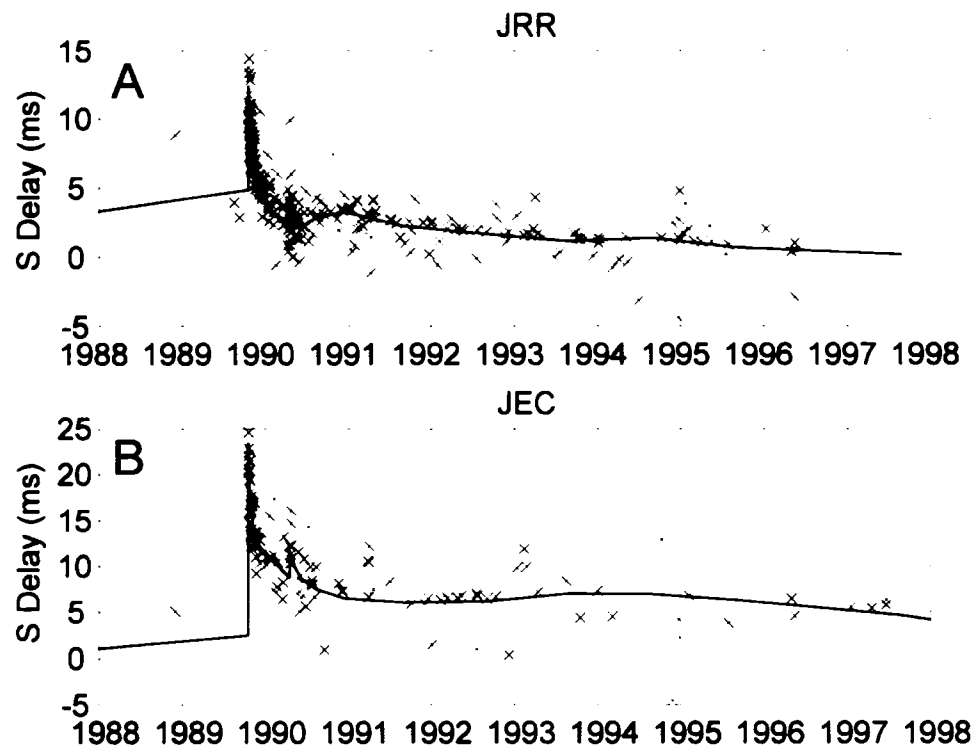


Figure 2.4: (a) Raw S -delay values are plotted versus time for all multiplets recorded by JRR. The model for JRR is overlain. To fit the raw values to the model predictions, the model prediction for the reference event for each multiplet is added to raw data values. This fits the raw data to the model because the delay value at the reference event is treated as zero in the delay calculation. (b) Same as figure 4a for multiplets recorded by JEC.

The amplitude of the S delays varies with time. We model this behavior as a time varying station S -delay function, similar to static station correction functions often used in earthquake location. The S -delay function behaves such that the relative delay between any two points in calendar time is simply the difference between the values of the station S -delay function evaluated at those two points in time. It is specific to the S -wave, because delays vary with time into the seismogram (Figure 2.3b, 2.3c). In our analysis, we treat this time varying delay as a discrete function with irregularly spaced sampling. We chose an irregularly sampled model for two reasons. First, we have irregularly sampled data; there are far more earthquakes that occur immediately after the two largest earthquakes in the region (the Loma Prieta Earthquake and its largest aftershock the M_w 5.4 Chittenden Earthquake) than at any other times between 1984 and

1999. Second, the rate of variation in the delay is not constant; the largest changes occur immediately after the Loma Prieta mainshock.

We assume that our measurements are differences of a time varying station correction function that is common to all multiplets. The 55 repeating earthquake sequences measure differences in this function at different times. We set up the inverse problem to reconstruct the underlying delay function from measurements of these differences in a manner similar to that used by *Beroza et al. (1995)* to characterize time variations in coda-Q. Our model has only 23 parameters for the 16-year interval 1984-1999 which includes four model parameters split between the days of the 2 largest earthquakes in the region (Loma Prieta and Chittenden) and the days immediately preceding these two earthquakes. We make the simplifying assumption that the delay function varies linearly between discrete model samples such that when an earthquake occurs between the times of two model points, the data point is represented as a linear combination of these two model points. For example, if an earthquake occurred on January 1, 1994 and we have model samples on January 1, 1992 and 1995, the data kernel weighting would be 0.33 and 0.67 for the model parameters for 1992 and 1995 respectively.

We fit the data subject to a smoothing constraint that simultaneously minimizes the model roughness based on a finite difference second derivative to regularize the inversion. Because we expect there to be large discontinuities in the station-lag function between the model point before Loma Prieta and the model point after Loma Prieta, smoothing is not applied over this interval. Smoothing is also not applied for the intervals spanning the April 18, 1990 M 5.4 Chittenden earthquake because we observe a significant increase in delay associated with this earthquake for some stations. The weight assigned to satisfying the smoothing norm relative to fitting the data is optimized using cross-validation (Wahba, 1990).

For each station, we calculate the least squares estimate of the temporal delay function. The results of this inversion are ignored if there are less than two reference event-data event pairs that sample the model point coincident with Loma Prieta to ensure that the model is robust for the period immediately surrounding Loma Prieta. We use the

model for each station to examine the influence of the Loma Prieta earthquake on *S*-wave arrival times. Specifically, we take the difference between the model values for the day immediately before and the day of the Loma Prieta Earthquake as the co-seismic *S* delay.

2.4 Results

The Loma Prieta Earthquake produces a distinct signal that many stations detect. All stations affected by the earthquake show a systematic increase in the relative delays, of varying strength, in all parts of the seismogram (Figure 2.5a-f). The greatest delay is coincident in time with the Loma Prieta mainshock and thus is apparent in the earliest aftershocks. Within a seismogram, delays are largest in the *S* coda (Figure 2.5a-f).

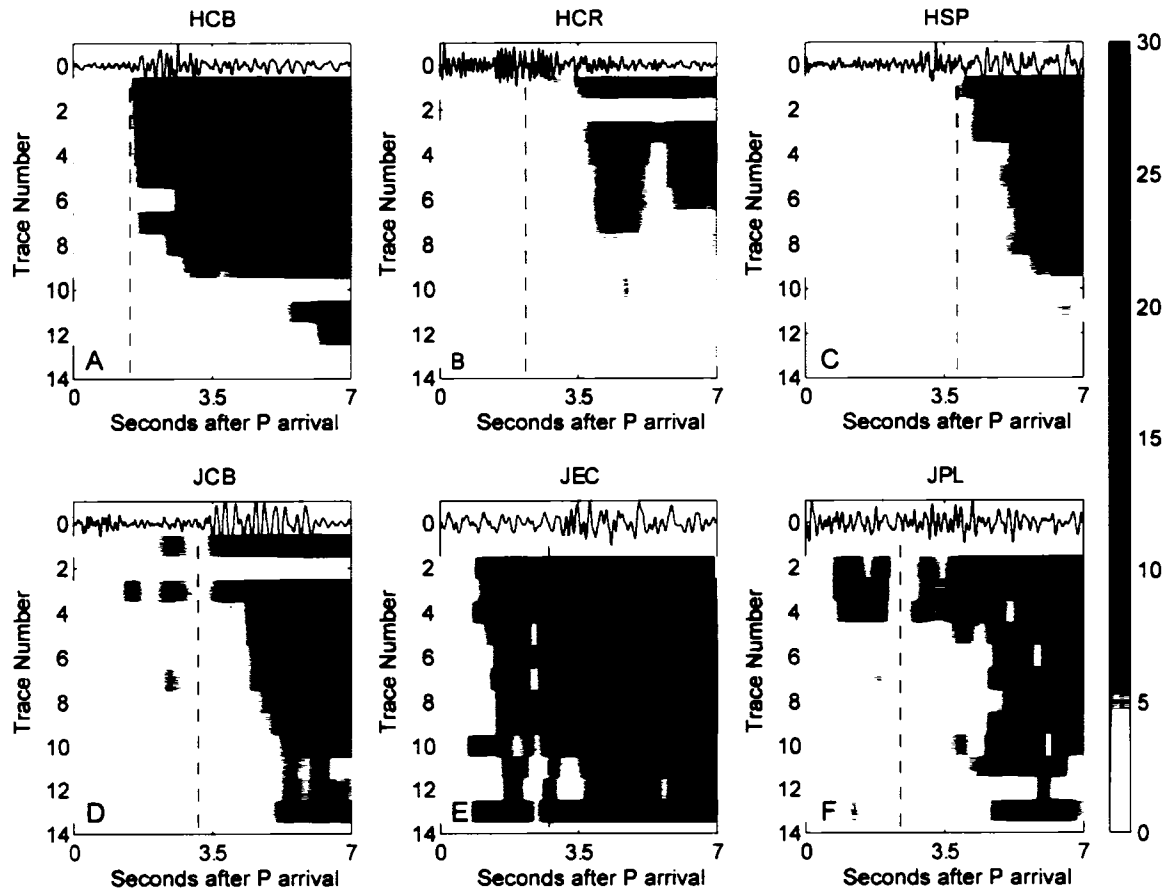


Figure 2.5a-f: Relative delays for multiplet 13 for stations HCB, HCR, HSP, JCB, JEC, and JPL. Reference seismogram for each multiplet-station pair plotted above delays. Vertical black line represents theoretical *S* arrival.

For example, delays of over 50 ms are observed at JEC in the *S* coda (Figure 2.5e). Delays for the direct *S* arrival are more modest, peaking at approximately 20ms (2 samples) at JEC (Figure 2.5g). The co-seismic increase in delays is indicative of a drop in seismic velocity caused by the earthquake. The delays gradually decrease to a level near those prior to the earthquake indicating that the seismic velocity heals following the co-seismic change. The healing is linear with the logarithm of time, such that the delays sharply decrease immediately after the earthquake and the rate of healing decreases with time (Figure 2.5h).

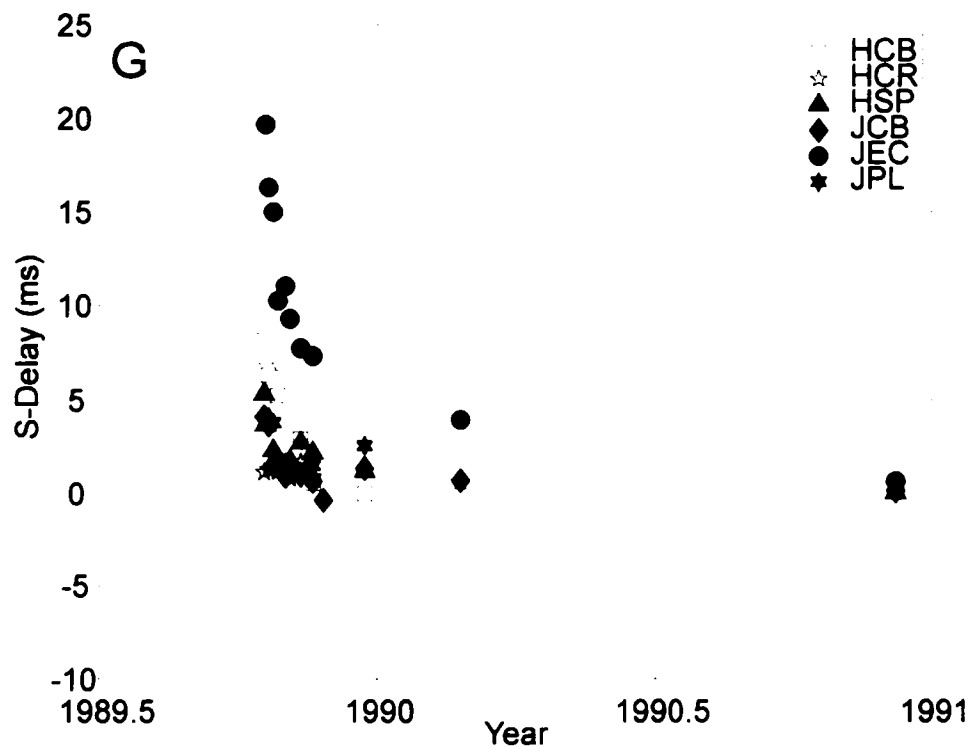


Figure 2.5g: Raw *S* delays for multiplet 13 as recorded by the same stations in Figures 5a-5f. Some stations may show less *S* delay measurements than the number traces shown in Figure 5a-f because some data have been eliminated based upon cross correlation coefficient or signal to noise minimums.

Our *S*-delay model reflects this behavior (Figure 2.5i-n). It should be noted that the delays we observe and compute a model for are specific to the *S*-waves, in that our initial waveform alignment method removes any delay in the *P* waves. As such, the delays observed should be considered as a minimum delay in the *S* arrival as any delay common to both the *P* and *S* arrivals will be removed in the initial alignment process.

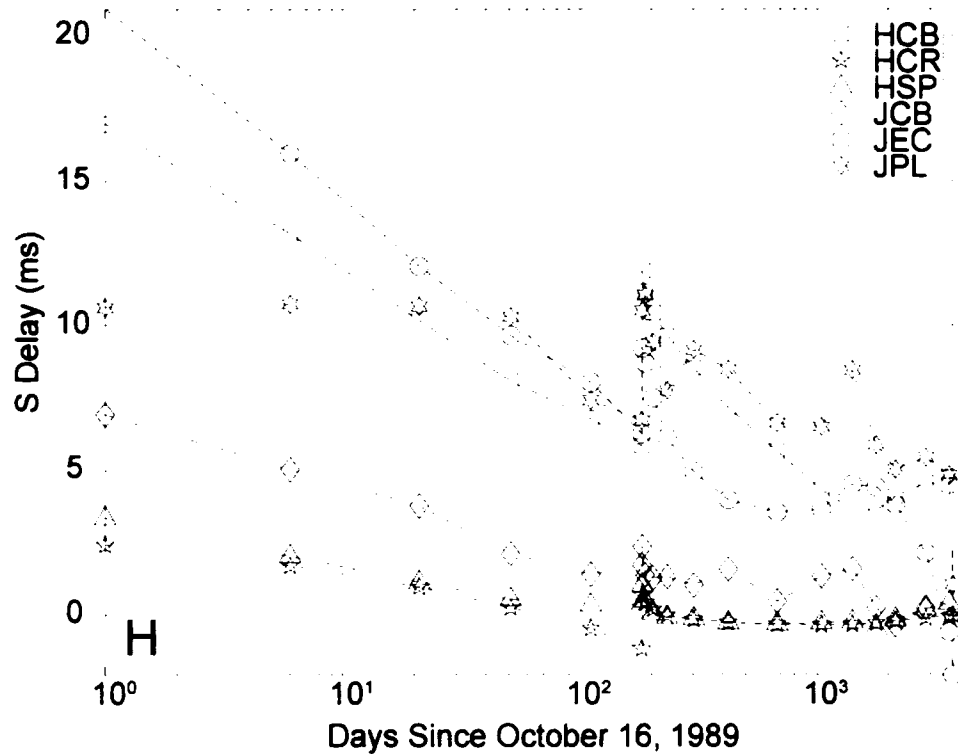


Figure 2.5h: Semilog plot showing the relative delay for multiplet 13 observed by the stations in Figures 2.5a-f plotted against the logarithm of the number of years after the day before the Loma Prieta earthquake.

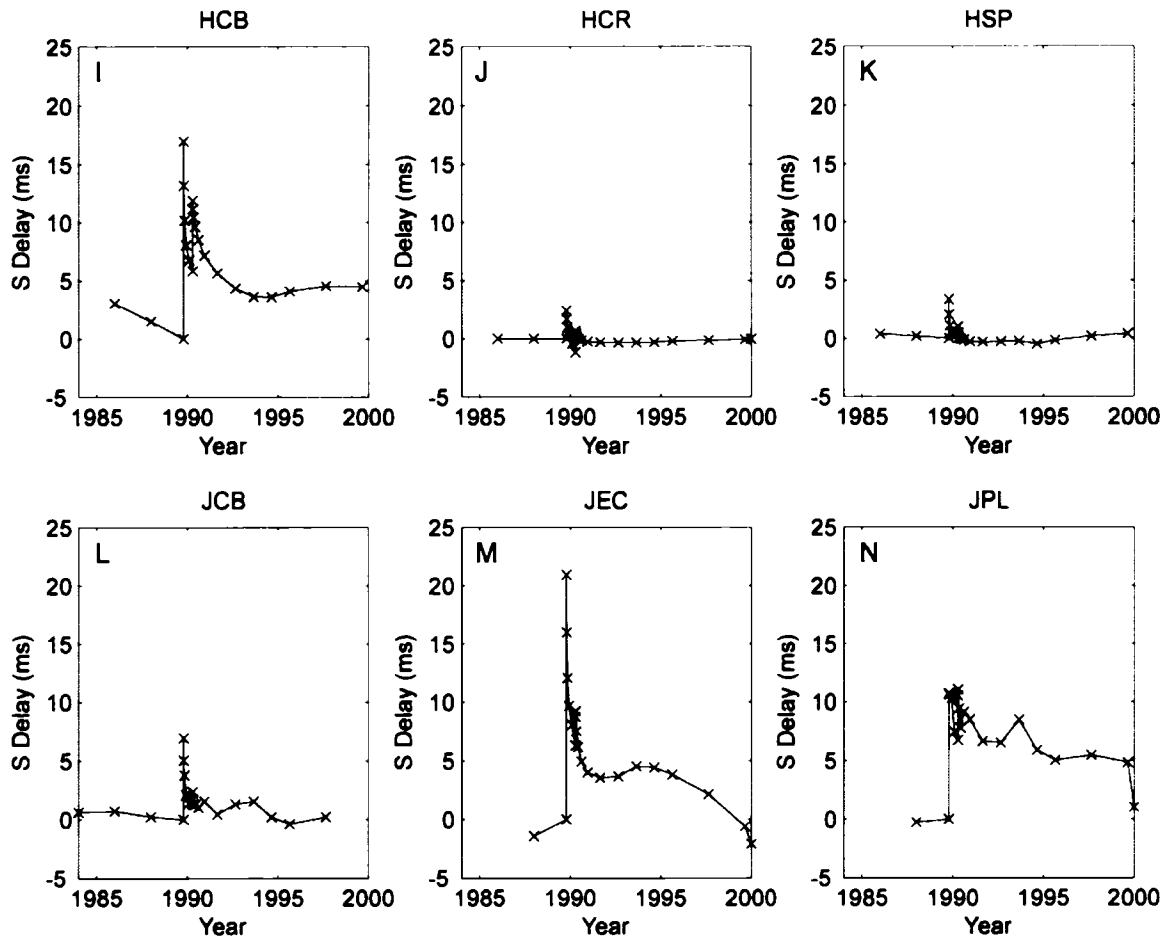


Figure 2.5i-n: Relative *S* delay model for the 6 stations shown in Figures 2.5a-2.5f. Note that the largest jump in delays at all of these stations is coincident in time with the Loma Prieta Earthquake.

Although the behavior of the response to the Loma Prieta Earthquake is consistent from station to station, the strength of this response varies greatly; however, there are some systematic patterns to the observed anomalies. Stations near the rupture typically have a much larger response to the Loma Prieta Earthquake than those that are more distant (Figure 2.6a, Table 2.1). Stations near the rupture have very large direct *S* delays in excess of 15 ms (e.g., JEC, JBZ, and HCB). Other stations, farther removed from the rupture, have much smaller delays of less than 5 ms (e.g. BSL, CSC, and HGS). Although the magnitude of delays decreases with distance from the rupture, we still observe a delay of over 3 ms at BCW, the station farthest from the rupture zone (~75km) that we examine.

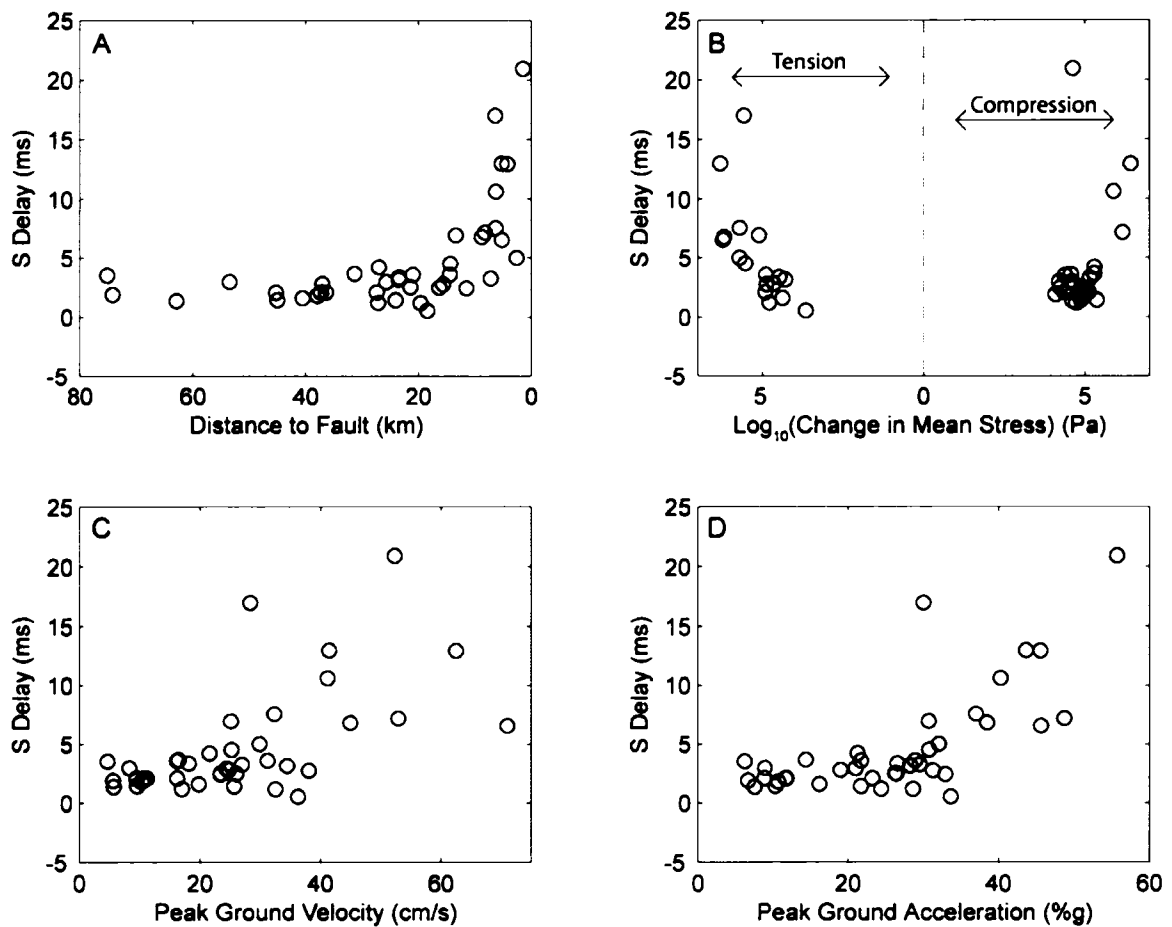


Figure 2.6: (A) Loma Prieta induced delay plotted versus distance to the vertical projection of the upper limit of the planar rupture described by *Marshall et al* (1991). (B) Loma Prieta induced delay plotted against the change in mean stress at the recording station. (C) Loma Prieta induced delay plotted against PGV for the recording station. (D) Loma Prieta induced delay plotted against PGA for the recording station.

2.5 Constraining the Source Region of the Delays

Prior to determining a mechanism for the observed delays, we attempt to localize the region in which they accumulate. The possible source regions are: near the earthquake, in the path between the earthquake and the receiver, near the receiver, or some combination of the three. For coda waves, there is the additional effect of the growth of the potential scattering volume with time into the coda. We have shown above

that near source effects aren't largely responsible for the observed delays. Below we examine how path and site effects might influence the observed velocity reductions.

Table 2.1: Station Parameters and Observations

Station	Latitude	Longitude	Distance to Fault (km)	Rock Unit*	Coda Amp. Factor*	Mean Stress Change (Pa)	PGV (cm/s)	PGA (%g)	S Delay Imparted by Loma Prieta (msec)
BCW	36.307	-121.567	75.15	--	--	0.24	4.65	6.20	3.52
BJO	36.611	-121.314	53.47	gr	1.4	0.16	8.29	8.93	2.96
BPC	36.573	-121.627	44.99	gr	0.8	0.76	9.58	10.34	1.44
BPR	36.407	-121.731	62.88	--	--	0.41	5.7	7.52	1.37
BSG	36.414	-121.255	74.16	gr	-0.1	0.12	5.61	6.64	1.89
BSR	36.667	-121.520	37.92	gr	0.9	0.70	10.26	10.72	1.80
BVY	36.746	-121.416	36.36	gr	-0.6	0.23	10.67	8.83	2.10
CAD	37.163	-121.624	21.45	ub	0.0	0.80	23.46	26.30	2.51
CAL	37.450	-121.800	37.30	KJf	-1.8	1.28	11.21	11.86	2.09
CCO	37.258	-121.675	27.04	Jk	-0.9	1.96	21.58	21.28	4.22
CMH	37.359	-121.758	31.33	Mm/Mu	-0.5	1.93	16.43	14.39	3.66
CSC	37.285	-121.773	24.04	KJf	-0.2	2.34	25.67	21.73	1.42
HAZ	36.885	-121.592	14.42	gr	-2.3	0.37	31.23	28.90	3.60
HBT	36.850	-121.552	19.63	phi	-0.9	0.55	32.53	28.64	1.18
HCA	37.025	-121.485	21.00	K	-0.9	-0.78	16.18	21.73	3.57
HCB	36.931	-121.662	6.34	phi	0.6	-3.78	28.31	30.02	16.99
HCR	36.957	-121.584	11.49	KJfv	-1.1	1.02	23.4	32.93	2.43
HDL	36.835	-121.645	16.35	gr	0.2	0.17	26	26.44	2.48
HFE	36.983	-121.403	27.40	Ku	-1.1	-0.81	16.22	23.25	2.09
HFH	36.888	-121.469	23.49	QP	1.7	-0.19	34.47	28.26	3.15
HGS	37.096	-121.448	27.16	KJf	-1.6	-0.61	16.99	24.41	1.20
HGW	37.017	-121.653	7.16	KJf	-2.0	1.42	26.95	29.50	3.25
HJS	36.817	-121.299	40.54	Ku	-1.6	-0.23	19.8	16.20	1.60
HLT	36.885	-121.309	37.03	Ku	-1.4	-0.44	24.74	19.02	2.80
HMO	36.600	-121.918	45.25	gr	-0.7	0.63	9.48	11.73	2.07
HOR	36.919	-121.515	18.43	Pc	0.4	-0.04	36.3	33.64	0.55
HPR	36.953	-121.695	2.58	Pml	1.2	-5.22	29.87	32.10	5.00
HSF	36.816	-121.498	25.70	Mv	0.6	0.39	24.42	21.00	2.94
HSP	37.115	-121.517	23.44	K	0.2	-0.30	18.14	26.56	3.35
JAL	37.158	-121.848	8.74	KJf	0.2	-15.54	44.97	38.49	6.78
JBL	37.128	-122.169	14.35	gr	-1.0	-3.42	25.23	30.77	4.52
JCB	37.112	-121.690	13.36	ub	0.1	-1.29	25.15	30.73	6.93
JEC	37.051	-121.810	1.42	Mm/Pml	0.7	0.43	52.31	55.72	20.91
JHL	37.109	-121.835	5.23	Ku	-0.8	-20.42	41.46	43.63	12.98
JPL	36.978	-121.834	6.25	Qc	0.9	7.78	41.19	40.25	10.62
JRG	37.038	-121.966	8.20	Pml	2.8	14.78	52.96	48.74	7.17
JRR	37.054	-121.728	6.28	KJf	-0.7	-5.09	32.33	37.01	7.56
JSS	37.170	-121.932	5.19	KJf	-1.0	-16.98	71.07	45.63	6.53
JST	37.206	-121.799	15.65	ub/KJf	-0.3	-0.76	38.09	31.28	2.75
JTG	37.029	-121.878	4.19	Pml	1.1	26.53	62.53	45.55	12.94

*Rock units described in Appendix 1

**From Phillips and Aki, 1986.

2.5.1 Path Effects

With the information we have available, it is difficult to localize the origin of the phase delays. We can't eliminate the possible contribution of whole-path effects on the signal; however, multiple aspects of the observed anomalies suggest that path effects are not the primary source of the delays. If delays largely accumulated along the entire source-receiver path, one would expect to observe the largest delays for paths that spend the largest amounts of time in or near the recently ruptured fault zone, as this is the region most strongly affected by earthquake rupture. The station JSS is at the opposite end of the rupture zone from the source multiplets, such that the source-receiver path largely traverses the ruptured fault zone. Were the path largely responsible for delays we would expect to observe the largest delays at JSS. This is not the case, the largest delays we observe are at JEC (20.9ms) and they are over three times larger than those observed at JSS (6.53ms). Were the observed delays accumulated along the entire path, we would expect that JSS would have significantly larger delays associated with it than nearby station JAL. JAL overlies the same rock, but the path to JAL from the multiplets does not path through the fault zone, and the path to JSS is straight through the fault zone. Instead, the delays observed at JAL (6.78ms) are comparable to the delays at JSS (6.53ms). Because paths that are long and largely confined to the fault zone do not have significantly larger delays associated with them than stations nearer the rupture, it suggests the delays are not accumulating gradually along the source-receiver path.

2.5.2 Site Effects

The site-specific aspects of the delays provide an even stronger argument against whole-path effects as an explanation for the delays. We observe large differences in the magnitude of delays at stations that are close to each other. For example stations HOR and HFH are located due east of the multiplet source region and overlie a Pliocene, nonmarine, sedimentary unit (Pc) and a Pleistocene nonmarine unit consisting of gravels, alluvial fan deposits, and sands (Qc), respectively. Neither source-receiver path crosses the rupture zone, so that near-rupture path effects are not a contributing factor in the *S* delays. If the delays were to accumulate along the path, the proximity of these two

stations would imply that similar delays should be observed at the two stations. Based on the strong ground motion and its closer proximity to the fault, one might expect HOR to have larger S delays than HFH. This is not the case, however, as delays of ~ 0.5 ms are observed at HOR, while delays of just over 3 ms are observed at HFH. This suggests that the geology local to the station may be the controlling factor in the strength of the observed delays. HFH is located on a much softer unit than HOR, which appears to make it more susceptible to velocity reductions. Site geology is consistently observed to influence the magnitude of delays (Table 2.1). This conclusion is further strengthened by the fact that the largest delays are observed in the S coda (e.g., Figure 2.3c), which is largely generated near the receiver (Dodge and Beroza, 1997). Figure 2.7 shows that stations where large delays are observed tend to have large site amplifications for coda waves (Phillips and Aki, 1986).

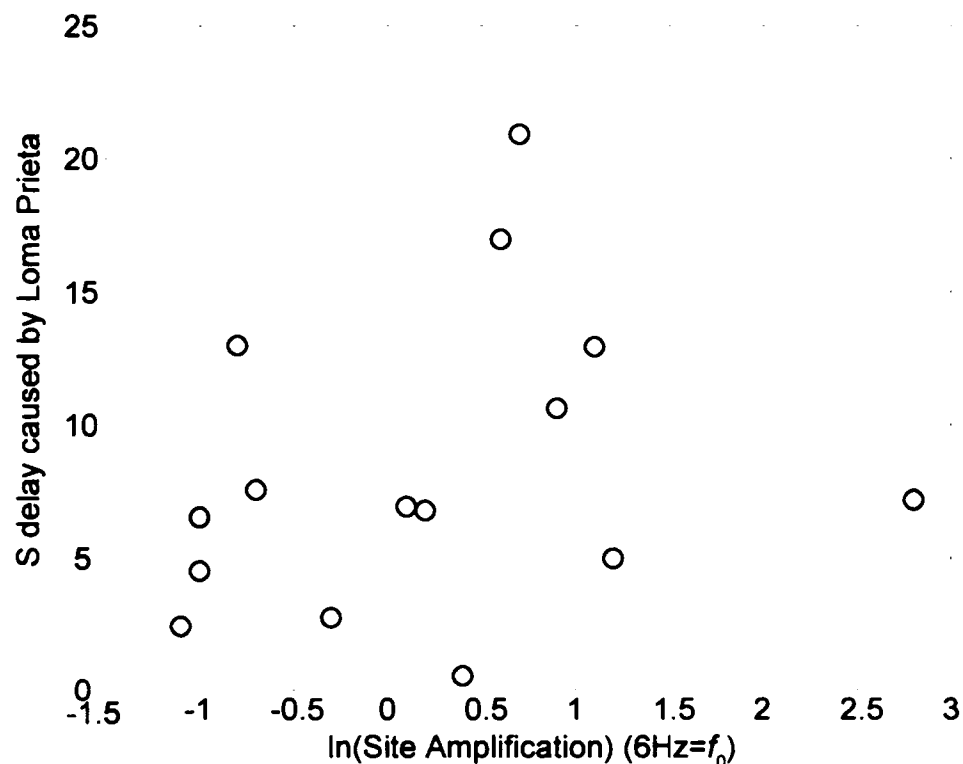


Figure 2.7: Loma Prieta induced delay plotted versus the natural logarithm of the coda derived site amplification factor determined by *Phillips and Aki* (1986). Only stations with peak ground acceleration greater than 30% are plotted.

2.6 Factors that Influence the Velocity Reductions

We now focus on the explanation for the observed anomalies. We explore the major factors that could influence the magnitude of the delays we observe. To explain our observations, we need to find a mechanism that allows large spatial variations over small distances, that is strongly expressed at distances of multiple fault lengths from the earthquake rupture, and that is of one sign only, like the observed co-seismic decrease in velocity. We first consider the possible effect of mainshock induced static stress changes on wave propagation in the Earth's crust.

2.6.1 Static Stress

Were the velocity changes imparted by static stress changes, we would expect the velocity changes to be caused by the preferential opening or closing of pre-existing cracks due to the change in stress. Assuming that the preexisting cracks are isotropically distributed, velocities should increase in regions of decreased mean stress (increased compression) and decrease in regions of increased mean stress because the stress would preferentially close (open) cracks in the case of compression (dilation) (Nur, 1971; Dodge and Beroza, 1997). We test this model by computing the change in mean stress in an elastic half space (Okada, 1985; Okada, 1992) at all the stations at which we record the repeating earthquakes using the Loma Prieta slip model of *Beroza* (1991).

We find that the change in mean stress imparted by the Loma Prieta earthquake does not predict the magnitude or the sign of the observed *S* delays (Figure 2.6b). In regions of dilation (increased mean stress), the delays increase, as expected; however, in regions of compression, the observed delays increase with increasing compression, contrary to what theory predicts. This indicates that porosity changes as a result of changes in the static stress field are not the cause of the observed phase delays.

We note that the assumption that the cracks are isotropically oriented is probably incorrect, and it is likely that there is some preferred orientation of cracks on both sides of the fault. Even so, any reasonable alignment of cracks would predict that there would be regions of both increased and decreased crack opening and hence areas of both

decreased and increased seismic velocity. We do not observe any regions where velocity increases co-seismically, therefore, we can rule out porosity changes induced by changes in mean static stress as the causative mechanism for the velocity reductions.

Unlike porosity changes induced by the change in the mean stress at a site, for which one cannot produce a distribution of velocity changes that are always negative, shear stress induced cracking will always result in reductions of seismic velocity. In this mechanism, the shearing induced by an earthquake (i.e., the change in shear stress) is believed to open of cracks. These cracks will have a highly anisotropic distribution, with the vast majority of cracks opening parallel to the direction of shear. This highly anisotropic crack distribution would result in large changes in velocity anisotropy. Recently, a number of authors have searched for earthquake induced changes in velocity anisotropy (Cochran *et al.*, 2003; *submitted*; Boness and Zoback, 2004; Peng and Ben-Zion, 2005). None of these studies were able to find changes in velocity anisotropy as a result of earthquakes, including two particularly precise studies that used repeating earthquakes as their sources (Boness and Zoback, 2004; Peng and Ben-Zion, 2005). The lack of observations of earthquake induced changes in velocity anisotropy suggests that shear induced cracking is not responsible for the large changes in seismic velocity that we observe here.

2.6.2 Strong Ground Motion

We find that the strength of strong ground motion correlates well with the observed *S*-delays. Figures 2.6c and 2.6d compare station specific peak ground acceleration (pga) values (in percent of gravity) and peak ground velocity (pgv) values (in cm/s) with the observed delays. Pga and pgv measurements are initially obtained from the Northern California Earthquake Data Center (NCEDC) from routinely computed ShakeMaps (Wald *et al.*, 1999; Boatwright *et al.*, 2003). Station specific pga and pgv measurements are then calculated by interpolation. After examining the relation between the *S* delay and strong ground motion, it appears that for pga and pgv there is a threshold, above which large delays start accumulating. This threshold is approximately 40 cm/s for velocity and 30 percent of gravity for acceleration. It should be noted that the pgv/pgv

values we compute are subject to considerable uncertainty. Although ShakeMaps do take rock type and topography into account, our simple interpolation scheme does not, such that site effects specific to other locations may contaminate our interpolated pga and pgv values.

Dynamic stresses during the strong shaking of the Loma Prieta Earthquake correlate much better with the observed phase delays than the earthquake's resultant static stresses. A simple computation of the dynamic stresses for a plane wave with a peak ground velocity of 40 cm/s (our threshold value for large observed delays) yields dynamic stresses of 8 MPa and 133 microstrain (assuming a Poisson solid with shear modulus of 20 GPa). The largest changes in mean static stress computed for any one station was 2.65 MPa. The large difference between the magnitude of the dynamic and static stresses suggests that the strong ground motion of the earthquake is potentially a much more potent agent to change velocities than the static stress field.

2.6.3 Lithology

We have shown that both site characteristics (site geology/coda amplification) and the strength of shaking experienced during Loma Prieta appear to influence the magnitude of the observed delays; however, these two factors are themselves highly correlated, regardless of the presence or absence of nonlinearity. Thus, we would like to disentangle the relative contributions of strength of shaking vs. susceptibility to nonlinearity. Figure 2.8 compares the affects of site characteristics: site geology, coda amplification factor (Phillips and Aki, 1986), and mainshock strong ground motion with respect to the magnitude of *S* delays.

Figure 2.8a compares the impact of coda amplification and the strength of ground shaking to the magnitude of the observed *S* delays. Intensity of strong shaking is clearly strongly correlated with the magnitude of the delays. Nearly every station that undergoes high values of peak ground acceleration (above 30%) has larger delays associated with it than stations that experience weaker ground motion. Coda amplification appears to be related to the magnitude of delays, as well. There are many more stations that have large delays associated with them that have coda amplification factors greater than zero than

those with coda amplification factors less than zero. This may be misleading, though, as there are more stations with high coda amplifications that also experience high strong ground motion than stations with low coda amplifications and high strong ground motion.

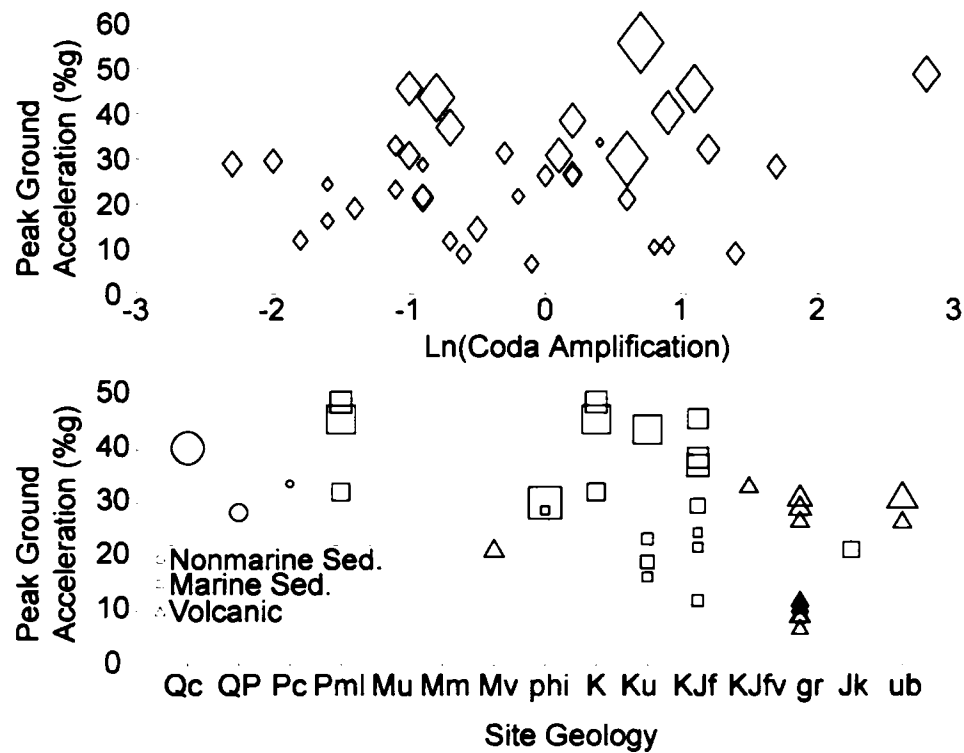


Figure 2.8: (a) Peak ground acceleration plotted against the natural logarithm of the site-specific coda amplification factor determined by *Phillips and Aki* (1986). The size of diamond indicates the magnitude of relative *S* delays recorded at that station. (b) Peak ground acceleration plotted against the geological unit over which the station is placed. The size of the symbol indicates the magnitude of delays recorded at that station. Circles indicate nonmarine sediments; squares indicate marine sediments; triangles indicate volcanic and meta-volcanic units. Age of the unit increases to the right.

Figure 2.8b is the same as figure 2.8a, but instead of coda amplification, it shows site geology on the horizontal axis. We find that the magnitude of delays correlates with the surface geology. Stations within the sedimentary (both marine and nonmarine) units exhibit large delays and the largest of them are observed at the sites located on the youngest rock. This implies that younger sedimentary rocks are more susceptible to

experience nonlinearity in strong ground motion than older sedimentary rocks, which are most likely harder and stronger than their younger counterparts.

If we consider different rock types (i.e. marine and non marine sediments and volcanic units) for which the level of strong ground motion is similar, we find that the geologic conditions at the site do not appear to control the magnitude of S delays. Because of the effects of site amplification, and the distribution of data we have, we are only able to compare stations where we don't expect the effect of nonlinearity to be strong. Therefore, this comparison, though suggestive, does not allow a definitive conclusion on the role of site geology, once site amplification is taken into account. The increasing magnitude of delays with decreasing age within the sedimentary units; however, suggests that geology does appear to have some control over the magnitude of delays.

From these comparisons, we can conclude that the primary factor in determining the magnitude of nonlinearity at any station is the magnitude of strong shaking. The strength of the geologic unit appears to be a secondary factor. Much of the preference for strength of shaking instead of site geology may be attributable to the amplification that the site geology causes, rather than increased susceptibility to nonlinearity at a given level of ground motion.

2.7 Physical Model

Other studies have identified velocity reductions following medium to large earthquakes (e.g., Poupinet *et al.*, 1984; Li *et al.*, 1994; Zhao *et al.*, 1996; Nishimura *et al.*, 2000; Li and Vidale, 2001; Vidale and Li, 2003; Schaff and Beroza, 2004). These studies have suggested a variety of mechanisms to account for the observed velocity reductions, including: static stress changes (Poupinet *et al.*, 1984; Nishimura *et al.*, 2000), changes in the hydrologic system (Poupinet *et al.*, 1984; Zhao *et al.*, 1996), physical damage to the fault zone caused by fault motion (Li *et al.*, 1994; Li *et al.*, 2002), and widespread physical damage caused by nonlinearity in the strong ground motion (Schaff and Beroza, 2004). We discount the static stress change model as inconsistent as argued above. Below we consider the fault zone damage and widespread damage models

for velocity changes in light of our observations. We will then consider the hydrologic implications of our preferred model. We favor a model that implicates near-surface physical damage to the Earth's crust caused by strong ground motion as the mechanism for the observed velocity reductions. We favor this model because it is the only one consistent with all of our observations.

2.7.1 Fault Zone Damage

We prefer a model of widespread physical damage, to that of damage localized on the fault zone for a number of reasons. First, the delay does not vary systematically with respect to the source-receiver path relative to the mainshock rupture zone. If damage were restricted to the fault zone, it would predict that delays would be large for paths crossing or traveling through the fault and small for paths that don't. The path from the repeating earthquake sequences to JSS, for example, traverses the length of the rupture zone, yet we do not observe particularly large lags at JSS. The paths from the repeating earthquakes to HCB, on the other hand, do not cross the rupture zone, yet they are quite large. Furthermore, the strong dependence of variation of S delays on the level of site-specific strong ground motion is incompatible with the fault zone damage model, as it implies that delays accumulate near the site. On the other hand, we cannot exclude the possibility that fault zone damage occurs, but that our measurements are not sensitive to it. Indeed, a zone of reduced seismic velocities several hundred meters wide such as found for the Landers and Hector Mine earthquakes (Li *et al.*, 2002; Li *et al.*, 1994) would be difficult to detect with our data, particularly since fault rupture in this earthquake was almost entirely deeper than 6 km (e.g., Beroza, 1991).

2.7.2 Widespread Damage Resulting From Strong Shaking

Our observations are consistent with a simple model in which the velocity reductions that we observe are the result of near surface damage imparted by the strong ground motion of the Loma Prieta Earthquake. Specifically, the strong shaking of the earthquake opened new cracks and enlarged preexisting cracks in the rock, which in turn reduced seismic velocities. The growth and creation of cracks along with the resultant

velocity reductions imply that the mainshock strong ground motion was nonlinear, i.e., that significant seismic energy was expended in damaging the rocks through cracking or crack extension. This phenomena has been observed in lab studies that show that strong ground motion can cause restructuring of the internal structure of rocks resulting in changes of detectable physical phenomena (Shamina *et al.*, 1990). Some have found fracturing to be the most common source of nonlinearity in strong ground motion (Shamina and Palenov, 2002). There are multiple lines of evidence that support our interpretation that fracturing (nonlinearity) resulting from the strong ground motion of the Loma Prieta Earthquake caused the velocity reductions we observe.

First, the velocity reductions we observe are strongly correlated with the level of mainshock strong ground motion. This dependence is consistent with laboratory observations that indicate the magnitude of nonlinearity is proportional to the level of dynamic strain (Guyer *et al.*, 1998; Ostrovsky *et al.*, 2000).

Second, our observations of the spatial variability of delays imply that the velocity reductions are very near surface. Nonlinearity should concentrate near the surface, considering that the strength of nonlinearity is inversely related to the effective pressure (Zinszner *et al.*, 1997; Ostrovsky *et al.*, 2000).

Third, the velocity reductions we observe are correlated with site conditions and are strongest at sites with relatively soft sedimentary lithology. This is consistent with the laboratory results of *Van Den Abeele and Van de Velde* (2000), who find a strong anticorrelation between measures of elastic strength (flexural strength, bending modulus, and tensile strength) and nonlinear susceptibility from laboratory experiments.

Fourth, the change in velocity is of one sign only, *viz* a co-seismic velocity reduction. This observation is inconsistent with mechanisms of stress-induced velocity change (Nur, 1971). It is, however, exactly what is observed in studies of nonlinearity in the laboratory (e.g., *TenCate et al.*, 2000 a, b).

Finally, the temporal behavior of the velocity change also follows observations made in the laboratory. *TenCate et al.* (2000 a, b) find that the velocity reduction due to nonlinear strain in the laboratory diminishes linearly with the logarithm of time once the large strains are removed – a behavior described as “slow dynamics” by the materials

science community. We find the same logarithmic time dependence for the velocity changes we observe.

It should be noted that laboratory studies of nonlinearity and slow dynamics are typically performed on intact rock samples while our study is of damaged country rock. This along with the issue of scaling from the lab to the macroscopic world may cast doubt as to the correlation between our observations and laboratory observations. We believe the comparisons we are making are valid because we are only comparing the general behavior and not specific numbers of country rock to intact lab samples.

To summarize, our observations are uniformly consistent with the interpretation that the velocity change we observe is a lingering effect of nonlinear wave propagation during mainshock strong ground motion. We find independent support for this interpretation in the form of hydrological changes following the Loma Prieta earthquake.

2.7.3 Supporting Evidence from Hydrology

Rojstaczer et al. (1995) documented an increase in streamflow coincident with the Loma Prieta Earthquake. They attribute this to a sudden increase in permeability associated with the Loma Prieta Earthquake. They observed the streamflow, over the course of a year, slowly return back to its initial level. Despite the difference in the time scale over which they heal, we suggest that the streamflow changes observed by *Rojstaczer et al. (1995)* and the velocity changes we observe are caused by the same mechanism. A sudden increase in crack density (porosity) should lead to both an increase in streamflow and seismic velocity reductions. A sudden increase in permeability (here caused by an increase in porosity) would immediately increase groundwater flow into streams. This would be followed by a drop in the water table due to the increase in groundwater flow without an increase in the recharge of water into the system (*Rojstaczer et al., 1995*). A sudden increase in porosity should also result in a reduction of seismic velocity as it drops the effective bulk and shear moduli of the medium. Although, the cause and mechanism of these two phenomena is the same, the time dependence of the recovery may not be. Streamflow is controlled by permeability (connectivity of pore space), while seismic velocity is controlled by porosity (density of

pore space). We would expect streamflow to heal faster than seismic velocity, as the removal of any pore space in connective cracks will reduce the permeability much more than the porosity. As such, the permeability will decrease more quickly than the porosity, effectively reducing the streamflow faster than the velocity increases, as observed.

Although major changes in the hydrologic system probably don't cause the observed velocity reductions, we do believe that the presence of water does influence the velocity perturbations we observe. Rock physics tells us that when water is present within cracks in a medium, S velocities will be decreased much more than P velocities because water cannot support shear (Mavko *et al.*, 1998). This implies that the delays for S and S coda will be larger than those for P and P coda (Li *et al.*, 2003). Although we cannot quantitatively measure delays for the P or the early P coda because they are used in our initial alignment, we can compare delays observed in the late P coda with delays in the early S coda. A cursory examination of stations shows delays in the late P coda are smaller than those in the early S coda (Figure 2.5a-f). Assuming that the source of our velocity reductions is cracks, the previous finding indicates that the cracks are saturated.

2.7.4 Other Evidence for Nonlinearity during Strong Ground Motion

It should not be surprising that the strong ground motion of Loma Prieta was nonlinear. Dynamic strains in the near field of the Loma Prieta earthquake were at least several hundred microstrain. Laboratory studies indicate that the onset of nonlinearity occurs at strains of less than a microstrain (Johnson and Rasolofosaon, 1996). Much of the seismological evidence for nonlinearity in strong ground motion has been equivocal. Nonlinearity was inferred by *Chin and Aki* (1991, 1996) at sediment sites for the Loma Prieta earthquake, for which they found that the accelerations predicted by a coda amplification factor, based on weak-motion records, were higher than those observed. The implication of their observation is that during the mainshock, amplitude dependent attenuation limited the amplification at sedimentary sites. Some have questioned the validity of their findings that there was nonlinearity in the strong ground motion of Loma Prieta, suggesting that the effect could be removed if site-specific amplifications were used (Wennerberg, 1996). Nonlinearity in site response has also been suggested for other

earthquakes, including: the 1994 Northridge Earthquake (Field *et al.*, 1997), the 2001 Nisqually Earthquake (Frankel *et al.*, 2002), the 1995 Kobe Earthquake (Pavlenko and Irikura, 2002), and three M6+ events in Taiwan (Wen *et al.*, 1994). Our results offer independent evidence that nonlinearity during the Loma Prieta earthquake was widespread.

2.8 Conclusions

Using repeating earthquake sequences located just to the south of rupture zone of the 1989 Loma Prieta Earthquake we have identified consistently late arriving *S* phases in these repeating earthquake sequences. We interpret the delays as reductions in near surface velocity. A strong correlation of the *S* delays with measures of strong ground motion indicates that strong ground motion is largely responsible for the observed delays. Specifically, when the strong ground motion exceeds the strength of rocks, cracks open, resulting in reduced seismic velocities. The nonlinear response of the crust is particularly strong at the near surface, which accounts for the rapid spatial variation in observed *S* delays and the correlation of the magnitude of these delays with the surface geology. It is likely that the magnitude of delays is largest for stations on softer rocks because soft rocks experience higher amplitudes when exposed to shaking and thus are more susceptible to nonlinear effects than harder rocks. We believe that the cracks opened in the strong motion of the Loma Prieta Earthquake are quickly filled with fluids, which results in *S* phases being delayed much more than *P* phases. Following the initial shock to the system, the seismic velocity heals back to its initial state in a log-linear fashion. This parallels the slow dynamic behavior observed by the materials science community, whereby creep processes close cracks and restore damaged rocks to their initial state. We believe the same sort of creep processes are at work here, driven by external stresses to close cracks and thereby increase velocity.

Acknowledgements:

The authors would like to thank Götz Bokelmann for many insightful discussions. We thank David Schaff for providing the repeating earthquake sequences used in this study and for offering many useful suggestions. This manuscript was improved by the

suggestions of Allan Rubin, Igor Beresnev, and an anonymous reviewer. All data used in this study were made available through the NCEDC. The data was provided by the NCSN, via the U.S. Geological Survey, Menlo Park. J.R. was partially supported by the Wells Family Stanford Graduate Fellowship. This work was supported by USGS grants 02HQGR0039 and 03HQGR0073.

References

- Arfken, G.B. and H.J. Weber (1995). *Mathematical Methods for Physicists: International Edition*, Academic Press, San Diego.
- Baisch, S. and G.H.R. Bokelmann (2001). Seismic waveform attributes before and after the Loma Prieta earthquake: Scattering change near the earthquake and temporal recovery, *J. Geophys. Res.*, **106**, 16,323-16,337.
- Beresnev, I.A. and K-L. Wen (1996). Nonlinear soil response—A reality?, *Bull. Seism. Soc. Am.* **86**, 1964-1978.
- Bishop, C.C. and R.H. Chapman (1967). Bouguer Gravity Map of California, Santa Cruz Sheet, Calif. Div. of Mines and Geol, Sacramento.
- Bokelmann, G.H.R. and H-P. Harjes (2000). Evidence for temporal variation of seismic velocity within the upper continental crust, *J. Geophys Res.*, **105**, 23,879-23,894.
- Beroza, G. C. (1991). Near-Source modeling of the Loma Prieta Earthquake: Evidence for heterogeneous slip and implications for earthquake hazard, *Bull. Seism. Soc. Am.* **81**, 1603-1621.
- Beroza, G.C., A. T. Cole, and W. L. Ellsworth (1995). Stability of coda wave attenuation during the Loma Prieta, California, earthquake sequence, *J. Geophys. Res.* **100**, 3977-3987.
- Boness, N.L. and M.D. Zoback (2004). Multi-scale seismic anisotropy in the region surrounding the San Andreas Fault near Parkfield, CA., *Eos Trans. AGU*, **85**, Fall Meet. Suppl. Abstract T11F-05.
- Booth, D.C., S. Crampin, and J.H. Lovell (1990). Temporal changes in shear wave splitting during an earthquake swarm in Arkansas, *J. Geophys. Res.* **95**, 11,151-11,164.
- Boatwright, J., H. Bundock, J. Luetgert, L. Seekins, L. Gee, and P. Lombard (2003). The dependence of PGA and PGV on distance and magnitude inferred from Northern California ShakeMap data, *Bull. Seism. Soc. Am.*, **93**, 2043-2055.
- Chin, B., and K. Aki (1991). Simultaneous study of the source, path, and site effects on strong ground motion during the 1989 Loma Prieta earthquake: A preliminary result on pervasive nonlinear site effects. *Bull. Seism. Soc. Am.*, **81**, 1859-1884.

- Chin, B. and K. Aki (1996). Reply to Leif Wennerberg's Comment on "Simultaneous study of the source, path, and site effects on strong ground motion during the 1989 Loma Prieta earthquake: A preliminary result on pervasive nonlinear site effects", *Bull. Seism. Soc. Am.*, **86**-1A, 268-273.
- Cochran, E.S., Y.-G. Li, and J.E. Vidale. Invariant anisotropy in the shallow crust observed around the San Andreas Fault before and after the 2004 M6 Parkfield earthquake, *submitted to Bull. Seism. Soc. Am.*
- Cochran, E.S., J.E. Vidale, and Y.-G.Li (2003). Near-fault anisotropy following the Hector Mine earthquake, *J. Geophys. Res.*, **108**, doi:10.1029/2002JB002352.
- Crampin, S., T. Volti, and R. Stefansson (1999). A successfully stress-forecast earthquake, *Geophys. J. Int.* **138**, F1-F5.
- Deichmann, N. and M. Garcia-Fernandez (1992). Rupture geometry from high-precision relative hypocentre locations of microearthquake clusters, *Geophys. J. Int.*, **110**, 501-517.
- Dodge, D.A. and G. C. Beroza (1997). Source array analysis of coda waves near the 1989 Loma Prieta, California, mainshock: Implications for the mechanism of coseismic velocity changes, *J. Geophys. Res.* **102**, 24,437-24,458.
- Field, E.H., P.A. Johnson, I.A. Beresnev, and Y. Zeng (1997). Nonlinear ground-motion amplification by sediments during the 1994 Northridge earthquake. *Nature*, **390**, 599-602.
- Frankel, A.D., D.L. Carver and R.A. Williams (2002). Nonlinear and linear site response and basin effects in Seattle for M6.8 Nisqually, Washington, Earthquake. *Bull. Seism. Soc. Am.* **92**, 2090-2109.
- Guyer, R. A., K. R. McCall, and K. Van Den Abeele (1998). Slow elastic dynamics in a resonant bar of rock, *Geophys. Res. Lett.*, **25**, 1585-1588.
- Jennings, C.W. and R.G. Strand (1958). Explanatory Data, Santa Cruz Sheet, Calif. Div. of Mines and Geol., Sacramento.
- Johnson, P.A. and P.N.J. Rasolofosaon (1996). Manifestation on nonlinear elasticity in rock: convincing evidence over large frequency and strain intervals from laboratory studies, *Nonlinear Processes in Geophys.*, **3**, 77-88.

- Li, Y.G. and J.E. Vidale (2001). Healing of the shallow fault zone from 1994-1998 after the 1992 M7.5 Landers, California, earthquake, *Geophys. Res. Lett.*, **28**, 2999-3002.
- Li, Y.G., K. Aki, D. Adams, A. Hasemi, and W.H.K. Lee (1994). Seismic guided waves trapped in the fault zone of the Landers, California, earthquake of 1992, *J. Geophys. Res.*, **99**, 11,705-11,722.
- Li, Y.G., J.E. Vidale, K. Aki, F. Xu, and T. Burdette (1998). *Science*, **279**, 217-219.
- Li, Y. G., J. E. Vidale, S. M. Day, D. D. Oglesby, E. Cochran (2003). Postseismic fault healing on the rupture zone of the 1999 M7.1 Hector Mine, California, Earthquake, *Bull. Seism. Soc. Am.* **93**, 854-869.
- Li, Y.G., J.E. Vidale, S.M. Day, D.D. Oglesby and the SCEC Field Working Team (2002). Study of the 1999 M7.1 Hector Mine, California, Earthquake Fault Plane by Trapped Waves, *Bull. Seism. Soc. Am.*, **92**, 1318-1332.
- Londono, John Makario (1996). Temporal changes in coda Q at Nevado del Ruiz Volcano, Colombia, *J. Volcanology and Geothermal Res.* **73**, 129-139.
- Marhsall, G. A., R.S. Stein, and W. Thatcher (1991). Faulting geometry and slip from co-seismic elevation changes: The 18 October 1989, Loma Prieta, California, earthquake, *Bull. Seism. Soc. Am.* **81**, 1660-1693.
- Mavko, G., T. Mukerji, and J. Dvorkin (1998). *The rock physics handbook*, Cambridge University Press.
- Nishimura, T. N., N. Uchida, H. Sato, M. Ohtake, S. Tanaka, and H. Hamaguchi (2000). Temporal changes of the crustal structure associated with the M6.1 earthquake on September 3, 1998, and the volcanic activity of Mount Iwate, Japan, *Geophys. Res. Lett.* **27**, 269-272.
- Nur, A., (1971). Effect of stress on velocity anisotropy in rocks with cracks, *J. Geophys. Res.*, **76**, 2022-2034.
- Okada, Y. (1985). Surface deformation due to shear and tensile faults in a half-space, *Bull. Seism. Soc. Am.* **75**, 1135-1154.
- Okada, Y. (1992). Internal deformation due to shear and tensile faults in a half-space, *Bull. Seism. Soc. Am.* **82**, 1018-1040.

- Ostrovsky, L. A., P. A. Johnson, and T. J. Shankland (2000). The mechanism of strong nonlinear elasticity in earth solids, in *Nonlinear Acoustics at the Turn of the Millenium: ISNA 15*, edited by W. Lauterborn and T. Kurz, pp. 75-84, American Institute of Physics.
- Pavlenko, O. and K. Irikura (2002). Changes in shear moduli of liquefied and nonliquefied soils during the 1995 Kobe Earthquake and its aftershocks at three vertical-array sites, *Bull. Seism. Soc. Am.* **92**, 1952-1969.
- Peng, J-Y, K. Aki, B. Chouet, P. Johnson, W.H.K. Lee, S. Marks, J.T. Newberry, A.S. Ryall, S.W. Stewart, and D.M. Tottingham (1987). Temporal change in coda Q associated with the Round Valley, California earthquake of November 23, 1984, *J. Geophys. Res.* **92**, 3507-3526.
- Peng, Z. and Y. Ben-Zion (2005). Spatiotemporal variations of crustal anisotropy from similar events in aftershocks of the 1999 M7.4 Izmit and M7.1 Duzce, Turkey earthquake sequences, *Geophys. J. Int.*, **160**, 1027-1043.
- Phillips, W. S. and K. Aki (1986). Site amplification of coda waves from local earthquakes in Central California, *Bull. Seism. Soc. Am.* **76**, 627-648.
- Poupinet, G., W. L. Ellsworth, and J. Frechet (1984). Monitoring velocity variations in the crust using earthquake doublets: An application to the Calaveras Fault, California, *J. Geophys. Res.* **89**, 5719-5731.
- Ratdomopurbo, A. and G. Poupinet (1995). Monitoring a temporal change of seismic velocity in a volcano: Application to the 1992 eruption of Mt. Merapi (Indonesia), *Geophys. Res. Lett.* **22**, 775-778.
- Rojstaczer, S., S. Wolf, and R. Michel (1995). Permeability enhancement in the shallow crust as a cause of earthquake-induced hydrological changes, *Nature* **373**, 237-239.
- Rubin, A. M. (2002). Using repeating earthquake to correct high-precision earthquake catalogs for time-dependent station delays, *Bull. Seism. Soc. Am.* **92**, 1647-1659.
- Saiga, A., Y. Hiramatsu, T. Ooida, and K. Yamaoka (2003). Spatial variation in the crustal anisotropy and its temporal variation associated with a moderate-sized earthquake in the Tokai region, central Japan, *Geophys. J. Int.* **154**, 695-705.

- Schaff, D. (2001). 4D high resolution seismology : repeating events and large scale relocation, Ph.D. thesis, Stanford University, Stanford, CA.
- Schaff, D. P., and G. C. Beroza (2004), Coseismic and postseismic velocity changes measured by repeating earthquakes, *J. Geophys. Res.*, **109**, B10302, doi:10.1029/2004JB003001
- Schaff, D. P., G. C. Beroza, and B. E. Shaw (1998). Postseismic response of repeating aftershocks, *Geophys. Res. Lett.*, **25**, 4549-4552.
- Su, Feng and K. Aki (1990). Temporal and spation variation of coda Q-1 associated with the North Palm Springs earthquake of July 8, 1986, *PAGEOPH* **133**, 23-52.
- Shamina, O.G. and A.M. Palenov (2002). Spectral Properties of Waves Propagating in a Fractured Medium: Dynamic and Static Cases, *Izvestiya: Physics of the Solid Earth*, **38**, 738-744.
- Shamina, O.G., A.M. Palenov, Z. Stopinskiy, V.S. Tkachenko, and N.A. Yakushina (1990). Influence of Ultrasonic Vibrations on Physicomechanical Properties of Rocks. *Izvestiya, Physics of the Solid Earth*, **28**, 694-700.
- TenCate, J. A., E. Smith, L. W. Byers, and T. J. Shankland (2000a). Slow dynamics experiments in solids with nonlinear mesoscopic elasticity, in *Nonlinear Acoustics at the Turn of the Millenium: ISNA 15*, edited by W. Lauterborn and T. Kurz, pp. 303-306, American Institute of Physics.
- TenCate, J. A., E. Smith, and R. A. Guyer (2000b). Universal slow dynamics in granular solids, *Phys. Rev. Lett.* **85**, 1020-1023.
- Van Den Abeele K. and K. Van de Velde (2000). Correlation between dynamic nonlinearity and static mechanical properties of corroded E-glass reinforced polyester composites, in *Review of Progress in Quantitative Nondestructive Evaluation*, edited by D.O. Thompson and D.E. Chimenti, pp. 1359-1366, American Institute of Physics.
- Vidale, J.E. and Y.G. Li (2003). Damage to the shallow Landers fault from the nearby Hector Mine Earthquake, *Nature* **421**, 524-526.
- Wahba, Grace (1990). *Spline Models for Observational Data*. Society for Industrial and Applied Mathematics.

- Wald, D. J., V. Quitoriano, T. H. Heaton, H. Kanamori, C.W. Scriver, C.B. Worden (1999). TriNet “ShakeMaps”: Rapid generation of peak ground motion and intensity maps for earthquakes in Southern California, *Earthquake Spectra* **15**, 537-555.
- Wang, J.H., T.L. Teng, and K.F. Ma (1989). Temporal variation of coda Q during Hualien earthquake of 1986 in eastern Taiwan, *PAGEOPH* **130**, 617-634.
- Wen, K-L., I.A. Beresnev, and Y.T. Yeh (1994). Nonlinear soil amplification inferred from downhole strong seismic motion data, *Geophys. Res. Lett.* **21**, 2625-2628.
- Wennerberg, L. (1996). Comment on “Simultaneous study on the source, path, and site effects on strong ground motion during the 1989 Loma Prieta Earthquake: A preliminary result on pervasive nonlinear site effects” by Byau-Heng Chin and Keiti Aki, *Bull. Seism. Soc. Am.* **86**-1A, 259-267.
- Zhao, D., H. Kanamori, H. Negishi, and D. Wiens (1996). Tomography of the source area of the 1995 Kobe Earthquake: Evidence for fluids at the hypocenter?, *Science*. **274**, 1891-1894.
- Zinszner, B., P. A. Johnson, and P. N. J. Rasolofosaon (1997). Influence of change in physical state on elastic nonlinear response in rock: Significance of effective pressure and water saturation, *J. Geophys. Res.* **102**, 8105-8120

Appendix 1

Table 2.2: Explanation of Rock Types

Qc	Pleistocene nonmarine
QP	Plio-Pleistocene nonmarine
Pc	Undivided Pliocene nonmarine
Pml	Middle/Lower Pliocene marine
Mu	Upper Miocene marine
Mv	Miocene volcanic
Mm	Middle Miocene marine
phi	Oligocene marine
K	Undivided Cretaceous marine
Ku	Upper Cretaceous marine
KJfv	Franciscan volcanic and metavolcanic rocks
KJf	Franciscan Formation
Jk	Knoxville Formation
gr	Mesozoic granitic rocks
ub	Mesozoic ultrabasic intrusive

Rock units determined from Phillips and Aki (1986) and Bishop and Chapman (1967). Rock unit description from Bishop and Chapman (1967) and Jennings and Strand (1958)

Chapter 3

Nonlinear Strong Ground Motion in the M_L

5.4 Chittenden Earthquake: Evidence that preexisting damage increases susceptibility to further damage

Abstract

We use 55 repeating earthquake sequences located near the 1989 Mw 6.9 Loma Prieta earthquake to identify time dependent velocity changes in the shallow crust. In addition to large delays caused by the Loma Prieta mainshock, the M_L 5.4 Chittenden earthquake, an aftershock of Loma Prieta, caused direct S wave delays of up to 6ms and S coda delays exceeding 15ms. We attribute the delays to cracks formed or opened during the strong shaking of the Chittenden earthquake, the same mechanism believed responsible for the delays observed following Loma Prieta. The magnitude of the delays caused by Chittenden strongly correlate with those caused by Loma Prieta. This suggests that rocks recently damaged by nonlinear strong ground motion are particularly

The material in this chapter has appeared in Rubinstein, J.L. and G.C. Beroza (2005), *Geophysical Research Letters*, **31**, L23614, doi:10.1029/2004GL021357.

susceptible to further damage until they are completely healed. Therefore, we expect that the onset of nonlinearity will occur at substantially lower ground motion for large aftershocks than would otherwise be anticipated.

3.1 Introduction

Previous studies have observed significant velocity reductions coincident with large ($M > 6$) earthquakes, including the Loma Prieta earthquake (Rubinstein and Beroza, 2004), the Morgan Hill earthquake (Schaff and Beroza, 2004), the Hector Mine earthquake (Li *et al.*, 2003), the Landers earthquake (Li *et al.*, 1998), and the Izmit and Duzce earthquakes (Peng and Ben-Zion, *in press*). For observations away from the fault (> 1 km), the velocity reductions are believed to be caused by strong shaking damaging rocks (nonlinear strong ground motion) (Rubinstein and Beroza, 2004; Schaff and Beroza, 2004; Vidale and Li, 2003). This mechanism requires particularly strong shaking (large earthquakes) to produce significant velocity changes. There is some evidence that medium magnitude earthquakes can also cause velocity reductions, albeit small ones; Rubin (2002) documented S delays of 2ms and P delays of 1ms at a station 10km away from a M4.7 earthquake.

In this study, we examine velocity reductions caused by another medium magnitude earthquake, the ML 5.4 Chittenden earthquake, the largest aftershock of the Mw 6.9 Loma Prieta Earthquake. The delays associated with it are much larger than those observed by Rubin (2002) in both magnitude (S delays > 5 ms) and spatial extent (S delays > 2 ms at distances exceeding 40km), despite the fact that the earthquakes are similar in size. To explain this difference, we propose a model whereby the preexisting damage from the Loma Prieta earthquake made these sites more vulnerable to further damage by the Chittenden earthquake.

3.2 Data and Methods

The data and techniques used in this paper are the same as those used in Rubinstein and Beroza (2004), where a complete description of the data and methodology can be found. Below is a summary of our data and methods.

We study 55 repeating earthquake sequences (multiplets) on the San Andreas Fault just south of the rupture zone of the 1989 Loma Prieta earthquake to identify time varying seismic velocity changes (Figure 3.1). Cross-correlation measurements reveal that events within multiplets are all located within meters of each other. These events were recorded by the Northern California Seismic Network (NCSN) and archived at the Northern California Earthquake Data Center (NCEDC). The NCSN is a network of high gain, short period seismometers that record at 100 samples per second. The events span from 1984 through the end of 1999. The aftershock sequences of Loma Prieta and Chittenden brought a sudden increase in the rate of repeating events (Schaff *et al.*, 1998), improving the temporal resolution at which we can observe the velocity changes.

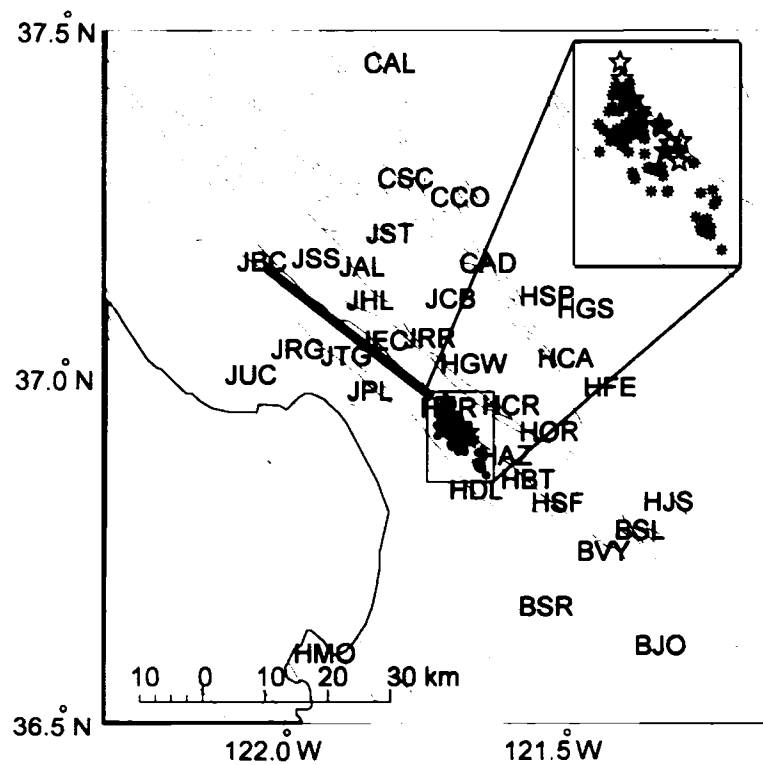


Figure 3.1: Map of the study region showing: NCSN stations used in this study, vertical projection of the upper limit of the Loma Prieta rupture (thick solid line) (planar model from Marshall *et al.* [1991]), epicenters of 55 multiplets (asterisks), events in the Chittenden earthquake sequence (unfilled stars), the ML 5.4 Chittenden earthquake (filled star), mapped faults (thin, grey lines).

The Chittenden earthquake sequence occurred April 18-19, 1990, approximately six months after the Loma Prieta earthquake (October 17, 1989) and was a period of increased seismic activity during which thirteen $M > 3$ earthquakes occurred in a small region just to the southeast of the rupture zone of the Loma Prieta earthquake. This swarm had a series of twelve $M > 3$ earthquakes within 4 hours on April 18 that was comprised of seven $M > 4$ earthquakes and two $M > 5$ earthquakes. The thirteenth $M > 3$ earthquake occurred approximately 24 hours after the first $M > 3$ earthquake. The largest earthquake in this sequence was ML 5.4, which we refer to as the Chittenden earthquake.

We use a moving window cross correlation technique to identify temporal changes in wavespeed manifest as late/early arriving phases in a repeating earthquake sequence (Figure 3.2a, 3.2b). We only examine vertical components and clipped data are removed. The correlation uses 128 sample windows that are weighted by a Hanning function and are shifted at 5 sample increments. Prior to the cross-correlation, all the traces for each multiplet at each station are aligned to the manually picked P arrival of the reference event for that multiplet-station pair. As a result, the delay that we compute is the difference between the S (or other phase) minus P times of the reference and data events.

Although delays are largest in the S coda (Figure 3.2c-e), we examine the delays of the direct S wave because it is more consistent from multiplet to multiplet than the early S coda. The delays we measure can be treated as differences between two points on a time varying station correction function (of S delays), hereafter referred to as the S delay function. We estimate the function at each station using the S delays computed from the cross-correlation measurements as the data (Figure 3.3). This function is discretized irregularly in time, with more samples following both the Loma Prieta and Chittenden earthquakes. The reasoning for this is twofold: there is more data (higher seismicity rate for the repeating earthquakes) immediately following these two earthquakes and the change in the S delay function is largest in these time spans as well. Using the S delay function, we compute the delays caused by the Chittenden and Loma Prieta earthquakes for each station. The coseismic delay is the difference between the value of the S delay function of the days before and after the earthquake.

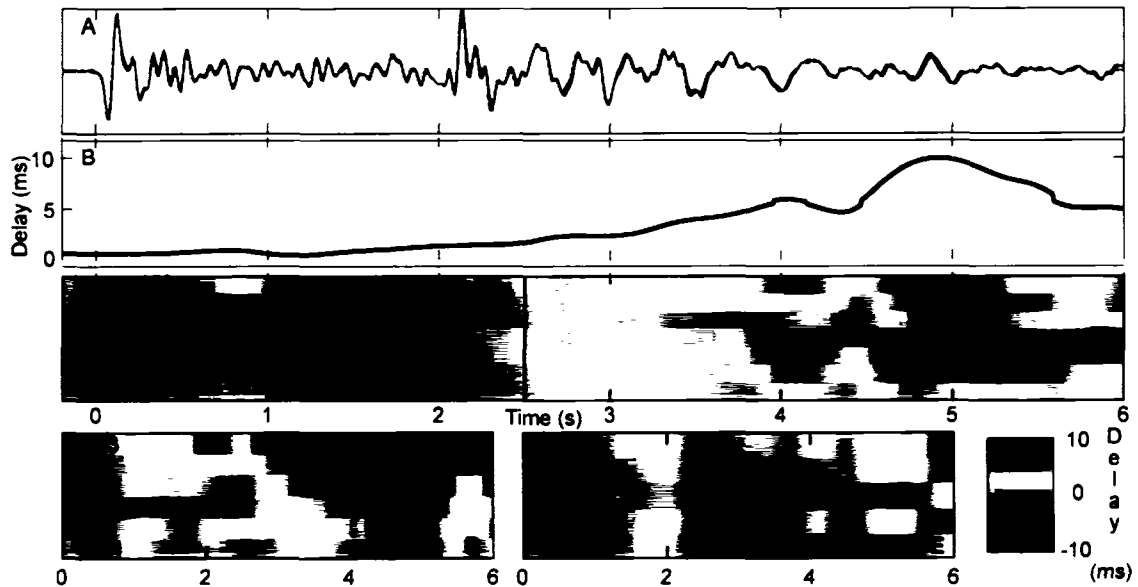


Figure 3.2: (a) Seismograms from events 3 (black) and 4 (red) in repeating earthquake sequence 27, recorded by HGW. Event 4 was one day after the Chittenden earthquake. Event 3 was 8 days before the Chittenden earthquake. The seismograms are aligned on the *P* arrival and plotted on the same time axis, where time is seconds after the *P* arrival. Note the separation between the two traces with time into the trace. (b) Relative delay between event numbers 3 and 4 for multiplet 27 at HGW. The largest delays are in the *S* coda. (c) Relative delays for all of repeating sequence 27 recorded at HGW. Each horizontal line represents a seismogram, with calendar time increasing down the y-axis. Shading represents the delay of the seismogram represented by the horizontal stripe relative to the reference seismogram. Warmer shades represent larger delays. The column of numbers at time=0.2s indicate the number of days after the Chittenden earthquake that the event occurred (negative numbers indicate number of days before it, Loma Prieta was 182 days before Chittenden). Note the first two events are soon after Loma Prieta and have large delays that decrease with time. The fourth event is just after Chittenden and shows a sudden increase in delays, which slowly decreases back towards zero. The dashed vertical line is a theoretical *S* arrival time pick, the solid vertical lines represent the bounds of the *S* wave window used to compute the *S* delay. (d) Multiplet 21 at JRR. (e) Multiplet 53 at HPR.

3.3 Results

3.3.1 Observations

Immediately following the Chittenden earthquakes, we observe a sudden increase in delays varying in strength throughout the seismogram at many stations (Figure 3.2). The delays are largest in the *S* coda, with changes in delays coincident with Chittenden exceeding 15ms (e.g. JEC). The delays for other phases are still significant, including the *S* arrival where delays can exceed 5ms (e.g. JTG). Following the Chittenden earthquake sequence, the delays decrease with calendar time (Figure 3.2c-e, 3.3, 3.4). The healing of these delays is log-linear with time, the most rapid healing occurring immediately after

the earthquake and healing slowing with increasing time after the earthquake (Figure 3.3, 3.4). Although the behavior of the delays is consistent from station to station (sudden increase following the Chittenden earthquake sequence, delays being largest in the *S* coda, and a log-linear decay of delays following the earthquake sequence), the strength of the delays varies significantly (Figure 3.5). This behavior parallels the behavior of delays caused by the Loma Prieta earthquake as observed by the same stations for the same repeating earthquake sequences (Rubinstein and Beroza, 2004). The similar time dependent behavior of the delays (both from event to event and within the individual seismograms) leads us to appeal to the same mechanism for both earthquakes, the growth and/or opening of cracks caused by the strong shaking of an earthquake.

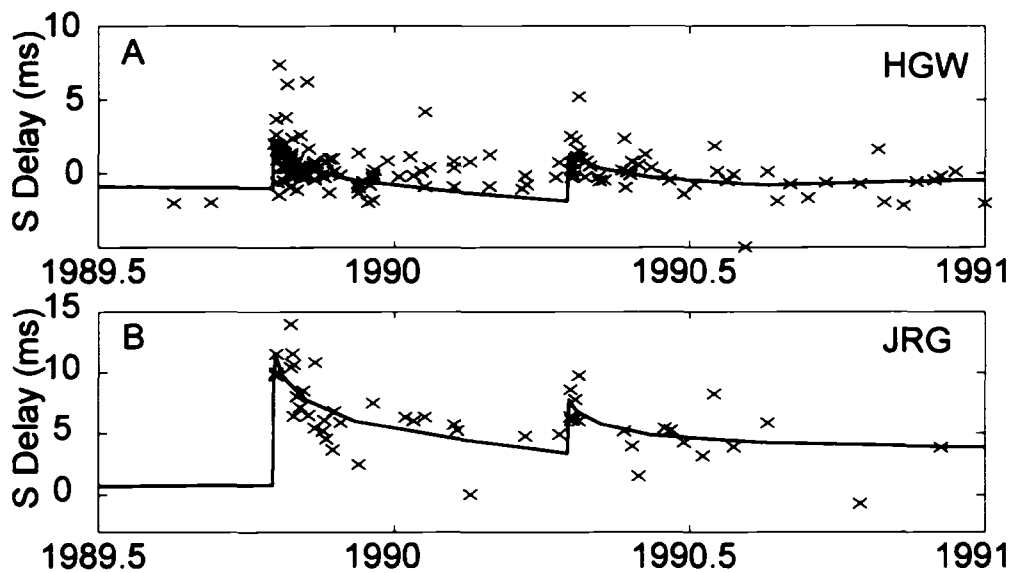


Figure 3.3: Raw *S*-delay values plotted versus time for all multiplets recorded by HGW (a) and JRG (b). The *S* delay function for each station is overlain. To fit the delay measurements to the predictions of the *S* delay function, the *S* delay predicted for the reference event of each multiplet is added to delay values. This fits the data to the model because the delay value at the reference event is treated as zero in the delay calculation.

3.3.2 Factors that Influence the Magnitude of Delays

There is a weak dependence of the strength of the delays caused by the Chittenden earthquake on the distance to the Chittenden earthquake (Figure 3.5a); the stations with

the largest delays tend to be closer to the Chittenden earthquake than those with smaller changes in delay. For example, station HPR is the closest station to the Chittenden earthquake. The change in *S* delays caused by the Chittenden earthquake at HPR is one of the largest we observe, exceeding 4ms. The correlation between the magnitude of Chittenden induced delays and distance to the Chittenden earthquake swarm, further supports our argument that nonlinearity in the strong shaking of the Chittenden earthquake caused the velocity reductions, because shaking should be strongest near the earthquake source. Unfortunately, strong motion “ShakeMaps” are unavailable for any of the members of the Chittenden earthquake sequence, so we cannot compare the strong shaking to the strength of observed delays. As a result, we are only left with distance to the earthquake as a measure of strong shaking.

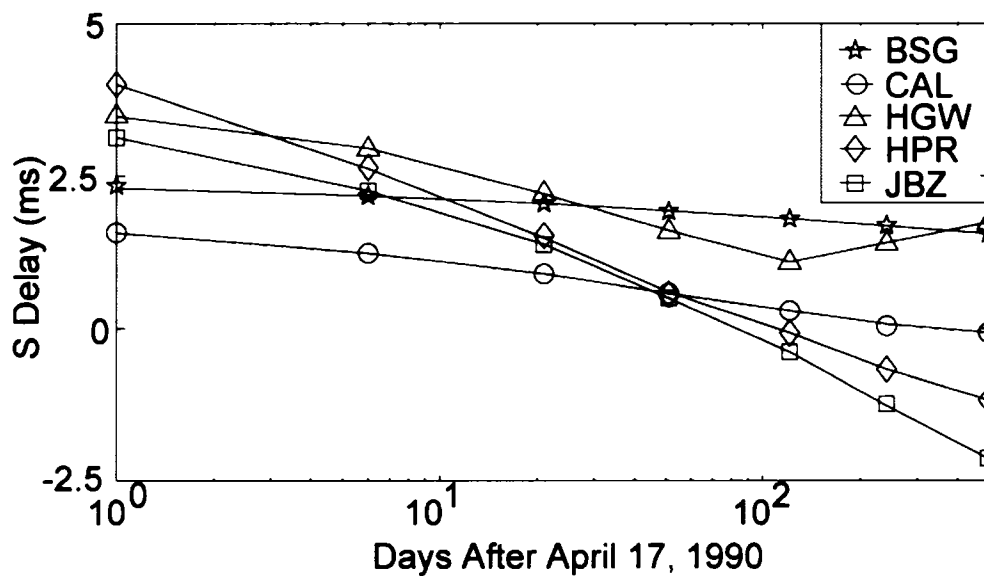


Figure 3.4: *S* delay function for stations BSG, CAL, HGW, HPR, and JBZ plotted against the logarithm of the number of days after April 17, 1990, the day before the Chittenden Earthquake.

We find that the magnitude of the delays imparted by the Chittenden earthquake depends strongly on the magnitude of the delays caused by the Loma Prieta earthquake (Figure 3.5b). As the magnitude of the *S* delay caused by the Loma Prieta earthquake increases, the *S* delay caused by Chittenden increases as well. This suggests that rocks

damaged by the Loma Prieta earthquake were more susceptible to further damage by strong ground motion in later quakes than those left undamaged by the Loma Prieta earthquake. To generalize, until a rock has completely healed from damage, it is in a weakened state and is more susceptible to further damage than it would be in an undamaged state. A similar phenomenon has been observed by *Vidale and Li (2003)* who observe increased delays in fault zone trapped waves on the not yet completely healed Johnson Valley Fault (damaged not by strong motion, but by the rupture of the 1992 Landers earthquake) caused by the 1999 Hector Mine earthquake, which occurred 7 years later and approximately 20-30km away.

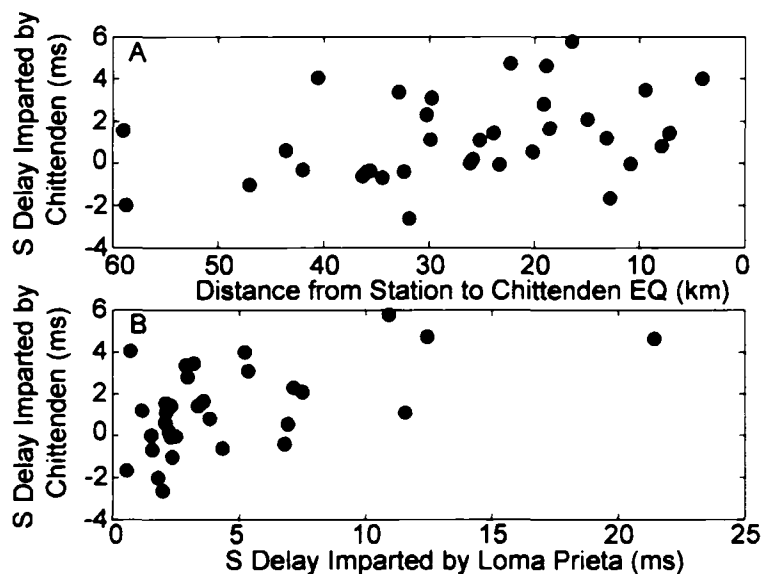


Figure 3.5: (a) S-delay caused by Chittenden plotted versus distance of station to the Chittenden earthquake. (b) S-delay caused by Chittenden plotted versus S-delay caused by Loma Prieta.

We believe that the weakened state of the shallow crust after the Loma Prieta earthquake allowed the Chittenden earthquake, a medium magnitude earthquake, to cause significantly more damage than it would have were it not soon after the Loma Prieta earthquake. To test this claim in detail would require a M5 earthquake that is isolated in time from larger earthquakes that has at least one repeat of a repeating earthquake sequence soon before and after it. We do not have data that meet these criteria.

It is also possible that the sites at which we observe damage induced by the Chittenden earthquake are simply those that are the most susceptible to damage by strong shaking. We discount this mechanism, as it would predict that the delays caused by Chittenden should be approximately proportional to the strong shaking the sites experienced in Chittenden, as we observe for Loma Prieta. Our observations do not support this. At the stations with the largest delays caused by Chittenden, we find that the Chittenden induced delays are on the order of 20-50% of the delays induced by Loma Prieta. Without strong ground motion parameterization it is impossible to be certain, but it is very likely that the strong shaking at these same sites in Chittenden was significantly less than 20% of that in Loma Prieta. This implies that the strong shaking of Chittenden, alone, would not be enough to cause the magnitude of delays we observe, even at the weakest sites.

3.3.3 Limitations and Outliers

We believe that the velocity reductions we observe were caused by the Chittenden earthquake because it was the largest earthquake in the Chittenden earthquake sequence. We are unable to be certain whether the damage was caused solely by the ML 5.4 Chittenden earthquake or if the accumulated effects of a number of events in the Chittenden sequence caused the delays. This cannot be tested because we have no repeats that occur in between events in the Chittenden sequence. Previous findings that show that the strength of shaking is the controlling factor in the strength of nonlinearity (Rubinstein and Beroza, 2004; Guyer *et al.*, 1998; Ostrovsky *et al.*, 2000) suggest that the majority of the damage was likely caused the ML 5.4 Chittenden earthquake.

For several stations the model indicates that there are negative delays coincident with the Chittenden earthquake, i.e. that the *S* wave is actually arriving faster immediately following Chittenden than it does prior to Chittenden (Figure 3.5). This would be in contrast to our findings for Loma Prieta and might suggest another mechanism; however, this effect is very small (< 2ms advance) at all but one of these stations. An exhaustive examination of individual delay measurements at these stations does not show a sudden decrease in *S* arrival time for these stations coincident with the

Chittenden earthquake. Instead, we find that these stations do not respond to the Chittenden earthquake, in that there is not a detectable increase or decrease in arrival times of any phase (not just the direct *S*) at these stations. The advance in arrival time that the *S* delay function shows is the continuing response to Loma Prieta (which at this point in time would be a healing of the delays caused by Loma Prieta—a decrease in delays). Our analysis allows this because in computing the *S* delay function we do not apply smoothing across the Chittenden earthquake.

There are two stations, BPR and BSR that show a decrease in *S* arrival times coincident with the Chittenden earthquake. Because the stations are both very far away (>30km) from the Chittenden earthquake, we suspect some process unrelated to the earthquake is affecting the near surface velocity at these stations.

3.4 Summary

We have used repeating earthquake sequences to identify *S* arrivals that are consistently late immediately following the Chittenden earthquake sequence. This behavior has been previously observed at the same stations for the Loma Prieta earthquake as well. The similarity of the delays caused by the Chittenden earthquake and the delays caused by the Loma Prieta earthquake suggests that they are caused by the same process: the growth and opening of cracks caused by the strong shaking of the earthquake exceeding the strength of the local rocks near the surface (nonlinear strong ground motion). We are unable to differentiate whether the largest earthquake in the Chittenden earthquake sequence, ML 5.4, is responsible for the observed change in delays or if the cumulative effect of some/all of the medium magnitude events in the sequence (five M4.0-4.9 events and two M5.0-5.4 events) that caused the velocity reductions. Because the shaking was strongest in the largest event, we believe that most, if not all, of the damage was caused by the ML 5.4 Chittenden earthquake. Either way, the magnitude of and the spatial extent to which we observe the delays caused by Chittenden exceed what we would expect had the Chittenden earthquake sequence not occurred in the aftermath of the larger, Loma Prieta earthquake. We believe that the weakened condition of rocks that Loma Prieta left facilitated and significantly increased the damage that the Chittenden earthquake sequence was able to cause. The correlation

between the strength of delays caused by the Loma Prieta earthquake and the delays caused by the Chittenden earthquakes supports this argument. From this, we infer that earth materials recently damaged by nonlinear strong ground motion are more susceptible to subsequent nonlinearity in strong shaking than they are in an undamaged state.

Acknowledgements

The authors would like to thank Götz Bokelmann for many insightful discussions. We thank David Schaff for providing the repeating earthquake sequences used in this study and for offering many useful suggestions. This manuscript was improved by the suggestions of Y.G. Li, A. Zollo, and an anonymous reviewer. All data used in this study were made available through the NCEDEC. The data was provided by the NCSN, via the U.S. Geological Survey, Menlo Park. J.R. was supported in part by the Wells Family Stanford Graduate Fellowship. This work was supported by USGS grants 02HQGR0039 and 03HQGR0073.

References

- Guyer, R. A., K. R. McCall, and K. Van Den Abeele (1998). Slow elastic dynamics in a resonant bar of rock, *Geophys. Res. Lett.*, **25**, 1585-1588.
- Li, Y.G., J.E. Vidale, K. Aki, F. Xu, and T. Burdette (1998), Evidence of shallow fault zone strengthening after the 1992 M7.5 Landers, California, Earthquake, *Science*, **279**, 217-219.
- Li, Y.G., J.E. Vidale, S.M. Day, D.D. Oglesby, and E. Cochran (2003), Postseismic healing on the rupture zone of the 1999 M7.1 Hector Mine, California, Earthquake, *Bull. Seism. Soc. Am.*, **93**, 854-869.
- Marshall, G.A., R.S. Stein, and W. Thatcher (1991), Faulting geometry and slip from co-seismic elevation changes: the 18 October 1989, Loma Prieta, California, earthquake, *Bull. Seism. Soc. Am.* **81**, 1660-1693.
- Ostrovsky, L. A., P. A. Johnson, and T. J. Shankland (2000). The mechanism of strong nonlinear elasticity in earth solids, in *Nonlinear Acoustics at the Turn of the Millenium: ISNA 15*, edited by W. Lauterborn and T. Kurz, pp. 75-84, American Institute of Physics.
- Peng, Z. and Y. Ben-Zion (in press). Temporal Changes of Shallow Seismic Velocity around the Karadere-Duzce Branch of the North Anatolian Fault and Strong Ground Motion, *PAGEOPH*.
- Rubin, A.M. (2002), Using repeating earthquakes to correct high-precision earthquake catalogs for time-dependent station delays, *Bull. Seism. Soc. Am.*, **92**, 1647-1659.
- Rubinstein, J.L. and G.C. Beroza, (2004), Evidence for Widespread Nonlinear Strong Ground Motion in the M_w 6.9 Loma Prieta Earthquake, *Bull. Seism. Soc. Am.*, **94**, 1595-1608.
- Schaff, D. P., G. C. Beroza, and B. E. Shaw (1998), Postseismic response of repeating aftershocks, *Geophys. Res. Lett.*, **25**, 4549-4552.
- Schaff, D.P. and G.C. Beroza (2004), Coseismic and postseismic velocity changes measured by repeating earthquakes, *J. Geophys. Res.*, **109**, B10302, doi:10.129/2004JB003011.
- Vidale, J.E. and Y.G. Li (2003), Damage to the shallow Landers fault from the nearby Hector Mine earthquake, *Nature*, **421**, 524-526.

Chapter 4

Depth Constraints on Nonlinear Strong Ground Motion from the 2004 Parkfield Earthquake

Abstract

We use the two target repeating earthquake sequences of SAFOD to identify time varying properties of the shallow crust in the Parkfield area at the surface and in shallow boreholes. At the surface, we find that the 2004 Parkfield earthquake caused direct S wave delays exceeding 7ms, and S coda delays exceeding 15ms. We attribute these delays to cracks formed or opened during the strong shaking of the Parkfield earthquake. Observations at depth show that the direct S wave arrival time was much less affected by the Parkfield earthquake. This provides evidence that damage caused by strong shaking (nonlinear strong ground motion), is limited to the very near surface (<100m).

The material in this chapter has appeared in Rubinstein, J.L. and G.C. Beroza (2005). *Geophysical Research Letters*, **94**, L14313, doi:10.1029/2005GL023189.

4.1 Introduction

A number of studies have identified nonlinear site response to strong ground motion (e.g., Field *et al.*, 1997; Frankel *et al.*, 2002; Wen *et al.*, 1994); typically using spectral ratios. Spectral ratios highlight the differences in the frequency response of a site with respect to other sites (to identify linear site response) or with respect to itself (to identify nonlinear site response). Rock sites are typically used as reference sites in spectral ratios, under the assumption that they don't have a significant site response. This assumption has been challenged by Steidl *et al.*, (1996), who showed that surface rock sites can have a significant site response. To avoid this possible bias, some studies use borehole seismometers as reference sites (e.g., Huang *et al.*, 2005; Wen *et al.*, 1994). Laboratory and theoretical studies have shown that susceptibility to nonlinear wave propagation decreases with increasing compressive stress (increasing depth) (Ostrovsky *et al.*, 2000; Zinszner *et al.*, 1997), implying that borehole sites are reasonable reference sites for studying nonlinear strong ground motion; however, there is scant corroborative evidence from field observations.

In this study, we use an alternative technique to identify the effects of nonlinear strong ground motion with the aim of testing whether strong ground motion is linear at shallow borehole depths (75-350m). We use repeating earthquakes (multiplets) to observe subtle, widespread changes in seismic velocity immediately following the 2004 Parkfield earthquake. Widespread coseismic velocity reductions have been shown to be indicative of damage induced by strong shaking of a number of earthquakes (Rubinstein and Beroza, 2004a,b; Schaff and Beroza, 2004; Peng and Ben-Zion, in press). This technique provides a direct measurement of the effects of nonlinear wave propagation, and therefore allows us to determine if wave propagation is linear at shallow depths.

Other studies have looked for changes in wave-propagation in the Parkfield region, with mixed results. For this same earthquake, a significant decrease and recovery of seismic velocities within the fault zone has been observed using fault zone trapped waves (Y.G. Li, pers. comm., 2005). Others have looked for changes in wave propagation in Parkfield during periods of seismic quiescence (no M6 earthquakes). Karageorgi *et al.*, (1992, 1997) found small changes in seismic velocity corresponding to

changes in fluid levels, fault creep, and variations in microseismicity. *Nadeau et al.* (1994) found no significant variation in seismic velocities using repeating earthquakes. *Niu et al.* (2003) identified the movement of scatters associated with an aseismic transient.

4.2 Data

We study two repeating microearthquake sequences that are the “target events” of the San Andreas Fault Observatory at Depth (SAFOD) to monitor the time dependence of seismic velocity in the Parkfield region (Figure 4.1). Cross-correlation measurements reveal that the member events of both repeating earthquake sequences are located within meters of each other. The two repeating earthquake sequences are separated by approximately 60-70m along the San Andreas Fault (*Nadeau et al.*, 2004). Both events repeated approximately one year prior to the Parkfield earthquake, on October 21st and 22nd 2003. Since the Parkfield earthquake, one has repeated twice, the other three times: they both repeated on September 28, 2004 (two days after the mainshock) and one sequence repeated October 24, 2004 and January 23, 2005, while the other repeated December 8, 2004. We examine these events using two seismic networks: the Northern California Seismic Network (NCSN), a network of high gain, short period, surface seismometers that record at 100 samples per second and the High Resolution Seismic Network (HRSN), a network of short period, shallow borehole seismometers (~70-350m depth) that record at 250 samples per second.

4.3 Method

We use a moving window cross-correlation technique to measure the relative arrival time of seismic phases of one event relative to a reference event in the same repeating earthquake sequence (Figure 4.2). The late/early arrivals indicate temporal changes in seismic velocity at the near surface. We examine unclipped, 1.28 second, Hanning tapered windows of zero-phase filtered vertical component seismograms. All the seismograms for each repeating earthquake sequence at each station are initially aligned to subsample precision to the manually picked *P* arrival of the reference event for that multiplet-station pair. As a result, the delays computed by the moving window cross

correlation reflect the change in the S (or other phase) minus P times from the reference event to the data events.

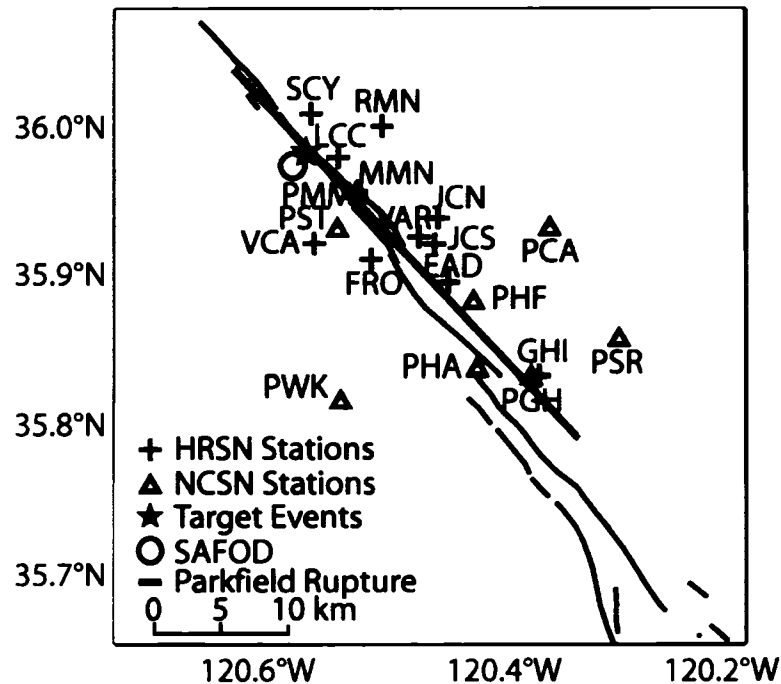


Figure 4.1: Map of the study region.

Although we find that delays are largest in the S coda (Figure 4.2b, 4.3), we choose to examine the delays of the direct S arrival. This provides a measure of the change in seismic velocity near the station that is relatively insensitive to scattering, unlike coda measurements. The arrival time of the direct S is determined under the assumption of a Poisson solid, given a precise computation of the P travel time that uses a manual P pick and precise origin times of the reference event determined by relative relocation (Waldhauser *et al.*, 2004). For each event-station pair, we compute the delay in the arrival of the S wave, relative to its reference event from October 2003. The delay of the S wave is computed as the median of the delay for windows centered on a time period spanning 0.1s before and 0.45 seconds after the theoretical S arrival time. To ensure data quality, we enforce a minimum correlation coefficient of 0.8 for both the P and S arrivals and a minimum signal to noise ratio of 4:1 at the P arrival.

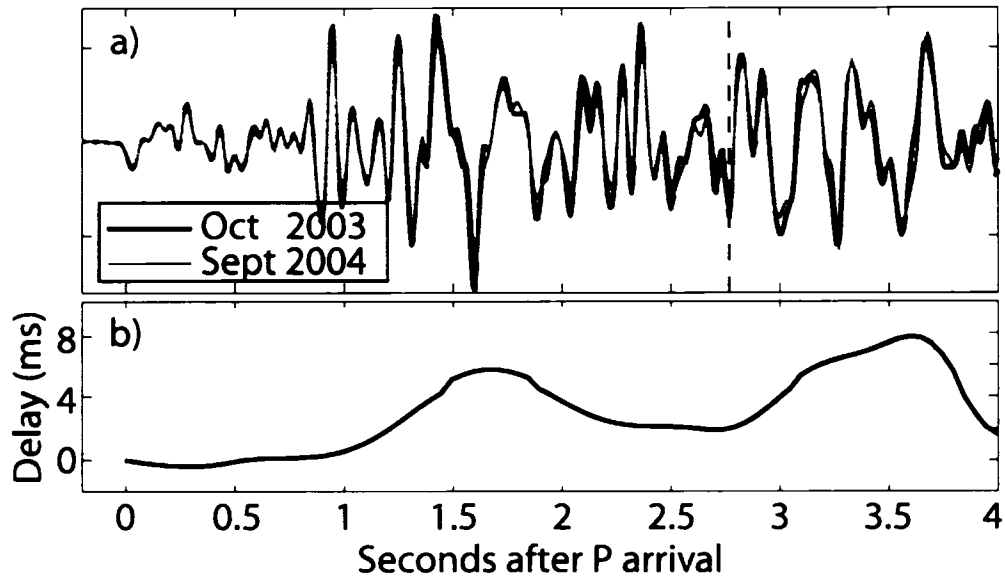


Figure 4.2: Repeating earthquake sequence 2, as recorded by NCSN station PHF. Vertical, dashed line indicates *S* Arrival. (b) Delay of September 2004 repeat of earthquake sequence 2 at PHF relative to October 2003 repeat.

We treat the *S* delays observed for the repeats immediately following the Parkfield earthquake as the coseismic change in delays. In doing this, we make the assumption that between October 2003 and the 2004 Parkfield earthquake there was no significant change in seismic velocities. Processes associated with aseismic transients have been shown to influence wave propagation (Niu *et al.*, 2003), however, no such transients were observed in this area between October 2003 and September 2004 (J.R. Murray, pers. comm., 2005). In this time period, the 2003 San Simeon earthquake also occurred nearby, so its influence must be considered. Unfortunately, we don't have the temporal resolution to measure any effect of the San Simeon earthquake, which implies that our "coseismic" measurements could be overprinted by a postseismic effect following San Simeon. However, the strong shaking of the San Simeon earthquake was much weaker than the shaking of the Parkfield earthquake at our sites, so we expect that its effect on seismic velocity will be significantly weaker. Furthermore, a number of studies have previously shown that earthquake induced seismic velocity changes heal logarithmically with time (Rubinstein and Beroza, 2004a,b; Schaff and Beroza, 2004). This indicates that any effect that the San Simeon earthquake had on local seismic

velocities would be mostly healed by the time the Parkfield earthquake occurred. For these reasons, we believe that the change in seismic velocities that we observe will be related to the Parkfield earthquake. In fact, the delays we observe should be considered a lower bound on the delays caused by the Parkfield earthquake as healing will have progressed for the first two days after the mainshock, for which we have no observations.

4.4 Observations

4.4.1 Surface Stations

At many of the NCSN stations, we find significant delays caused by the Parkfield earthquake. The delays vary in strength throughout the seismogram (Figure 4.2, 4.3a). The largest delays are in the *S* coda, exceeding 25ms at PMM. Delays of the direct *S* arrival can exceed 7ms (e.g., PMM). In the second repeat of both repeating earthquake sequences after the Parkfield earthquake, we find the delays have decreased significantly throughout the seismogram (Figure 4.3a). This implies that the local damage is healing with time.

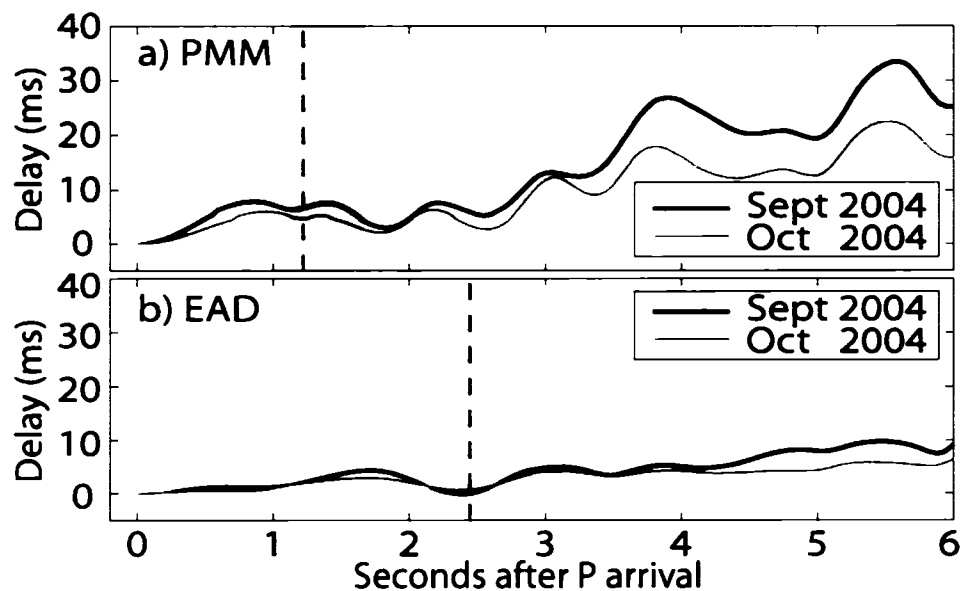


Figure 4.3: Delay of September and October 2004 repeats of repeating earthquake sequence 1, relative to October 2003 repeat at NCSN station PMM and HRSN station EAD. Vertical dashed lines represent *S* arrivals. Shaded area marks window over which median *S* delay is computed..

4.4.2 Borehole Stations

Our observations at the HRSN stations are significantly different than those for the surface seismometers (NCSN). Typically, there is little or no delay (<2 ms) in the S arrival following the Parkfield earthquake (Figure 4.3b, 4.4). Similar to the NCSN stations, at many of the HRSN stations we observe delays in the P and S codas that increase with time into the coda (Figure 4.3b). For those borehole stations that observe delays in the P and S codas, we find that the coda delays show healing between the first and second repeats (Figure 4.3b).

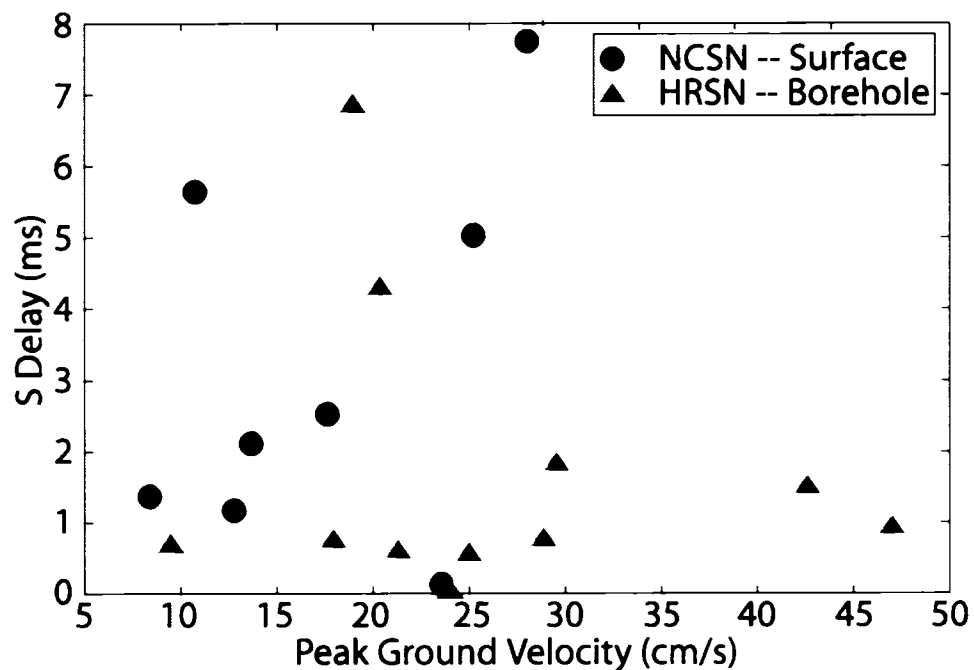


Figure 4.4: Coseismic S delay of each station plotted against peak ground velocity experienced in the 2004 Parkfield earthquake. The S delay is the mean of the measurements computed for the September 2004 repeats of both multiplets relative to their October 2003 repeats.

4.5 Discussion

The different behaviors of the delays observed at NCSN (surface) stations and HRSN (borehole) stations, suggests that the upper 100m of the Earth's crust responds differently to strong ground motion than do deeper materials. The relation between strong ground shaking and S delays for the two networks accentuate this point, as we see

a clear scaling between strong ground motion and S delays for the surface stations and no scaling of S delays to strong ground motion for the borehole stations (Figure 4.4). We don't observe a scaling of S delays to strong ground shaking at depth because the borehole records are from far below the shallow layers damaged by the Parkfield earthquake.

4.5.1 Physical Model and Interpretation

To explain the delays observed at the NCSN stations, we appeal to a model in which the strong shaking of the Parkfield earthquake caused cracks to grow and/or open near the surface, effectively damaging the medium (nonlinear wave propagation). We have observed similar phenomena for the Loma Prieta, Chittenden, and Morgan Hill earthquakes (Rubinstein and Beroza, 2004a,b; Schaff and Beroza, 2004). The behavior of the delays induced by the Parkfield earthquake parallel the delays induced by the Loma Prieta and Morgan Hill earthquakes: S delays scale with strong ground shaking, decrease with time following the mainshock, and are largest in the coda.

Unlike the surface stations, we find that the S arrival is not delayed at the HRSN borehole stations. Because the S-P time stays consistent before and after the Parkfield earthquake, we believe that there are no velocity reductions local to the HRSN borehole stations. This implies that the strong shaking of the Parkfield earthquake is not causing damage below depths of $\sim 100\text{m}$. What delays are present in the S and P codas, we attribute to scattered energy that is coming from nearer the surface where nonlinear strong ground motion has reduced seismic velocities. This suggests that even the minimal amount of pressure that rocks are under in the shallow boreholes of the HRSN is enough to prevent damage during strong ground motion.

Li et al. (1998, 2003) also appeal to earthquake induced cracking to explain velocity reductions following the Landers and Hector Mine earthquakes. Their observations are made much closer to the fault than ours ($< 500\text{m}$). With this data, they see significant velocity changes extending much deeper than we do (3km for Landers and 5km for Hector Mine, Y.G. Li, pers. comm.). This difference can be explained by either 1) the presence of a different damage mechanism in the fault zone (e.g., shearing induced

damage) or 2) differing conditions (e.g., high fluid pressures within the fault zone increasing the susceptibility to damage, or stronger shaking resulting in deeper damage).

Some suggest that damage caused by the passage of seismic waves, the same phenomenon that we study here, is responsible for triggering of earthquakes at large distances (Gomberg and Johnson, 2005; Johnson and Xia, 2005). We find that strong shaking does not damage earth materials detectably, even at modest depths (100-300m), suggesting that for this triggering model to work, pore fluid pressures would have to be nearly lithostatic, such that the effective stresses were comparable to those at 100m depth. A related observation was made on the Landers fault, which was shown to be damaged by the strong shaking of the nearby Hector Mine earthquake (Vidale and Li, 2003). This suggests that the high fluid pressures needed for this triggering mechanism are plausible.

4.5.2 Outliers?

In general, the borehole stations do not have a significant response to the Parkfield earthquake, with the exception of VCA and RMN that have coseismic *S* delays of 4.3 and 6.9ms respectively (Figure 4.4). Because these sites do not experience particularly strong ground shaking, relative to the other HRSN stations, it may be that fluid pressures at these sites were particularly high. Raising fluid pressures would increase susceptibility to strong ground motion induced damage, allowing for the large coseismic *S* delays we observed. RMN is also the shallowest of the HRSN stations (73m), which might contribute to a greater susceptibility to damage due to a lower overburden. The coupling at RMN is also known to be somewhat poor (R. Nadeau, pers. comm.), which could provide an alternative explanation to the anomalously high delays observed there.

For the surface stations, we observe a trend of increasing *S* delays with increasing strong motion. PCA and PST lie significantly above and below the trend, respectively (Figure 4.4). We have previously appealed to variations in rock strength to explain scatter in the correlation between strong shaking and velocity reductions (Rubinstein and Beroza, 2004a). This does not explain the observations at PCA and PST as their site

geologies are not significantly weaker or stronger than the average site. These variations must then come from our incomplete understanding of subsurface geology or from other limitations in our analysis. A likely source of these variations is our parameterization of strong ground motion. Our strong ground motion parameters for each site are spatially interpolated from ShakeMap. ShakeMap is a routinely produced map of strong motion parameters for earthquakes M3.5 and larger (method described in Boatwright *et al.*, 2003). The interpolation immediately introduces uncertainty into our measurement. The accuracy of ShakeMap's measurements is limited by the number and proximity of strong motion observations used in its computation. Specifically for PCA, there are not many nearby strong ground motion stations. ShakeMap also cannot account for localized effects (e.g., topographic effects, resonances, etc.) that may cause increased or decreased strong shaking. Although we have shown previously that strength of shaking correlates well with coseismic velocity reductions, factors other than the peak ground motion (e.g., duration of strong shaking) may control the ultimate amount of near-surface damage caused by an earthquake.

4.6 Conclusions

We have used repeating earthquakes near Parkfield to identify near surface reductions in seismic velocity. Specifically, we identify delays in S arrival times at surface stations, and the general absence of delays at shallow borehole seismometers (depths ~100-300m). Previous studies have shown that strong shaking of earthquakes damaging rocks can cause delays in S arrival times. The depth dependence of the S delays therefore implies that the pressure at the depth of shallow boreholes prevents strong shaking from damaging rocks at depth. This allows us to conclude that nonlinear wave propagation and the damage that it induces is limited to the very near surface or to regions of particularly high pore fluid pressure.

Acknowledgements

We are grateful to F. Waldhauser and R. Nadeau for providing the catalog information for the repeating earthquake sequences used in this study. We thank D. Oppenheimer, H. Macbeth, and D. Neuhauser for their assistance and expedience in providing access to data. M. Thayer kindly provided the preliminary results of his mapping of the Parkfield area. This paper was improved by the suggestions of J. Vidale, Z. Peng, A. Zollo, and an anonymous reviewer. Conversations with P. Johnson and J. Gomberg improved this work. All data used in this study were made available through the NCEDEC. NCSN data was provided by the U.S. Geological Survey, Menlo Park. HRSN data was provided by the Berkeley Seismological Laboratory of UC Berkeley. Research supported by the U.S. Geological Survey (USGS), Department of the Interior, under USGS award number 05HQGR0007. The views and conclusions contained in this document are those of the authors and should not be interpreted as necessarily representing the official policies, either expressed or implied, of the U.S. Government.

References

- Boatwright, J., H. Bundock, J. Luetgert, L. Seekins, L. Gee, and P. Lombard (2003). The dependence of PGA and PGV on distance and magnitude inferred from Northern California ShakeMap data, *Bull. Seism. Soc. Am.* **93**, 2043–2055.
- Field, E.H., P.A. Johnson, I.A. Beresnev, and Y. Zeng (1997). Nonlinear ground-motion amplification by sediments during the 1994 Northridge earthquake, *Nature*, **390**, 599-602.
- Frankel, A.D., D.L. Carver, and R.A. Williams (2002). Nonlinear and linear site response and basin effects in Seattle for the M6.8 Nisqually, Washington, earthquake, *Bull. Seism. Soc. Am.*, **92**, 2090-2109.
- Gomberg, J. and P. Johnson (2005). Dynamic triggering of earthquakes, *Nature*, **437**, 830.
- Huang, H-C., S-W. Huang, and H-C. Chiu (2005). Observed evolution of linear and nonlinear effects at the Dahan Downhole Array, Taiwan: Analysis of the September 21, 1999 M7.3 Chi-Chi earthquake sequence, *PAGEOPH*, **162**, 1-20.
- Johnson, P.A. and X. Jia (2005). Nonlinear dynamics, granular media and dynamic earthquake triggering, *Nature*, **437**, 871-874.
- Karageorgi, E., R. Clymer, and T.V. McEvelly (1992). Seismological Studies at Parkfield II. Search for temporal variations in wave propagation using vibroseis, *Bull. Seism. Soc. Am.*, **82**, 1388-1415.
- Karageorgi, E., T.V. McEvelly, and R. Clymer (1997). Seismological Studies at Parkfield IV: Variations in controlled-source waveform parameters and their correlation with seismicity, 1987 to 1995, *Bull. Seism. Soc. Am.*, **87**, 39-49.
- Li, Y.G., J.E. Vidale, K. Aki, F. Xu, and T. Burdette (1998). Evidence of Shallow Fault Zone Strengthening After the 1992 M7.5 Landers, California, Earthquake. *Science*, **279**, 217-219.
- Li, Y. G., J. E. Vidale, S. M. Day, D. D. Oglesby, E. Cochran (2003). Postseismic fault healing on the rupture zone of the 1999 M7.1 Hector Mine, California, Earthquake, *Bull. Seism. Soc. Am.* **93**, 854-869.

- Nadeau, R., M. Anatolik, P.A. Johnson, W. Foxall, and T.V. McEvilly (1994). Seismological studies at Parkfield III: Microearthquake clusters in the study of fault-zone dynamic, *Bull. Seism. Soc. Am.*, **84**, 174-263.
- Nadeau, R.M., A. Michelini, R.A. Uhrhammer, D. Dolenc, and T.V. McEvilly (2004). Detailed kinematics, structure, and recurrence of micro-seismicity in the SAFOD target region, *Geophys. Res. Lett.*, **31**, L12S08, doi:10.1029/2003GL019409.
- Niu, F., P.G. Silver, R.M. Nadeau, and T.V. McEvilly (2003). Stress-Induced Migration of Seismic Scatterers Associated with the 1993 Parkfield Aseismic Transient Event, *Nature*, **426**, 544-548.
- Ostrovsky, L. A., P. A. Johnson, and T. J. Shankland (2000). The mechanism of strong nonlinear elasticity in earth solids, in *Nonlinear Acoustics at the Turn of the Millennium: ISNA 15*, edited by W. Lauterborn and T. Kurz, pp. 75-84, American Institute of Physics.
- Peng, Z. and Y. Ben-Zion (in press). Temporal Changes of Shallow Seismic Velocity around the Karadere-Duzce Branch of the North Anatolian Fault and Strong Ground Motion, *PAGEOPH*.
- Rubinstein, J.L. and G.C. Beroza (2004a). Evidence for widespread nonlinear strong ground motion in the Mw 6.9 Loma Prieta Earthquake, *Bull. Seism. Soc. Am.*, **94**, 1595-1608.
- Rubinstein, J.L. and G.C. Beroza (2004b). Nonlinear strong ground motion in the ML 5.4 Chittenden earthquake: Evidence that preexisting damage increases susceptibility to further damage, *Geophys. Res. Lett.*, **31**, L23614, doi: 10.1029/2004GL021357.
- Schaff, D.P. and G.C. Beroza (2004). Coseismic and postseismic velocity changes measured by repeating earthquakes, *J. Geophys. Res.*, **109**, B10302, doi: 10.1029/2004JB003011.
- Steidl, J.H., A.G. Tumarkin, R.J. Archuleta (1996). What is a reference site? *Bull. Seism. Soc. Am.*, **86**, 1733-1748.
- Vidale, J.E. and Y.G. Li (2003). Damage to the shallow Landers fault from the nearby Hector Mine Earthquake, *Nature*, **421**, 524-526.
- Waldhauser, F., W. L. Ellsworth, D. P. Schaff, and A. Cole (2004), Streaks, multiplets, and holes: High-resolution spatio-temporal behavior of Parkfield seismicity, *Geophys. Res. Lett.*, **31**, L18608, doi:10.1029/2004GL020649.

Wen, K-L, I.A. Beresnev, and Y.T. Yeh (1994). Nonlinear soil amplification inferred from downhole strong seismic motion data, *Geophys. Res. Lett.*, **21**, 2625-2628.

Zinszner, B., P. A. Johnson, and P. N. J. Rasolofosaon (1997). Influence of change in physical state on elastic nonlinear response in rock: Significance of effective pressure and water saturation, *J. Geophys. Res.* **102**, 8105-8120.

Chapter 5

Seismic Velocity Reductions Caused by the 2003 Tokachi-Oki Earthquake

Abstract

We use four repeating earthquake sequences located near Hokkaido to identify velocity changes caused by the M_w 8 2003 Tokachi-Oki earthquake. Using a moving window cross-correlation technique we identify delays in the arrival time of seismic waves that accumulate linearly with time into the seismogram. This behavior is indicative of repeated scattering within a medium where the seismic velocity has been reduced. For all of our earthquake/receiver geometries we find evidence that there are significant velocity reductions close to the receiver. The correlation of the size of the velocity reductions with both strong shaking and site characteristics suggest that these velocity reductions are caused by strong motion induced damage to near surface materials during nonlinear strong ground motion. For earthquake/receiver geometries where the seismic waves cross the Tokachi-Oki rupture zone, we identify particularly large increases in slowness as a result of the earthquake. For these geometries, we believe that the rupture zone of the Tokachi-Oki earthquake or the shallow crust above it represent a second region where seismic velocities are reduced as a result of the mainshock.

The material in this chapter is in preparation for publication in the *Journal of Geophysical Research* with co-authors N. Uchida and G.C. Beroza.

5.1 Introduction

For years seismologists have searched for changes in wave propagation both prior to and as a result of large earthquakes. Studies have suggested temporal changes in coda Q (e.g., Su and Aki, 1990), anisotropy (e.g., Saiga *et al.*, 2003), scattering (e.g., Baisch and Bokelmann, 2001) and seismic velocity (e.g., Uchida *et al.*, 2002) following earthquakes. Recently, seismic velocity changes caused by earthquakes have been intensively studied, as one only needs a repeating source, either natural (e.g., repeating earthquakes) (e.g., Poupinet *et al.*, 1984; Rubinstein and Beroza 2004a; Schaff and Beroza, 2004; Peng and Ben-Zion, in press) or artificial (e.g., explosions) (e.g., Li *et al.*, 1998; 2003), to identify changes in seismic velocity. Typically, authors appeal to strong motion induced damage (Schaff and Beroza, 2004; Rubinstein and Beroza, 2004a; 2004b; 2005; Peng and Ben-Zion, in press), static stress induced closure/opening of cracks (Poupinet *et al.*, 1984; Nishimura *et al.*, 2000) or damage to the fault zone itself (e.g., Li *et al.*, 1998; 2003) as the sources of velocity changes caused by the earthquakes.

In this study we are afforded a unique opportunity to observe multiple regions of velocity reductions associated with M_w 8 2003 Tokachi-Oki earthquake. We observe the influence of velocity reductions at the near-surface, and also near the rupture zone of the Tokachi-Oki earthquake. Our results are consistent with previous observations of nonlinear strong ground motion (site effects). We also see evidence of evidence of similar velocity reductions due to either fault zone damage or multiple scattering near the Earth's surface along the source-receiver path.

5.2 Data

We study four repeating microearthquake sequences (multiplets) in the Hokkaido region of Japan to monitor the influence of the September 26, 2003 Tokachi-Oki earthquake on seismic velocity (Figure 5.1). These four repeating earthquake sequences represent a subset of 294 repeating earthquake sequences identified near the Tokachi-Oki earthquake (Uchida *et al.*, in preparation). All the repeating earthquake sequences we study are characterized by high coherence values that exceed 0.95 over a broad range of

frequencies (1-8Hz) for 40 second long seismograms at a minimum of two stations. These criteria ensure that the member events of every repeating earthquake sequence are co-located. All these events are located on or near the the plate interface, which is dipping to the northwest. The depths determined from the JMA catalog for events 1-4 are: 39km, 51km, 60km, 44.5km respectively.

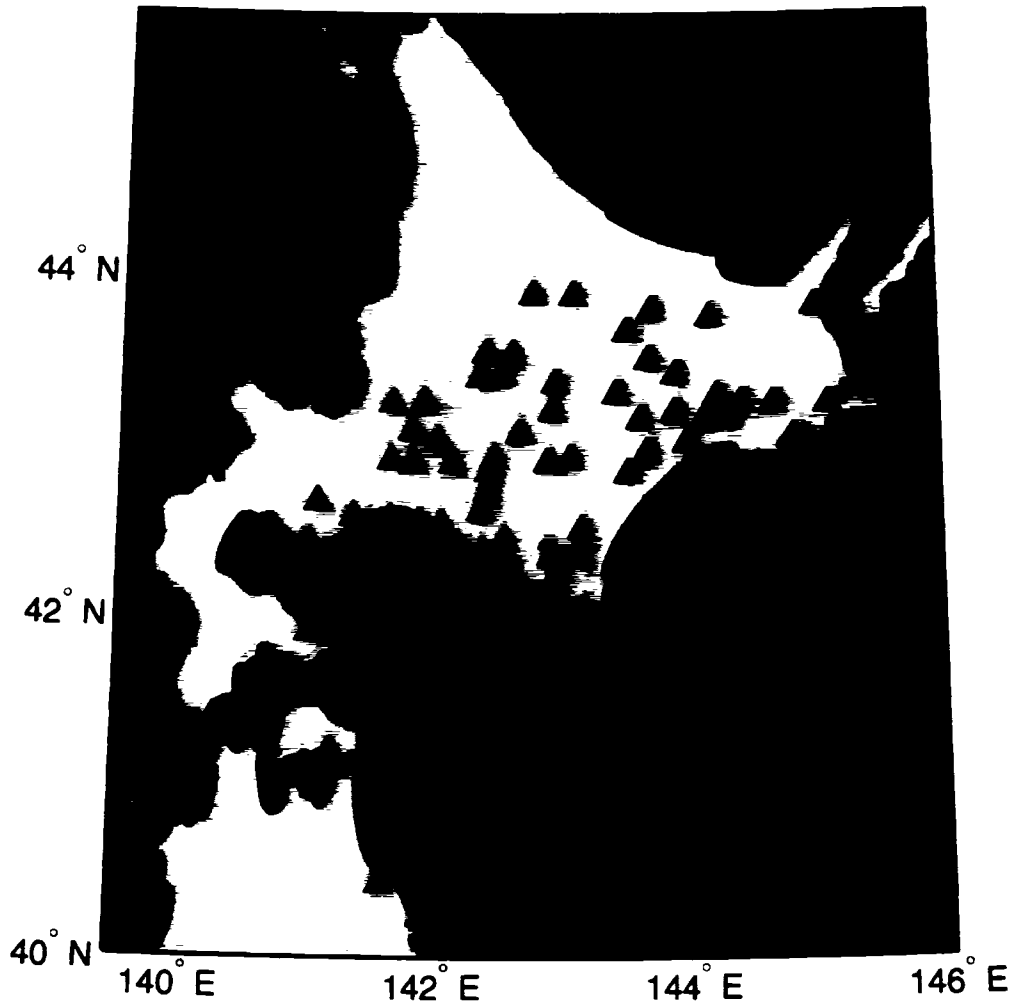


Figure 5.1: Map of Hokkaido and Northern Tohoku showing: station locations (triangles), location of repeating earthquakes (stars—number indicates repeat number), and approximate slip distribution of the Tokachi-Oki earthquake (blue contours) (Yamanaka and Kikuchi, 2003).

We examine the recordings of these earthquakes using seismometers from four different seismic networks: the Hokkaido University seismic network, the Tohoku

University seismic network, Hi-Net, and F-Net. The instruments within the university networks are high-gain, short period instruments and are typically located within vaults, although some instruments are placed at the surface. Hi-Net is a network of high-gain, short period velocity seismometers placed in deep boreholes (>100 meters depth). F-Net is a network of broadband seismometers placed in shallow vaults (<50 meters depth). All of the instruments within these networks record at a rate of 100 samples per second.

Previous studies of velocity changes induced by large earthquakes have shown that healing of velocity changes is most rapid immediately after the earthquake and slows with time (Li *et al.*, 2003; Vidale and Li, 2003; Schaff and Beroza, 2004; Rubinstein and Beroza, 2004a; 2004b; 2005; Peng and Ben-Zion, in press). Therefore, to ensure that the influence of the Tokachi-Oki earthquake on seismic velocities would be large, we select the multiplets that repeat within two months after the Tokachi-Oki mainshock. The timing of the events in each repeating earthquake sequence is shown in Table 5.1 and described in the following section.

Table 5.1: Timing of Repeating Earthquake Sequences Used

Repeating Earthquake Sequence	Event Number*	Date
1	1r	09/27/2003
	2	12/31/2003
2	1r	02/14/2001
	2	10/29/2003
3	1	08/23/2001
	2r	09/10/2003
	3	11/03/2003
4	1r	09/24/2003
	2	10/25/2003
	3	04/04/2004

* r indicates that the event was used as the reference event

5.3 Method

Prior to any data analysis the seismograms in this data set are normalized and causally filtered with a bandpass window of 1-10Hz. For each repeating earthquake sequence at each station, we then use cross correlation to align the seismograms to sub-sample precision to a manually picked P arrival. Once all the events within an individual sequence are aligned, we use a moving window cross-correlation technique to measure the relative arrival time of seismic phases of one event relative to a reference event in the same repeating earthquake sequence (Figure 5.2). As input to the moving window correlation, we use 128 sample windows of the vertical component seismogram weighted by a Hanning function. The windows are stepped forward at increments of 5 samples (0.05s). We obtain sub-sample precision to the correlation data by fitting a parabola to the peak of the cross-correlation function (Deichmann and Garcia-Fernandez, 1992). To ensure data quality, we enforce a minimum correlation coefficient of 0.9 on the P arrival, a minimum correlation coefficient of 0.8 on the first 20 seconds of the seismogram, and a minimum signal to noise ratio of 4:1. Previous studies have shown that delay values determined using cross correlation provide useful information for earthquake location for correlation coefficients as low as 0.7 (Schaff *et al.*, 2004). Therefore, we use 0.7 as a minimum threshold for the correlation coefficient for any individual correlation measurement. Any delay values associated with correlation coefficients less than 0.7 are not included in our further processing.

Using this technique we find that following the Tokachi-Oki earthquake the delays at many stations increase linearly as a function of time into the seismogram shortly after the S wave arrives (e.g., Figure 5.2b). Schaff and Beroza (2004) and Niu *et al.* (2003) have shown that if the velocity within a medium has been reduced, as later phases within the coda spend progressively longer amounts of time within this altered medium the seismogram should be stretched and delays should increase linearly as a function of time into the seismogram. To interpret these delays, we follow the method of Schaff and Beroza (2004). We first select a window of the delay function, specifically where the delays appear to increase/decrease linearly as a function of time. The data within these windows must satisfy the signal to noise criterion discussed above, as well as have a

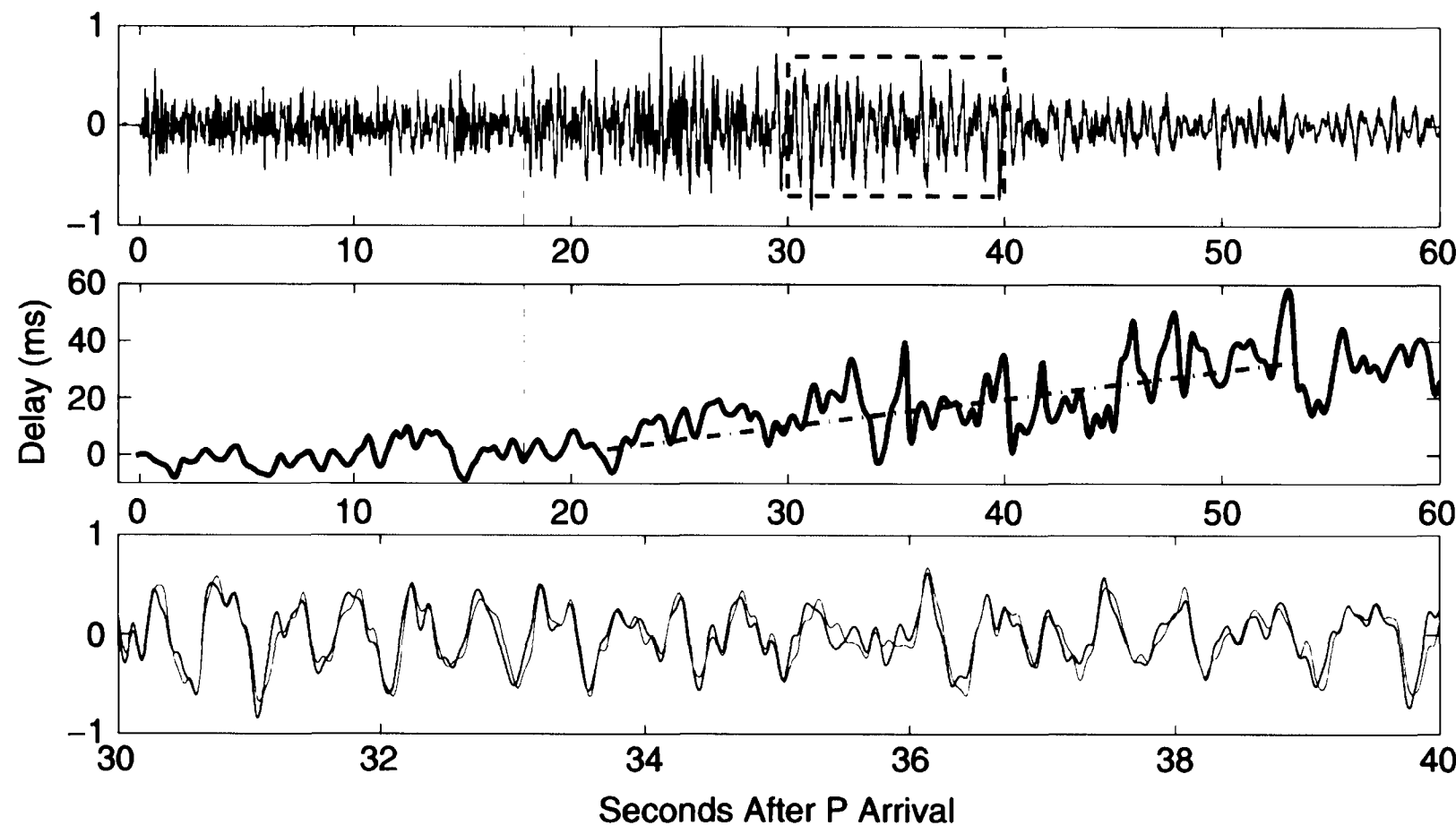


Figure 5.2: (a) Events 3 (black) and 4 (red) of repeating earthquake sequence #3 recorded by Hi-Net station SNSH. S arrival is indicated by the magenta dashed line. Note that the seismograms align nicely at the P arrival, but separate further into the seismogram, in particular after the S arrival. Region within the dashed black box is shown at larger scale in (c). (b) Delay of event 4 relative to event 5 (blue). Line fit to delay within a manually selected window (red).

minimum length of 5 seconds. The windows average approximately 30 seconds in length, but exceed 50 seconds for some stations. We then fit a line to the delays within this window, the slope of which has been shown to represent the fractional change in slowness (Figure 5.2b) (Schaff and Beroza, 2004). This fractional change in slowness represents a path averaged value, meaning that the velocity reductions may be localized and much larger. For those stations where significant delays are not apparent, we still fit a line to the delay function, such that we can quantitatively identify those stations where the change in slowness is indistinguishable from zero.

This method allows us to estimate error bars on the slowness change based upon the formal standard errors of the slope from the line fit. These errors do not take into account all the potential sources of error involved in using this technique. A major source of error is window selection. Windows are selected where delays are seen to vary linearly with time, i.e., where the data is most consistent with our model. We also see significant deviations from the linear trend in the form of peaks and valleys in delays (e.g., Figure 5.2). Numerical experiments have shown that sudden, short-lived peaks in the delay function may represent a movement of scatters rather than a change in velocity (Niu *et al.*, 2003). These sharp peaks and valleys are often observed when the correlation coefficient is particularly low, which suggests that the delay values they provide may be unreliable.

The delay values that are determined by cross-correlation methods describe changes in the medium that occurred at some point in time between the two repeating events being correlated. Because we are interested in changes induced by the Tokachi-Oki earthquake we try to minimize the time between our reference events and our data events such that any changes we observe are likely a result of the Tokachi-Oki earthquake. For repeating earthquake sequences 3 and 4, our reference events are events 2 and 1, which occur 16 and 2 days prior to the Tokachi-Oki earthquake, respectively. In sequences 3 and 4, the next event occurs 5 weeks and 4 weeks after the Tokachi-Oki earthquake, respectively. The short window of time between the reference and data events for these sequences indicates that Tokachi-Oki is likely responsible for any large differences observed between the reference events and these data events. There is more uncertainty in the timing of delays observed using repeating earthquake sequence 2. For

this sequence, there is an event that occurs approximately 5 weeks after Tokachi-Oki, but its reference event occurs in 2001, over 2½ years prior to Tokachi-Oki. If seismic velocities between 2001 and 2003 remained constant, the measurements from repeating earthquake sequence 2 should reflect Tokachi-Oki induced changes. Considering that there were no major tectonic events within the region from 2001 to 2003 (prior to Tokachi-Oki), we expect that the velocities remained constant and any changes in wave propagation that we observe using this repeating earthquake sequence are a result of the Tokachi-Oki earthquake. The delays of event 1 (8/23/2001) relative to event 2 (9/10/2003) in repeating earthquake sequence 3 offer further evidence that regional velocities remained constant from 2001 to 2003, as we don't observe significant delays between these two events (Figure 5.3). The lack of changes in seismic velocity from 2001 to shortly prior to Tokachi-Oki indicate that the measurements made using repeating earthquake sequence 2 should be comparable to those from multiplets 3 and 4, which had data events at approximately the same time as multiplet 2. The effect that we observe with repeating earthquake sequences 2-4 should be considered a lower bound on the coseismic reduction of seismic velocity induced by the Tokachi-Oki earthquake. It is a lower bound because the velocity reductions are shown to heal with time after the mainshock (Figures 5.4, 5.5) and these repeating earthquake sequences have no events within the first month after the Tokachi-Oki mainshock, so velocity reductions induced by the earthquake probably healed significantly by the time any of these repeating earthquake sequences repeated after the Tokachi-Oki earthquake.

The fourth repeating earthquake sequence we consider in this paper (#1) does not have a repeat prior to Tokachi-Oki. This means that we cannot directly observe the delays caused by Tokachi-Oki. Instead, we observe the healing of Tokachi-Oki induced velocity reductions by comparing an event the day after Tokachi-Oki and a repeat that occurred 3 months later (Figure 5.4). As a result, we see negative delays that reflect a decrease in slowness (velocity increase). The percentage decrease in slowness from September 2003 to December 2003 that we observe using repeating earthquake sequence 1 is often larger than the percentage increase in slowness we observe at the same stations using repeating earthquake sequences 2-4 (Figure 5.6). It is not surprising that we observe larger changes in slowness with multiplet 1 than the others because the repeats

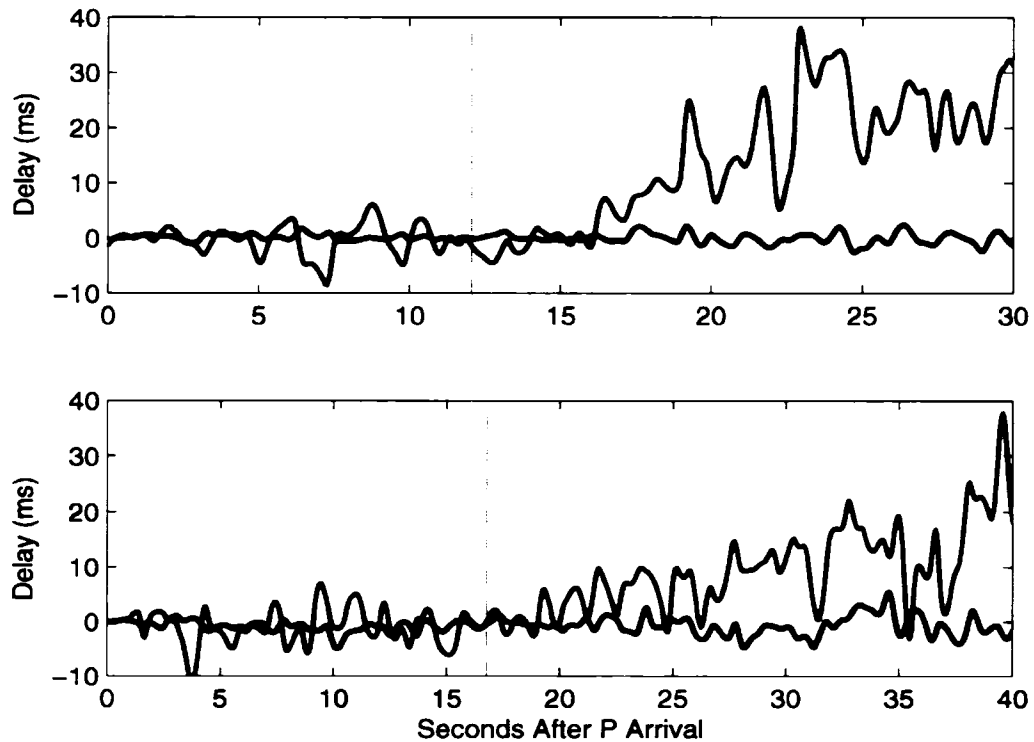


Figure 5.3: Delay plotted as a function of time for repeating earthquake sequence 3 at Hi-Net stations MMRH (a) and HBTH (b). The red line indicates event number 3 (11/03/2003). The blue line indicates event number 1 (08/23/2001). S arrival is indicated by the magenta dashed line.

within events 2-4 occur 1 month after the Tokachi-Oki earthquake allowing for a significant amount of healing before the effects of the velocity changes can be measured. As a result, the slowness change measurements we compute for repeating earthquake sequence 1 are useful for understanding the spatial behaviors of the delays, but should not be compared in amplitude to slowness change measurements made for repeating earthquake sequences 2-4. For this reason when we compute the mean slowness changes at a station we do not include those determined from repeating earthquake sequence one in these computations.

5.4 Observations

The Tokachi-Oki earthquake produces a distinct signal that is detected at many stations. Nearly all of our stations show a systematic increase in arrival times in the *S* coda following the Tokachi-Oki earthquake. For those repeating earthquake sequences

where we have multiple repeats after the Tokachi-Oki earthquake (1 and 4), we see that the delays decrease with time after the mainshock. This suggests that the seismic velocity reductions caused by Tokachi-Oki heal with time after the mainshock (Figure 5.4, 5.5). Interestingly, we do not typically observe any significant change in the arrival times of the *P* coda (Figures 5.2, 5.3). Although the general response to the Tokachi-Oki earthquake is consistent from station to station, in that they reflect a decrease rather than increase in velocity, the size of the velocity changes varies significantly from station to station and from repeating earthquake sequence to repeating earthquake sequence (Figure 5.6, 5.7). Below we search for systematic controls on this variation to localize where the velocity reductions are occurring.

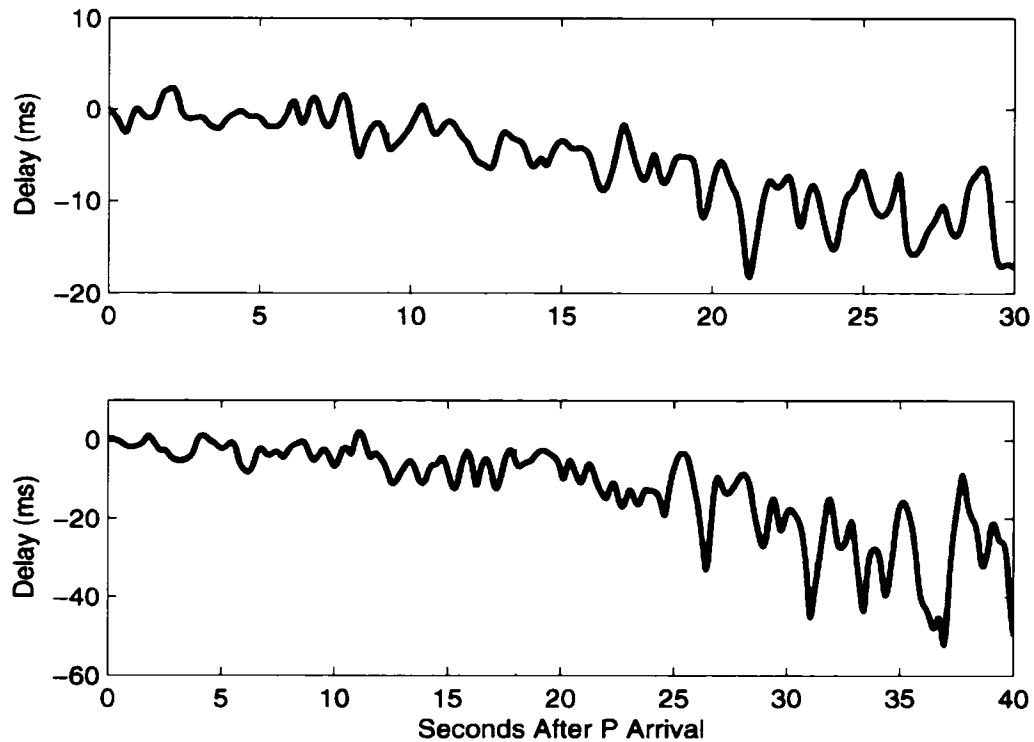


Figure 5.4: Delay plotted as a function of time for event 2 relative to event 1 within repeating earthquake sequence 1 at (a) Hokkaido University station AKK and (b) Hi-Net station AYWH. *S* arrival is indicated by the magenta dashed line. Negative delays indicate that phases are arriving sooner in December than they are in September.

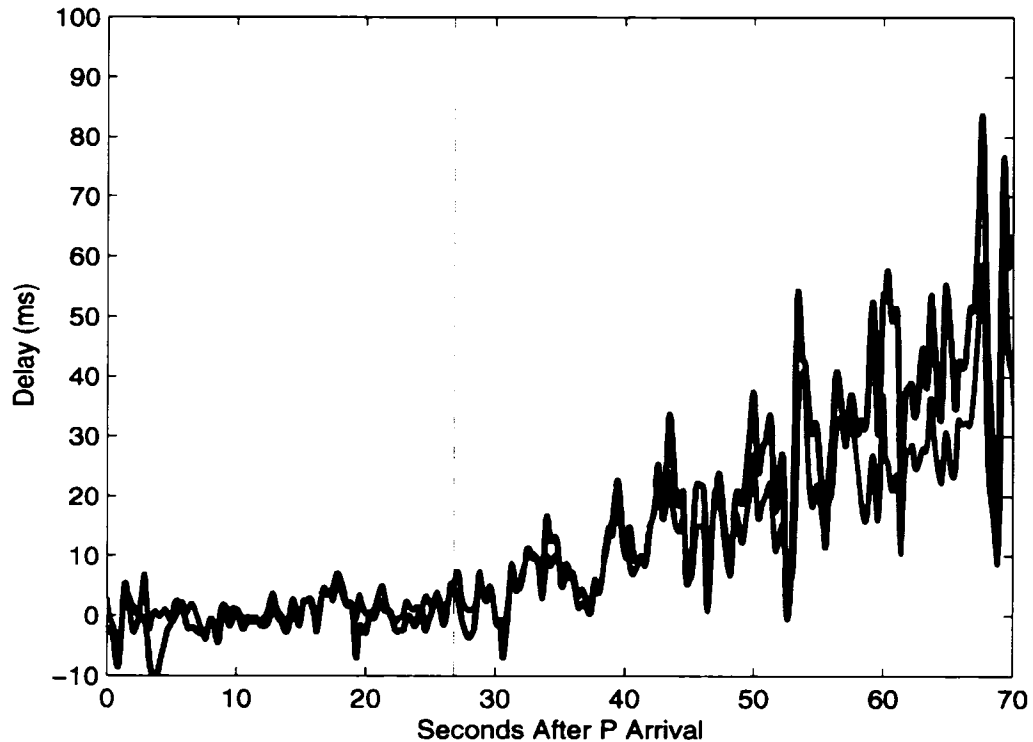


Figure 5.5: Delay plotted as a function of time for events 2 (blue) and 3 (red) of repeating earthquake sequence 4 at Hi-Net station SKNH. *S* arrival is indicated by the magenta dashed line. The much smaller delays and shallower slope of event 3 relative to event 2 indicate that the velocity reductions caused by Tokachi-Oki are healing.

If we examine a map showing the average increase in slowness caused by the Tokachi-Oki earthquake plotted at all our stations there is a very striking feature in that the slowness increases are largest in the east and west of Hokkaido, while the increase in slowness in the central region of Hokkaido is much smaller (Figure 5.7). This correlates very nicely with the topography of Hokkaido; the central region of Hokkaido is very mountainous, while the regions to the east and west of it are plateaus (Figure 5.7). In fact, there appears to be a threshold of approximately 100m altitude; almost all the largest slowness changes are observed at stations of 100m altitude or less (Figure 5.8). This correlation may be a result of our measurement technique. Our technique identifies linear increases in delay, which are believed to be the result of repeated scattering within a medium with reduced seismic velocities. Topographic effects in the mountains may prevent energy from being trapped locally. This appears to be true for the mountains of

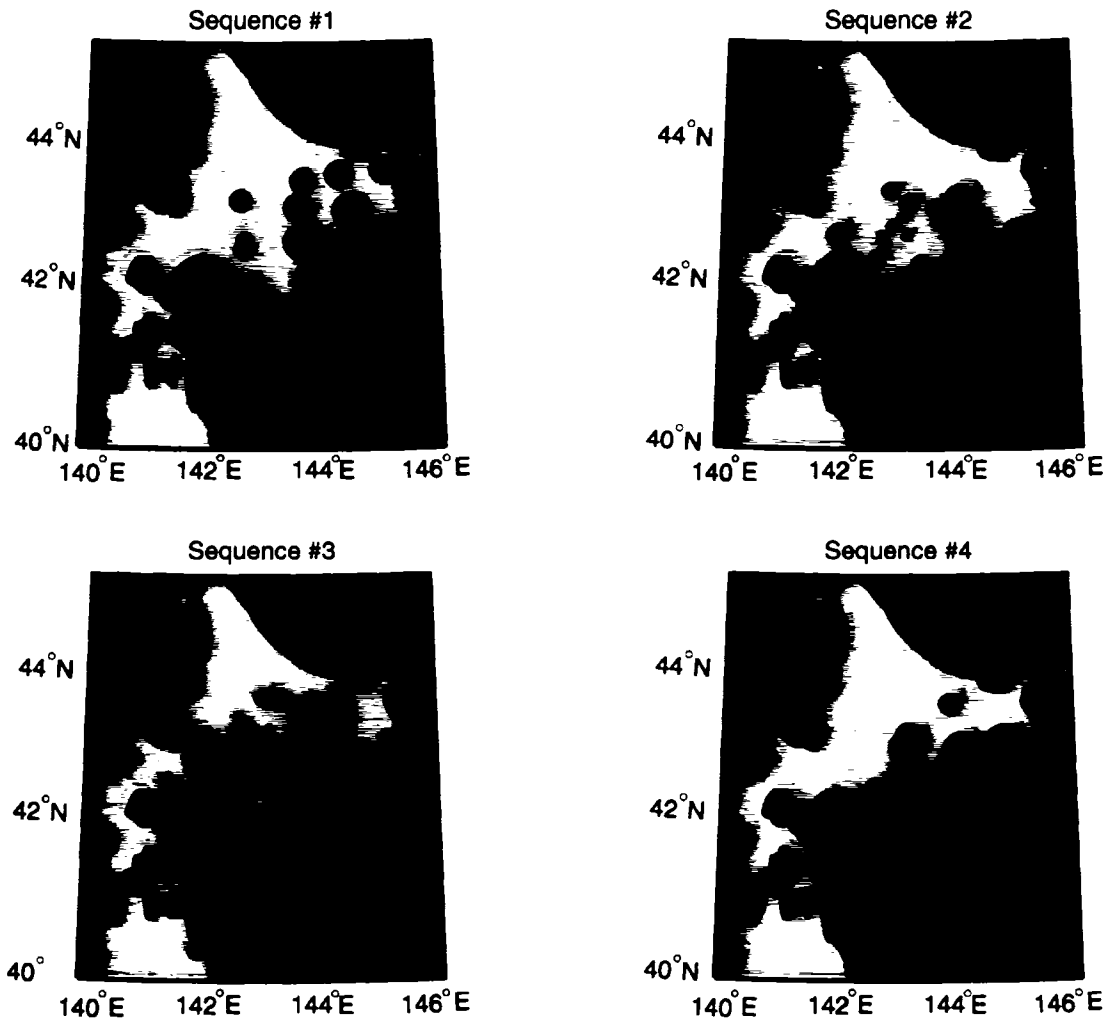


Figure 5.6: The increase in slowness at each station caused by the Tokachi-Oki earthquake is plotted as a circle at the location of each station. Each panel represents a different repeating earthquake sequence and the associated observations with it. The size of the circle indicates the amount by which the path averaged slowness increased (decreased) at that station for stations marked in blue (red). The scale is shown in the upper left panel, which depicts the delays observed using repeating earthquake sequence 1. The black circles represent stations where the error bars to the change in slowness indicate that the change in slowness is not significantly different from zero at the 95% confidence level. Pink stars indicate the location of the repeating earthquake sequences. The circles for repeating earthquake sequence 1 are all red because these measurements reflect the healing from 9/27/2003 to 12/31/2003, and therefore the slowness should be decreasing.

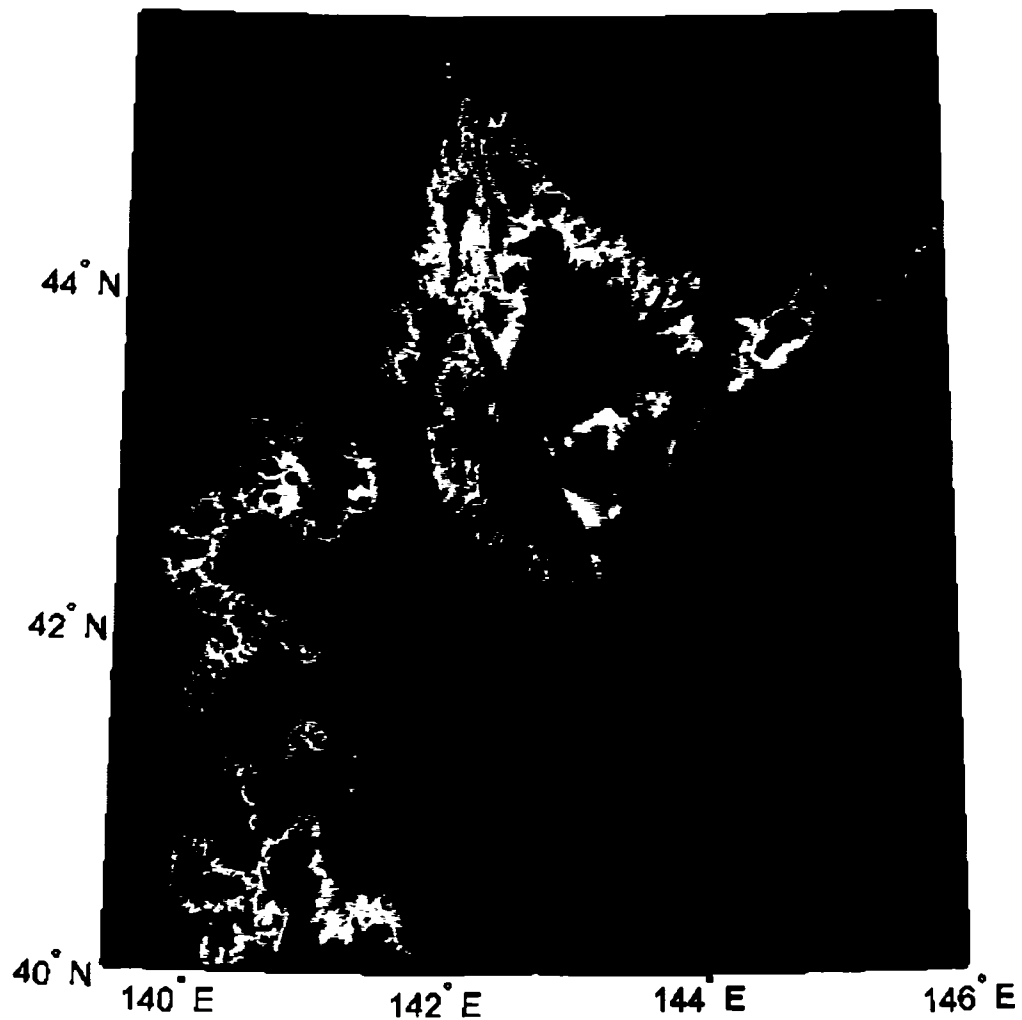


Figure 5.7: The average increase in slowness at each station caused by Tokachi-Oki. This averages over all repeating earthquake sequences (within multiplets 2-4) available at any individual station. The number of observations for each station varies, so this may affect the relative values of the delays.

Hokkaido. The majority of the scattered energy in the Hidaka Mountains (southern end of the central mountain region of Hokkaido) appears to be scattering at depths of 50km or greater (Taira and Yomogida, 2004). On the other hand, plateaus and other regions with layered geology, may have trapped or standing waves within them. This suggests that a larger percentage of the coda energy is locally generated and remains within an altered, near-surface medium for plateaus than in mountainous regions. Should these assertions be true, the delays within plateau regions should be larger than those in mountainous regions. There is an alternative explanation for the correlation of the velocity reductions

and the station altitude, which relates to the local geology. It is probable that the rocks within the mountains are harder than those elsewhere and thus less subject to damage from the Tokachi-Oki earthquake.

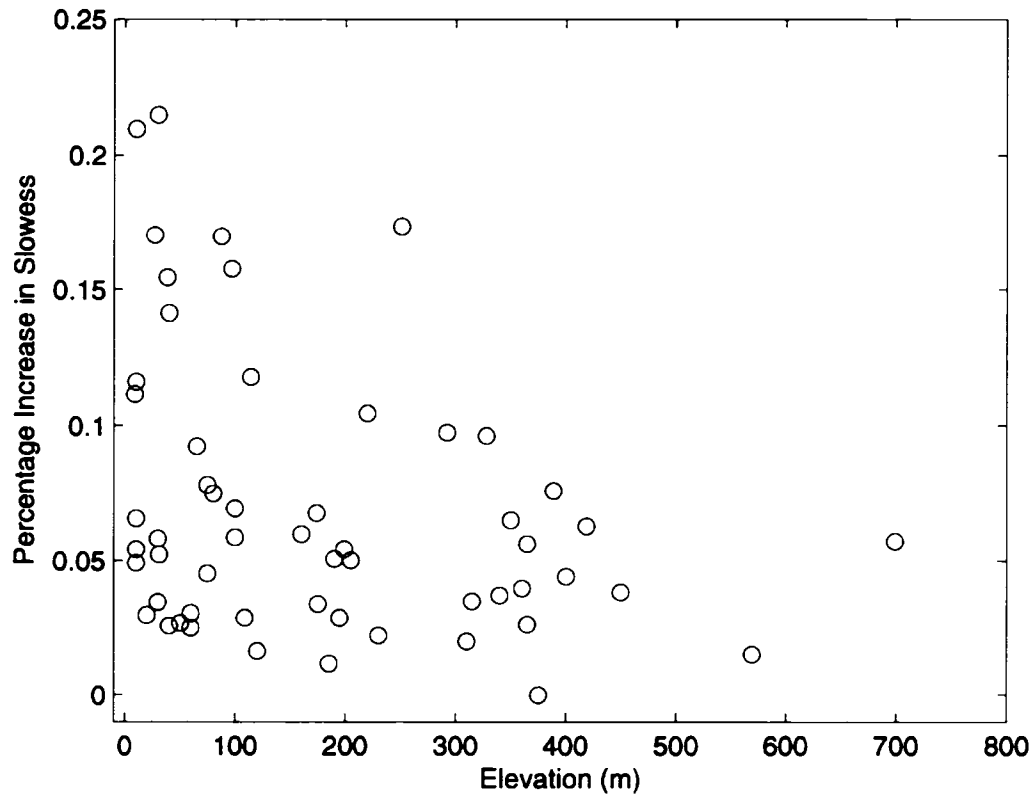


Figure 5.8: The average increase in slowness at each station plotted against elevation. Elevation is determined at the borehole adit (for borehole stations) or surface elevation (surface stations). The intent is to understand the influence of local topography on velocity reductions and our method.

We also note that the influence of Tokachi-Oki is particularly small in the north of Honshu (Tohoku area). The lack of changes in Tohoku is expected, as these stations are further from the mainshock than the majority of the stations on Hokkaido. This means that the influence of the Tokachi-Oki earthquake should be smaller there.

5.5 Constraining the Source Region of the Delays

Before determining a mechanism for the observed decreases in seismic velocity associated with Tokachi-Oki earthquake, we attempt to localize the region in which the delays are accumulating. The possible source regions for these delays are near the earthquake sources, in the path between the earthquakes and the receivers, near the receivers, or some combination of the three. We have previously argued that a significant percentage of the delays are a result of scattering within a volume near our receivers. Below, we offer further evidence that a large percentage of the delays are accumulating near the receivers. We also find evidence that substantial delays are accumulating in the path between the sources and receivers. We rule out near source effects as a significant source of the delays that we observe. If delays were accumulating near the repeating earthquake sources, we would expect that they would be approximately constant at all of our stations for any individual repeating earthquake sequence. We see very large variations in the slowness increases at different stations for the same repeating earthquake source (Figure 5.6). This wide range in the slowness increases for any repeating earthquake sequence indicates that any delays that are accumulating near the repeating earthquake sources are much smaller than those accumulating elsewhere. As such, velocity reductions near the earthquake sources should be considered an insignificant source of the delays that we observe.

5.5.1 Site Effects

We believe that a large percentage of the delays that we observe are accumulating very close to the sites that we are observing them at. We have shown previously that delays are much smaller in the mountainous regions than they are in the plateau regions (Figure 5.7). We believe this to be the result of the lack of repeated scattering within mountainous regions, therefore our method is less likely to observe velocity reductions in these regions. Mountainous regions are also more likely to have harder rocks, which are less likely to be damaged (and have their seismic velocities temporarily reduced) than the softer rocks found in plateaus and elsewhere. We can observe this effect if we compare site-specific amplification factors to the observed slowness increases (Figure 5.9). The

most convincing evidence, though, that a large percentage of the delays are accumulating near the site is the strong variation in slowness with location. We observe very large difference in the slowness changes observed at nearby sites (Figure 5.6, 5.7). At nearby sites, the difference in path and source effects should be negligible, so any difference between sites should reflect differences in their site responses.

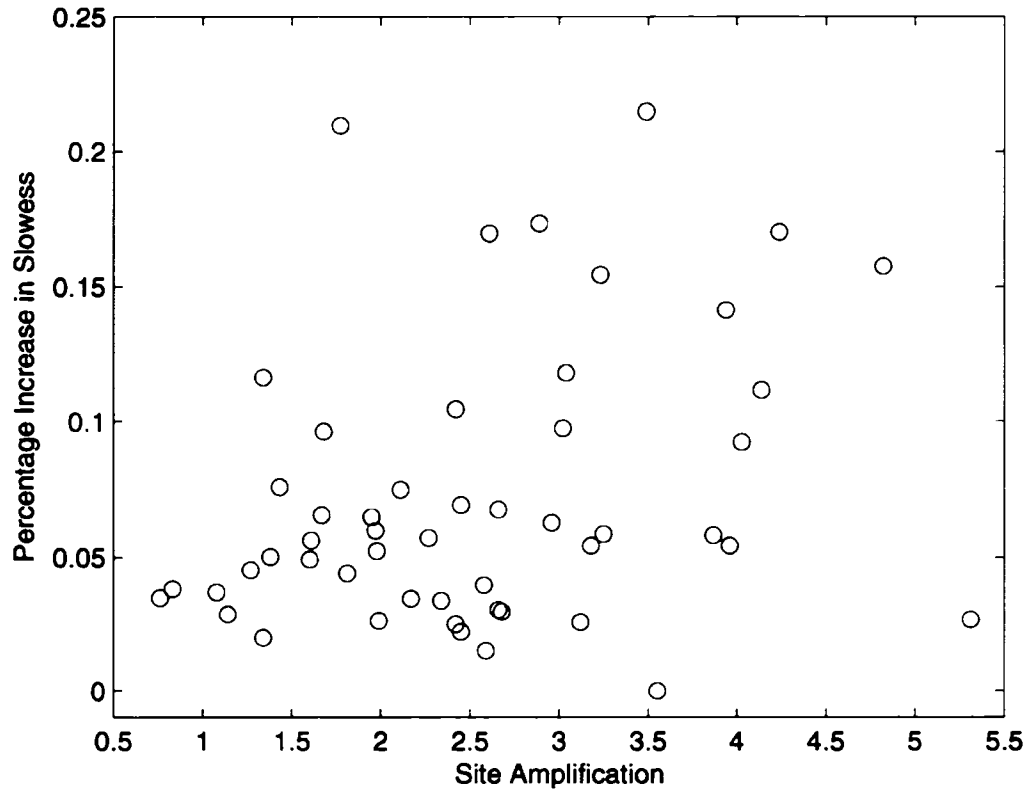


Figure 5.9: Mean slowness increase at each station plotted against peak ground velocity (PGV) amplification factors. Site amplification factors were determined based on the ratio of observed peak amplitudes versus theoretical peak amplitudes computed based on magnitude and hypocentral distance (Watanabe, 1971) for a suite of 64 $M > 3.5$ earthquakes within 900km of Hokkaido. Amplification factors were not determined for the 6 F-Net stations used in this study and so these 6 data points are not plotted.

5.5.2 Path Effects

As noted above, the strength of the observed velocity reductions is strongest in the plateau regions in the east and west of Hokkaido, while slowness increases in the central, mountainous region of Hokkaido are significantly smaller. The strength of observed

slowness increases in the central mountain region of Hokkaido appears to vary depending upon the source locations. Using the multiplets that are located downdip of the Tokachi-Oki rupture (sequences 2 and 3), we find that the slowness increases in the central region of Hokkaido are much smaller than they are in the plateau regions to the east and the west (Figure 5.6). Making this same comparison using the multiplets that occur to the east and southeast of the mainshock rupture (repeats 1 and 4), we find that the slowness changes in the central region are much more comparable in magnitude to the plateau areas. We believe that the difference in slowness changes for the central mountain region for repeating earthquake sources in different locations is related to the path that the waves take to the stations. For multiplets 1 and 4, the paths to the stations in the central region cross the rupture zone of the Tokachi-Oki earthquake, while for sequences 2 and 3 the paths to the central region do not cross regions of high slip (Figure 5.1). The difference between the two paths is illustrated clearly if we compare the slowness changes for repeating sequences 2-4 observed by stations in this region where some paths cross the rupture zone (paths from repeat 4) while others don't (paths from repeats 2-3) (Figure 5.10). Slowness changes for paths that cross the rupture zone of Tokachi-Oki are consistently larger than those that don't, strongly suggesting that delays are not just accumulating near the receiver for paths that cross the rupture zone. For those paths that cross the rupture zone of Tokachi-Oki, we expect that a significant percent of the delays that we observe are accumulating in the region immediately surrounding the mainshock rupture..

Further evidence supporting the argument that some stations are seeing delays accumulate both at the site and in the region surrounding Tokachi-Oki can be found by comparing repeating earthquake sequences 1 and 4. For repeating earthquake sequence 1, the slowness increases in the central region are approximately 50% the size of the slowness increases to the east, while for repeating earthquake sequence 4 the slowness increases in the central region of Hokkaido are equivalent in amplitude with those to the east (Figure 5.6). The waves from repeating earthquake sequence 4 traverse the entire width of the rupture zone and the region of highest slip en route to the central region of Hokkaido, while the waves from repeating earthquake sequence 1 cross a smaller portion of the rupture zone (Figure 5.1). This suggests that both the amount of time waves spend

crossing the rupture zone of the Tokachi-Oki earthquake and the amount of slip on the rupture zone in which the waves are traveling are important in determining the amplitude of slowness changes observed at the stations in the central region.

5.6 Physical Mechanism for Seismic Velocity Reductions

As discussed in the previous section, we appear to be observing velocity reductions in the near surface near our receivers. For those paths that cross the rupture zone of the Tokachi-Oki earthquake, we also see velocity reductions somewhere

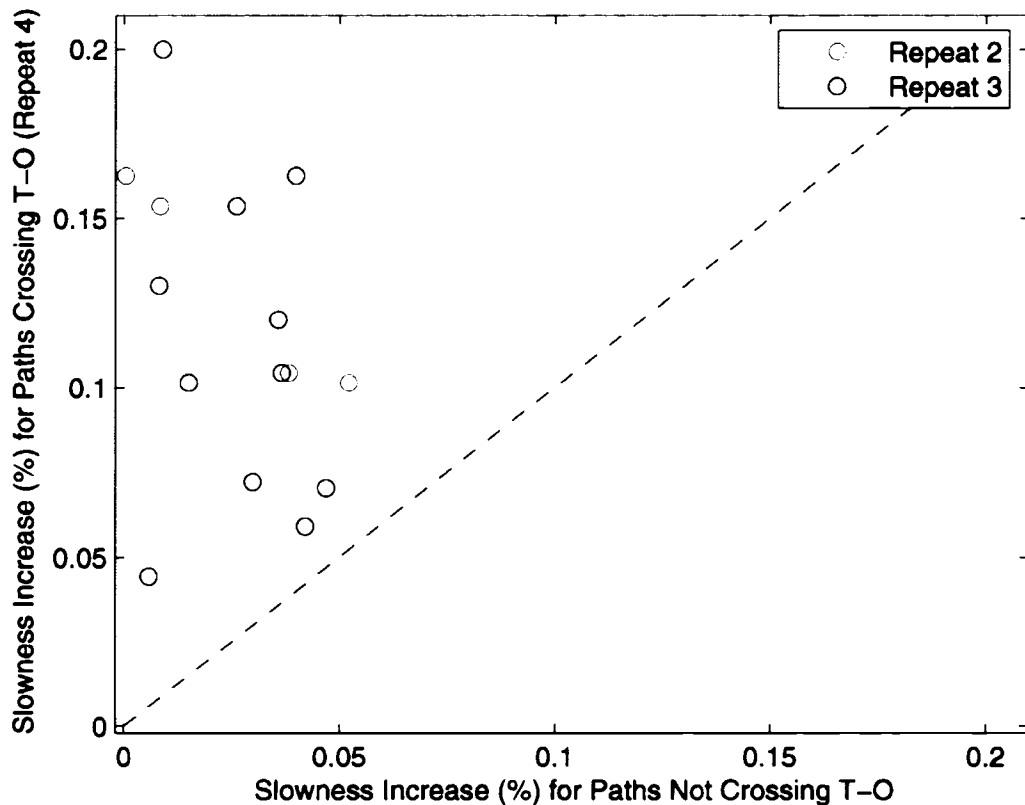


Figure 5.10: Slowness increase for repeating earthquake sequence 4 for stations where the path crossed the Tokachi-Oki earthquake plotted against the slowness increases observed at those same stations using repeats 2 (red) and 3 (blue). We consider paths for repeating earthquake sequence 4 to cross the Tokachi-Oki earthquake if the station is located to the west of 144°E. A one to one line is provided as reference.

in the path between our repeating earthquakes and receivers, likely near the Tokachi-Oki earthquake. In this section we attempt to determine the physical mechanisms responsible

for both sets of velocity reductions. We believe that the velocity reductions that are accumulating near the receivers are a result of nonlinear strong ground motion in the Tokachi-Oki earthquake, i.e., strong ground motion damaging near surface materials resulting in velocity reductions. The cause of the velocity reductions that we believe to be in the region of the Tokachi-Oki rupture zone is less clear. To explain the velocity reductions near the Tokachi-Oki rupture zone we posit two hypotheses: 1) the linear increase in delays that we observe for these paths may result from delays accumulated by phases that reflect multiple times off the surface (where velocities will have been reduced by nonlinear strong ground motion), 2) the linear increase in delays results from repeated scattering within the plate interface in the rupture zone itself.

5.6.1 Site Effects

To explain the increases in slowness caused by the Tokachi-Oki earthquake that appear to be localized to the near surface near our sites, we appeal to nonlinear strong ground motion as the causative agent for the velocity reductions. Nonlinear strong ground motion has been widely documented for many earthquakes, including: the 1994 Northridge earthquake (Field *et al.*, 1997), the 1999 Chi-Chi earthquake (Huang *et al.*, 2005), the 1995 Kobe earthquake (Aguirre and Irikura, 1997), and the 2003 Tokachi-Oki earthquake (Yamanaka and Kikuchi, 2003). The physics and the effects of nonlinear strong ground motion have been thoroughly reviewed in (Beresnev and Wen, 1996) and more recently in (Ostrovsky and Johnson, 2001). Nonlinear strong ground motion is characterized by the strong shaking of large earthquakes resulting in damage (the growth and/or opening of microcracks) to geomaterials. This damage results in a decrease in the elastic moduli of the medium, and therefore a decrease in the seismic velocities.

The strength of nonlinearity and its damage are expected to be positively correlated with the strength of shaking (Guyer *et al.*, 1998; Ostrovsky *et al.*, 2000; Rubinstein and Beroza, 2004a; 2004b; 2005; Peng and Ben-Zion, in press). Our observations parallel this expectation, as there only appear to be large slowness increases at stations that experienced strong shaking from the Tokachi-Oki earthquake exceeding 100 cm/s^2 (or approximately 10 percent the acceleration of gravity) (Figure 5.11). The

strong shaking parameters that we use are subject to considerable uncertainty. These values are simple interpolations of the K-net strong motion observations of the Tokachi-Oki earthquake and any site effects specific to the K-net sites are included and those specific to our observations sites are not. There are also many of our sites that are quite distant from the closest K-net site, adding further uncertainty. We have previously shown that the slowness increases caused by the Tokachi-Oki earthquake correlate with site amplifications (Figure 5.9). This behavior is also predicted by nonlinear strong ground motion, as softer materials are more susceptible to damage by nonlinear strong ground motion than hard materials (Van Den Abeele and Van de Velde, 2000; Rubinstein and Beroza, 2004a; 2004b).

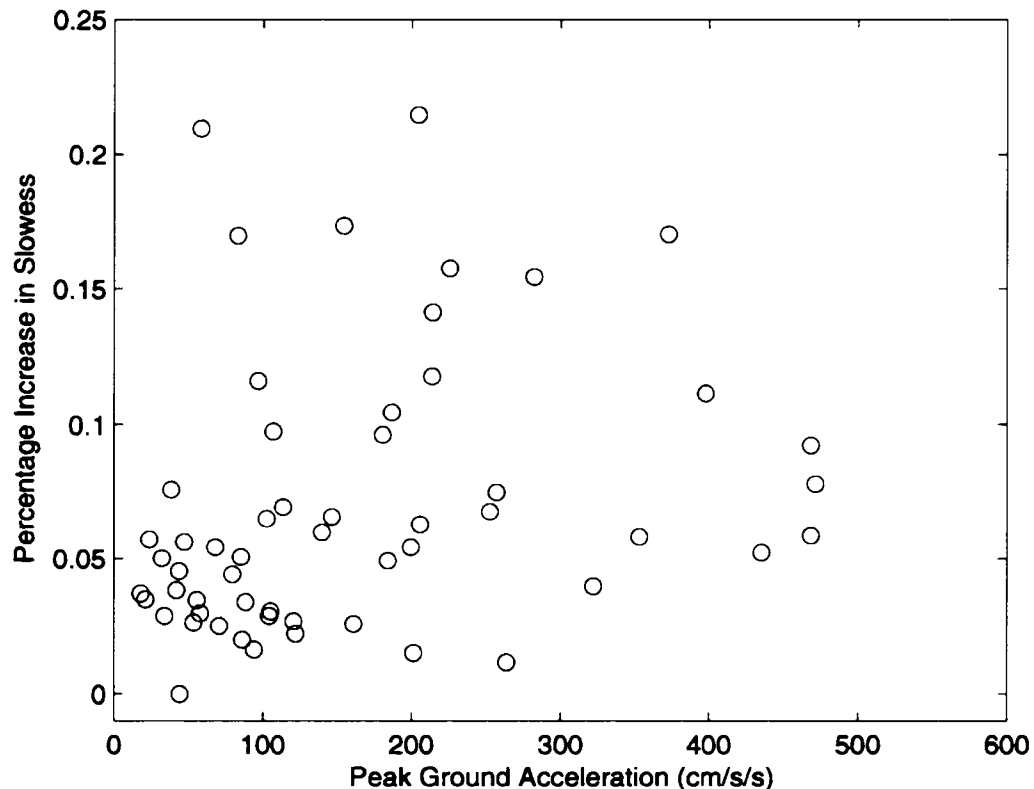


Figure 5.11: Mean slowness increase at each station plotted against peak ground acceleration in Tokachi-Oki earthquake. Site specific PGA values are interpolated from the PGA values determined at K-net stations. These values reflect the peak acceleration on 1 component. The peak, vector acceleration, although probably more directly correlated to our observations, is not readily available. Furthermore, the value we examine and the peak, vector acceleration are likely to closely related.

One other prediction of nonlinear strong ground motion is that damage caused by it should be limited to the very near surface as the susceptibility to nonlinearity decreases with increasing compressive stress, and hence with increasing depth (Zinszner *et al.*, 1997; Ostrovsky *et al.*, 2000). Field evidence from the 2004 Parkfield earthquake indicates that the damage caused by strong shaking is limited to the very near surface (depth < 100m) (Rubinstein and Beroza, 2005). Here we do not find such a correlation (Figure 5.12). We expect that there is a depth dependence to the damage for our sites, but our method of measuring slowness changes cannot resolve this detail. Our method is unable to resolve the depth dependence of the damage caused by Tokachi-Oki because the scattering volume that is contributing to the coda likely extends deeper than our deepest stations. Therefore, the delays at any site should be relatively depth independent. Rubinstein and Beroza (2005) were able to identify the depth dependence of nonlinear strong ground motion by examining the change in the *S-P* time at a number of sites. The *S* arrivals at many of our sites are very emergent, making it impossible to properly use this technique.

5.6.2 Path Effects

We are less certain of the physical mechanism responsible for the delays that seem to accumulate along the paths that cross the Tokachi-Oki rupture zone. We offer two hypotheses for the source mechanism of these velocity reductions.

We first suggest that damage induced by nonlinear strong ground motion at the near surface above Tokachi-Oki is resulting in the delays that we observe. Most likely, the shaking of the Tokachi-Oki earthquake was strongest at the near surface, directly above the rupture. Because this region experienced the strongest shaking, the strong motion induced damage will likely be largest. This damage will likely be particularly large because the ocean sediments which overlie the rupture zone are probably poorly consolidated and therefore particularly subject to nonlinearity. Therefore we expect velocity reductions at the near surface above the Tokachi-Oki to be quite large. While it is particularly likely that the damage induced by the strong motion of the Tokachi-Oki earthquake was particularly strong directly above the rupture zone; for these velocity

reductions to be observed as a linear increase in delays at our stations onshore, a significant percentage of the S-coda energy recorded at our seismometers onshore must be multiply reflected at the near surface in this region.

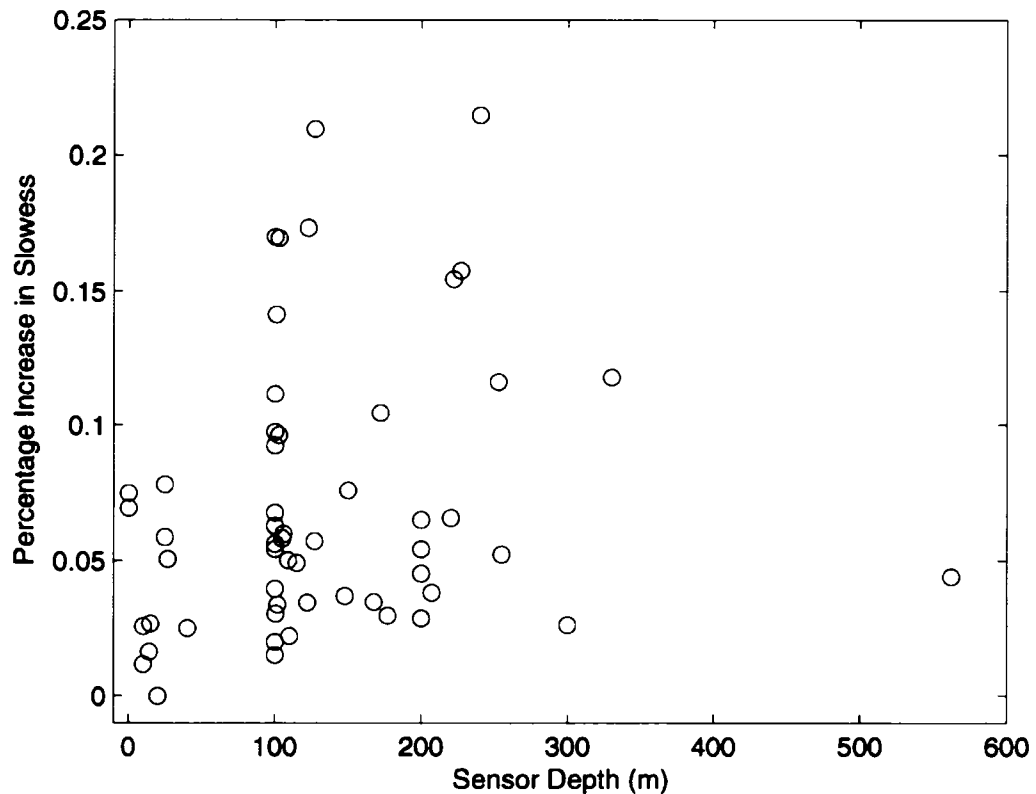


Figure 5.12: Mean slowness increase at each station plotted against sensor depth.

In our second hypothesis we suggest that delays are accumulating within the rupture zone of the Tokachi-Oki earthquake. This model requires that there be significant velocity reductions within the rupture zone. Studies of strike-slip earthquakes in California have provided evidence that earthquake rupture can result in significant velocity reductions within a narrow region surrounding the rupture (Li *et al.*, 1998; 2003; submitted). For fault zone velocity reductions to result in the linear increase in delays that we observe, it requires that much of the energy pass through this region and scatter repeatedly. It is likely that the energy from these repeating earthquakes does pass

through the rupture zone of the Tokachi-Oki earthquake, as both the repeating events and the Tokachi-Oki earthquake are located on the plate interface, with the mainshock located downdip from the smaller, repeating events. The distances between the repeating earthquakes and receivers range approximately between 100 and 250km, which ensures that the majority of the energy arriving at the stations will have departed the earthquake in a downgoing direction. This suggests that a significant portion of the energy from the repeating earthquakes will cross the Tokachi-Oki rupture zone.

The waveguide nature of fault zones could allow for repeated scattering and a linear increase in delays for fault-zone trapped waves. There is an uncertainty, though, in how much energy will escape the waveguide and reach the surface. There is evidence that the subduction interface in Hokkaido is a large source of scattered energy in the coda, albeit at very high frequencies (14-18Hz) (Taira and Yomogida, 2003). Thus the plate interface (and therefore the rupture zone of the Tokachi-Oki earthquake) is a potential source for the scattered energy we are observing late into the *S* coda and therefore a potential location where the delays could be accumulating.

5.6.3 Fluids?

While we see significant changes in the arrival times of the *S* coda for both path and site effects on the seismic velocities, we don't generally see significant changes in the *P* arrival times (e.g., Figure 5.2, 5.3). This may suggest that fluids have somehow been introduced, as the inability of fluids to support shear would make the changes in arrival time of the *S* coda arrivals much more dramatic than those for the *P* coda. It may also be that the delays in the *P* coda are more difficult to observe. First, we have less time to observe an accumulation of delays in the *P* coda than we do for the *S* coda. We can only look for changes in the arrival times of the *P* coda until the *S* wave arrives (typically 5-20s for this data set), whereas for the *S* arrival, we often have 50-60s of coda to examine. The higher velocity of *P* also makes it harder to observe changes in arrival time than for *S* because the same percentage reduction in *S* and *P* velocities will result in significantly larger delays for the *S*. All this considered, we do occasionally see what

appear to be linear increases in delay for the P coda caused by the Tokachi-Oki earthquake (e.g., Figure 5.4).

5.7 Summary

We have used repeating earthquake sequences near the Tokachi-Oki earthquake rupture to identify time-dependent changes in the seismic velocity. We identify increases of up to 0.3% in path-averaged slowness caused by the Tokachi-Oki earthquake. Our varied recording geometry allows us to identify velocity reductions both near the receivers and in the region surrounding the mainshock rupture. The near-receiver velocity reductions, we expect are a result of nonlinear strong ground motion. The velocity reductions nearer the rupture we believe are either a result of damage in the kilometers immediately surrounding the Tokachi-Oki rupture or damage induced by nonlinear strong ground motion directly above the Tokachi-Oki mainshock.

5.8 Acknowledgements

The authors would like to thank Hiroe Miyake for assistance with strong motion data and descriptions of site response. The waveform data were provided by Hokkaido University, Tohoku University, NIED Hi-Net and NIED F-Net. We thank M. Kasahara and M. Ichiyangi for their corporation in using data from Hokkaido University seismic network. Strong motion parameterization was provided by NIED K-Net. This work was supported by USGS grant 05HQGR0007. J.R. was partially supported by the William K. Whiteford Fellowship.

References

- Aguirre, J., and K. Irikura (1997), Nonlinearity, liquefaction and velocity variation of soft soil layers in Port Island, Kobe, during the Hyogo-ken Nanbu earthquake, *Bull. Seism. Soc. Am.*, **87**, 1244-1258.
- Baisch, S., and G. H. R. Bokelmann (2001), Seismic waveform attributes before and after the Loma Prieta earthquake: scattering change near the earthquake and temporal recovery, *J. Geophys. Res.*, **106**, 16323-16337.
- Beresnev, I. A., and K.-L. Wen (1996), Nonlinear soil response--A reality?, *Bull. Seism. Soc. Am.*, **86**, 1964-1978.
- Deichmann, N., and M. Garcia-Fernandez (1992), Rupture geometry from high-precision relative hypocentre locations of microearthquake clusters, *Geophys. J. Intl.*, **110**, 501-517.
- Field, E. H., P. A. Johnson, I. A. Beresnev, and Y. Zeng (1997), Nonlinear ground-motion amplification by sediments during the 1994 Northridge earthquake, *Nature*, **390**, 599-602.
- Guyer, R. A., K. R. McCall, and K. Van Den Abeele (1998), Slow elastic dynamics in a resonant bar of rock, *Geophys. Res. Lett.*, **25**, 1585-1588.
- Huang, H.-C., S.-W. Huang, and H.-C. Chiu (2005), Observed evolution of linear and nonlinear effects and the Dahan Downhole Array, Taiwan: Analysis of the September 21, 1999 M7.3 Chi-Chi earthquake sequency, *PAGEOPH*, **162**, 1-20.
- Li, Y.-G., J. E. Vidale, K. Aki, F. Xu, and T. Burdette (1998), Evidence of shallow fault zone strengthening after the 1992 M7.5 Landers, California earthquake, *Science*, **279**, 217-219.
- Li, Y.-G., J. E. Vidale, S. M. Day, D. D. Oglesby, and E. Cochran (2003), Postseismic fault healing on the rupture zone of the 1999 M7.1 Hector Mine, California, earthquake, *Bull. Seism. Soc. Am.*, **93**, 854-869.
- Li, Y.-G., P. Chen, E. S. Cochran, J. E. Vidale, and T. Burdette (submitted), Seismic evidence for rock damage and healing on the San Andreas Fault associated with the 2004 M6 Parkfield earthquake, *Bull. Seism. Soc. Am.*

- Nishimura, T., N. Uchida, H. Sato, M. Ohtake, S. Tanaka, and H. Hamaguchi (2000), Temporal changes of the crustal structure associated with the M6.1 earthquake on September 3, 1998, and the volcanic activity of Mount Iwate, Japan, *Geophys. Res. Lett.*, **27**, 269-272.
- Niu, F., P. G. Silver, R. M. Nadeau, and T. V. McEvilly (2003), Stress-induced migration of seismic scatterers associated with 1993 Parkfield aseismic transient event, *Nature*, **426**, 544-548.
- Ostrovsky, L. A., and P. A. Johnson (2001), Dynamic nonlinear elasticity in geomaterials, *La Rivista del Nuovo Cimento*, **24**, 1-46.
- Ostrovsky, L. A., P. A. Johnson, and T. J. Shankland (2000), The mechanism of strong nonlinear elasticity in Earth solids, in *Nonlinear Acoustics at the Turn of the Millenium: ISNA 15*, edited by W. Lauterborn and T. Kurz, pp. 75-84, American Institute of Physics, College Park, Md.
- Peng, Z., and Y. Ben-Zion (in press), Temporal Changes of Shallow Seismic Velocity around the Karadere-Duzce Branch of the North Anatolian Fault and Strong Ground Motion, *PAGEOPH*.
- Poupinet, G., W. L. Ellsworth, and J. Fréchet (1984), Monitoring velocity variations in the crust using earthquake doublets: an application to the Calaveras Fault, California, *J. Geophys. Res.*, **89**, 5719-5731.
- Rubinstein, J. L., and G. C. Beroza (2004a), Evidence for widespread nonlinear strong ground motion in M_w 6.9 Loma Prieta Earthquake, *Bull. Seism. Soc. Am.*, **94**, 1595-1608.
- Rubinstein, J. L., and G. C. Beroza (2004b), Nonlinear strong ground motion in the ML 5.4 Chittenden earthquake: Evidence that preexisting damage increases susceptibility to future damage, *Geophys. Res. Lett.*, **31**, L23614, doi:10.1029/2004GL021357.
- Rubinstein, J. L., and G. C. Beroza (2005), Depth constraints on nonlinear strong ground motion from the 2004 Parkfield earthquake, *Geophys. Res. Lett.*, **32**, L14313, doi: 10.1029/2005GL023189.
- Saiga, A., Y. Hiramatsu, T. Ooida, and K. Yamaoka (2003), Spatial variation in the crustal anisotropy and its temporal variation associated with a moderate-sized earthquake in the Tokai region, central Japn, *Geophys. J. Intl.*, **154**, 695-705.
- Schaff, D. P., and G. C. Beroza (2004), Coseismic and postseismic velocity changes measured by repeating earthquakes, *J. Geophys. Res.*, **109**, B10302, doi:10.1029/2004JB003001.

- Schaff, D. P., G. H. R. Bokelmann, W. L. Ellsworth, E. Zankerka, F. Waldhauser, and G. C. Beroza (2004), Optimizing correlation techniques for improved earthquake location, *Bull. Seism. Soc. Am.*, **94**, 705-721.
- Su, F., and K. Aki (1990), Temporal and spatial variation of coda Q^{-1} associated with the North Palm Springs earthquake of July 8, 1986, *PAGEOPH*, **133**, 23-52.
- Taira, T. a., and K. Yomogida (2003), Characteristic of small-scale heterogeneities in the Hidaka, Japan, region estimated by coda envelope level, *Bull. Seism. Soc. Am.*, **93**, 1531-1541.
- Taira, T. a., and K. Yomogida (2004), Imaging of three-dimensional small-scale heterogeneities in the Hidaka, Japan region: coda spectral analysis, *Geophys. J. Intl.*, **158**, doi: 10.1111/j.1365-246X.2004.02333.x.
- Uchida, N. *et al.* (2002), Temporal change of seismic-wave velocity associated with the 1998 Northern Iwate Prefecture, Japan Earthquake, *Zisin*, **55**, 193-206 (in Japanese with English abstract).
- Uchida, N. *et al.* (in preparation), A M7 earthquake induced by afterslip of the 2003 Tokachi-Oki earthquake (M8.0),
- Van Den Abeele, K., and K. Van de Velde (2000), Correlation between dynamic nonlinearity and static mechanical properties of corroded E-glass reinforced polyester composites, in *Review of progress in quantitative nondestructive evaluation*, edited by D. O. Thompson and D. E. Chimenti, pp. 1359-1366, American Institute of Physics, College Park, Maryland.
- Vidale, J. E., and Y.-G. Li (2003), Damage to the shallow Landers fault from the nearby Hector Mine earthquake, *Nature*, **421**, 524-526.
- Watanabe, H. (1971), Determination of earthquake magnitude at regional distance in and near Japan, *Zisin II*, **24**, 189-200 (in Japanese).
- Yamanaka, Y., and M. Kikuchi (2003), Source processes of the recurrent Tokachi-oki earthquake on September 26, 2003, inferred from teleseismic body waves, *Earth Planets Space*, **55**, e21–e24.
- Zinszner, B., P. A. Johnson, and P. N. J. Rasolofosaon (1997), Influence of change in physical state on elastic nonlinear response in rock: Significance of effective pressure and water saturation, *J. Geophys. Res.*, **102**, 8105-8120.

Chapter 6

Full Waveform Earthquake Location: Application to Seismic Streaks on the Calaveras Fault, California

Abstract

We use a novel technique based upon source array analysis to locate three moderate earthquakes that occur at the edge of previously identified streaks of seismicity on the Calaveras Fault, California. Our method determines centroid locations for earthquakes, in addition to the hypocenters previously determined using first-break picks. Application of the method to smaller earthquakes indicates that the errors associated with the locations are on the order of 100m, much less than the rupture dimensions of the $M > 4.5$ events that we have analyzed. We treat high-precision locations of microearthquakes near the earthquakes we want to locate as source arrays and compute the slowness of waves leaving these source arrays. We then use the slowness parameters to locate the earthquakes of interest. We find that the medium magnitude events nucleate on the streaks and rupture into a zone devoid of seismicity. Based on this, we argue that streaks represent the boundary between creeping and locked sections of a fault. Our location

The material in this chapter is in preparation for publication in the *Journal of Geophysical Research* with co-author G.C. Beroza.

technique has the potential for wide application, including circumstances where it may be desirable to locate earthquakes without using direct arrivals.

6.1 Introduction

Like their larger relatives, microearthquakes occur on active faults and interact with each other, but they occur much more frequently and hence provide an opportunity to test theories over reasonably short time frames. Precise hypocentral locations are fundamental to understanding the complex physical processes involved in earthquake interaction. Accurate descriptions of both the spatial and temporal offset between microearthquakes are needed to complete studies of earthquake recurrence and interaction. Such studies are now becoming possible as seismologists continually improve the precision of earthquake locations.

A significant source of error in earthquake location arises from inaccurate arrival time measurements. Arrival times are usually picked manually or automatically generated, making them subject to operator error and errors due to emergent onsets. Measurements based on these techniques are also limited in precision by the sampling rate of the seismometers. For example, the timing precision of first arrivals is often on the order of 10-30 msec for Northern California Seismic Network (NCSN) data with 100 sample per second digitization. The computation of relative arrival times of earthquakes using waveform cross-correlation (Poupinet *et al.*, 1984) can reduce the error of relative arrival time measurements to ~1 msec for similar earthquakes. This improvement allows relative earthquake location with errors on the order of meters to tens of meters. The extent to which cross-correlation can be used to improve relative arrival times has been thoroughly explored by *Schaff et al* (2004). Others have reduced the error in earthquake locations by minimizing the influence of unknown earth structure using the “double-difference” method (Waldhauser and Ellsworth, 2000) and by using differential measurements to solve for both hypocenters and velocity structure (Zhang and Thurber, 2003).

While cross-correlation measurements are useful for improving relative arrival time measurements for seismicity in many cases, they fail when waveform similarity is

too low, typically due to a difference in Green's functions (i.e., the earthquakes are located too far from each other to produce a reliable estimate of their relative arrivals) or when focal mechanisms differ. Cross-correlation measurements also fail in the event that the seismogram is clipped, as cross-correlation is dependent upon both phase and amplitude. This leads to the unfortunate situation where the relocations of medium magnitude and large earthquakes, which are often the earthquakes of primary interest, have higher uncertainties than those of nearby microearthquakes. Considering that the stresses released and strains associated with these larger earthquakes are far larger than those of microearthquakes, knowing their locations accurately is particularly important to understand the physical behavior of any fault system. Ironically, the locations of these earthquakes are particularly poorly constrained due to the goals of most earthquake monitoring networks, which often are to record and locate the largest number of earthquakes, and hence the smallest earthquakes, possible. Accelerometer networks supplement high-gain networks and allow for the precise description of larger events ($M > 5.5$). The strong shaking of medium magnitude earthquakes ($M 3.5-5.5$), though, often does not trigger recording on enough accelerometers to produce good quality locations. As a result, medium magnitude earthquakes often have particularly large uncertainties in their locations.

In the interest of improving the locations of the population of medium magnitude earthquakes, we developed a new technique based upon seismic array analysis to improve earthquake locations for sparsely recorded earthquakes. A number of studies have recently used array analysis, based upon receiver arrays, to locate seismic sources (Kao and Shan, 2004; Kao *et al.*, 2005) and image larger events (Ishii *et al.*, 2005; Krüger and Ohrnberger, 2005a; 2005b; Walker *et al.*, 2005; Fletcher *et al.*, submitted). In our method, we treat the precise microearthquake locations made possible by cross-correlation and double difference relocation methods as an array of seismic sources (Niazi, 1969). Using standard array analysis methods, we are able to determine the velocity and propagation direction of energy that is recorded at a single station for many different time windows. With this description of the slowness parameters, we are able to relocate nearby events by finding the location where its waveform best matches that predicted by the source array.

6.2 Geologic Setting and Motivation

We focus our attention on the interplay of medium magnitude earthquakes and recently discovered microearthquake streaks. Streaks are lineations of seismicity within an individual fault. They were first discovered on the south flank of Kilauea volcano, Hawaii (Gillard *et al.*, 1996), and have since been identified on the central San Andreas Fault (Rubin *et al.*, 1999; Waldhauser *et al.*, 2004), the Hayward Fault (Waldhauser *et al.*, 1999; Waldhauser and Ellsworth, 2002), and the Calaveras Fault (Schaff *et al.*, 2002). In all of these locations, the orientation of the streaks is approximately parallel to the direction of slip on the fault. This suggests that streaks are a slip-driven process. Streaks are also consistently found in regions where a significant portion of the slip budget appears to be accommodated by creep. This suggests that the interplay between creep-slip and stick-slip behaviors may play a key role in the generation of this highly organized seismicity pattern. Thus, understanding streaks is important as we expect they will provide clues to the physics underpinning fault mechanics and how slip is partitioned on faults between creep and earthquakes.

For this study, we apply our method to determine precisely the locations of 3 medium magnitude earthquakes. These earthquakes are the largest events that occurred in our study region over a period of 15 years. It follows that these events have had the strongest influence on other earthquakes and creep within the area. The preliminary locations of these earthquakes (M4.5, 4.8, and 5.3) indicate that they are located at the ends of 3 streaks on the Calaveras Fault (Figure 6.1, 6.2) (Schaff *et al.*, 2002). These locations were determined using the double-difference relocation method HypoDD (Waldhauser and Ellsworth, 2000), but cross-correlations were not possible for the waveforms of these earthquakes as the high gain channels on the NCSN were strongly clipped. As a result, only first breaks were used in the relocations of these events, so we expect the locations of these earthquakes will represent their hypocenters, but with larger location errors than for surrounding events as they lack the benefit of precise relative arrival time measurements. This differs from the locations for the cross correlation measured microearthquakes, which represent centroid locations. The onset of clipping of the NCSN, comes first from bandwidth limitations of the telemetry system rather than

clipping of the sensor. Fortunately, within the NSCN, some stations have both low-gain channels and high-gain channels, such that the medium magnitude earthquakes we are interested in were recorded unclipped at a handful of stations.

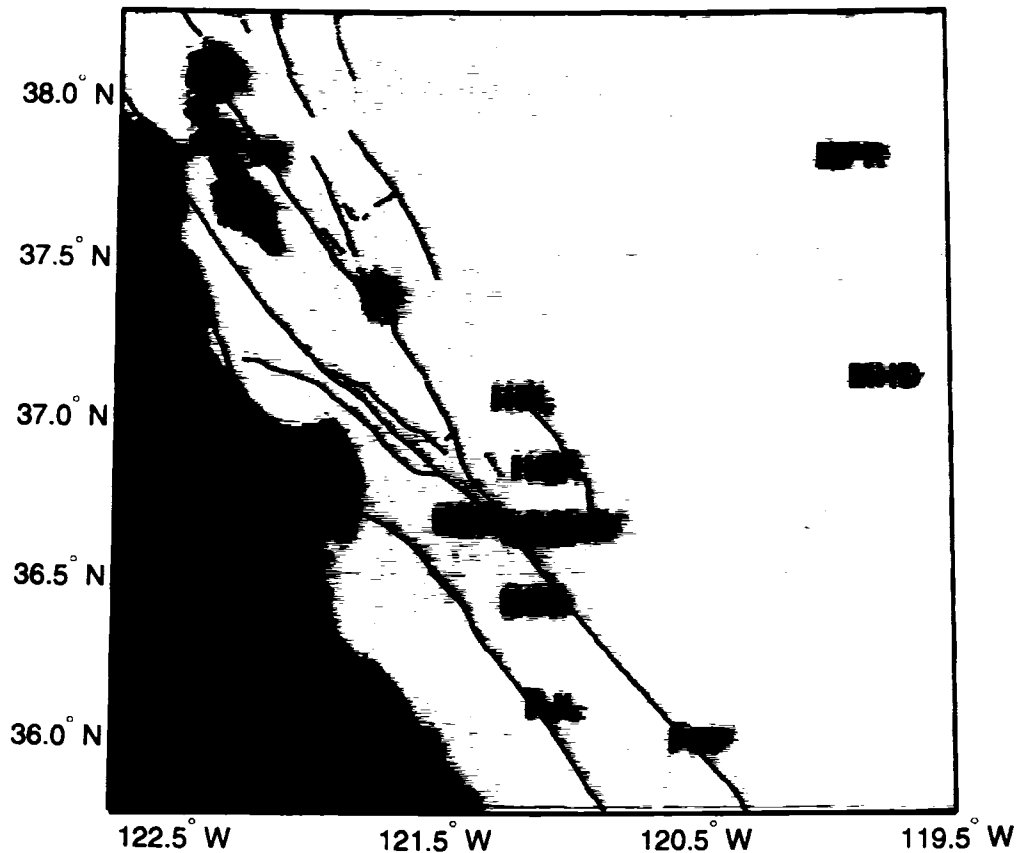


Figure 6.1: Map of the study region and the seismometers used. Blue stars indicate locations of the medium magnitude earthquakes we are locating. Red lines indicate faults.

6.3 Method

Our technique is based upon standard array processing techniques. A thorough review of array techniques can be found in *Rost and Thomas (2002)*. In standard array analysis, seismologists typically assume plane wave propagation through an array of receivers with known locations to predict the relative arrival time of phases within the receiver array. We use the reciprocal geometry, where we have an array of seismic sources and one receiver to determine the propagation patterns within our source array.

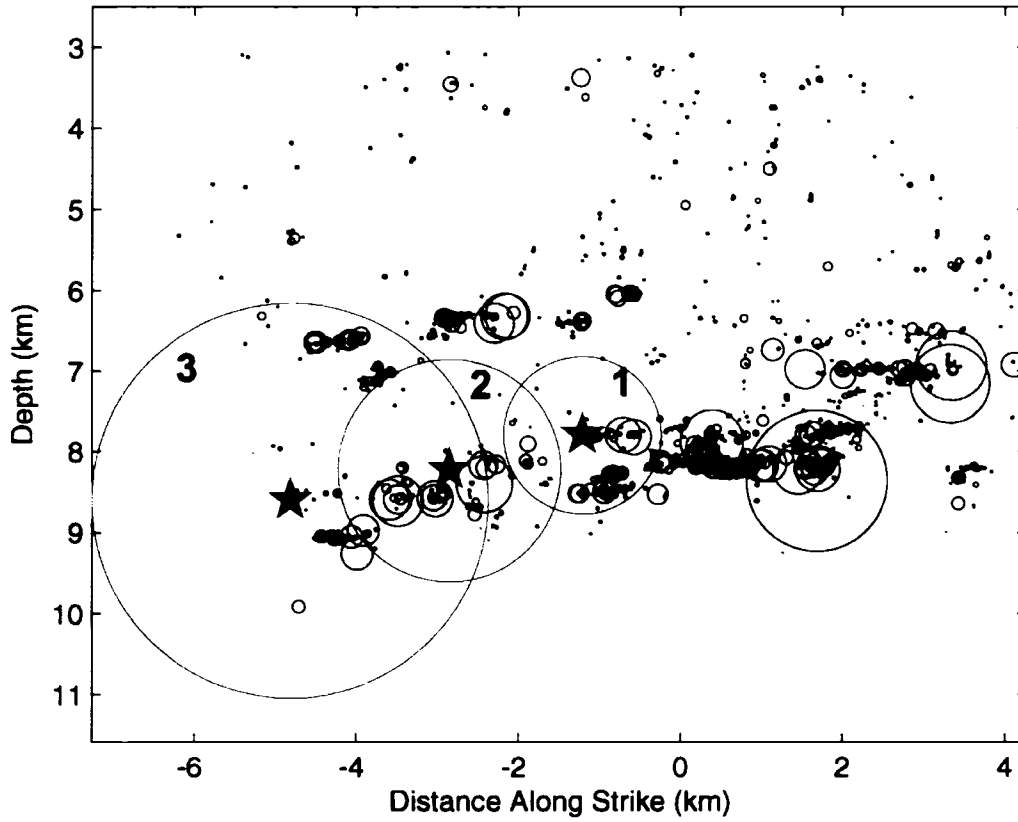


Figure 6.2: Cross section showing locations of seismicity on the Calaveras fault determined by *Schaff et al.* (2002). Circle size represents approximation of the source given the assumptions of circular rupture with a 30 bar stress drop. The red circles represent the approximate rupture extent of the three medium magnitude earthquakes we are re-locating. The red stars represent hypocenters of these earthquakes as determined by double-difference relocation by *Schaff et al.* (2002). The numbers indicate the earthquake number as referred to in the paper.

A schematic description of this technique can found in Figure 6.3, which is Figure 2 from *Dodge and Beroza* (1997). This method was first proposed by *Niazi* (1969) and again by *Spudich and Bostwick* (1987). Others have developed more advanced techniques that utilize both source and receiver arrays (double beam analysis (*Krüger et al.*, 1993) and double beam imaging (*Scherbaum et al.*, 1997) to produce refined images of the mantle and the core mantle boundary region. Here we use source-array beamforming to determine slowness parameters for multiple time windows for source arrays centered on the earthquakes that we want to locate. Once we have the slowness parameters, we then search for the optimal location of the earthquake based upon the stacks of the source

array and the waveforms of the earthquake we are locating. We discuss the method more fully below.

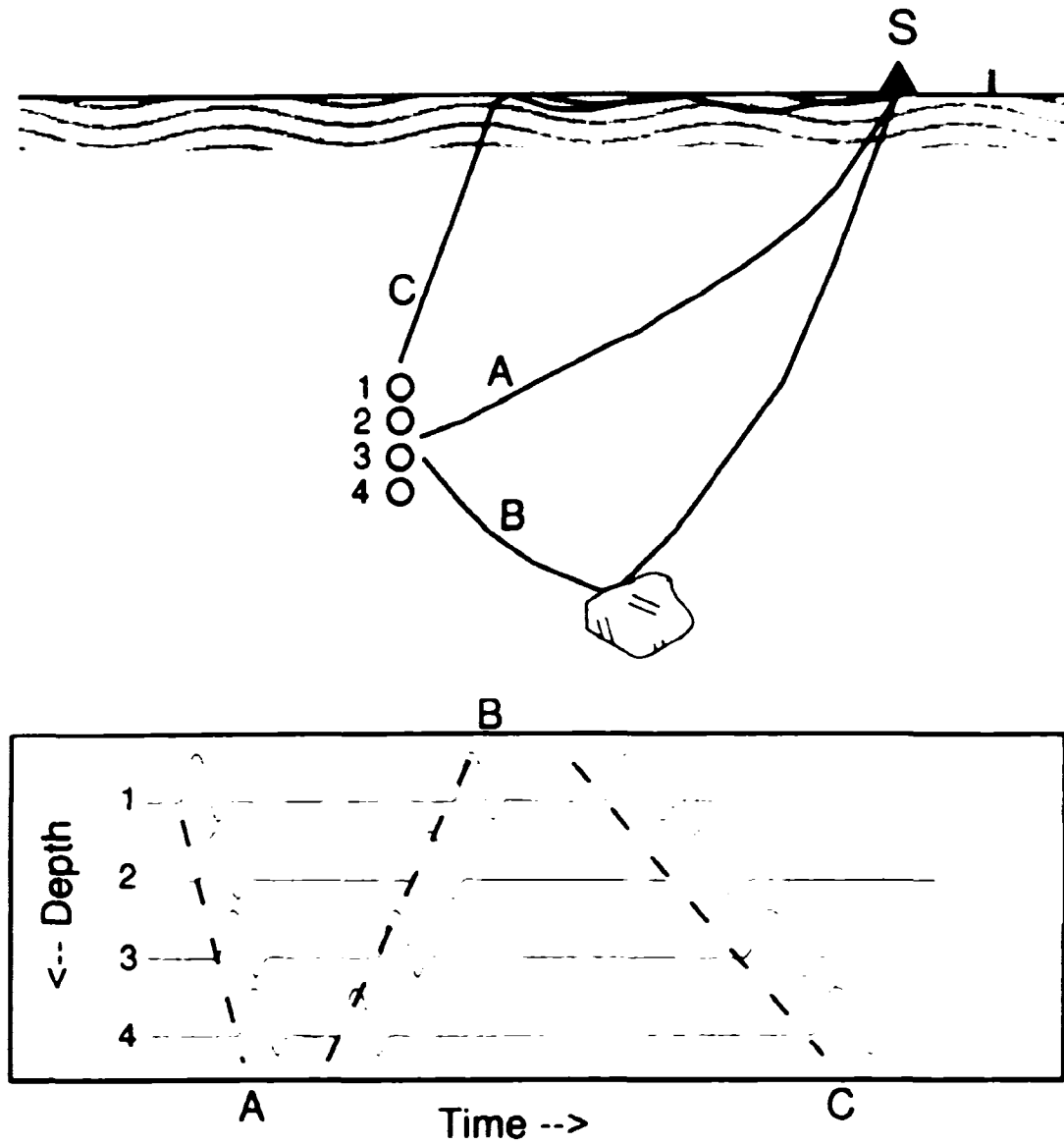


Figure 6.3: Schematic representation of source array analysis from *Dodge and Beroza (1997)* which has a vertical column of earthquake hypocenters numbered 1 to 4 and the raypaths for three arrivals A, B, and C. Lower panel shows simplified waveforms for these three arrivals and their differing moveouts that depend on the path that they took leaving the source array.

6.3.1 Precise Determination of Slowness Parameters

We use the catalog of earthquakes produced by *Schaff et al. (2002)* as the basis of locations for this study. For each medium magnitude earthquake that we are trying to locate, we choose a source array of earthquakes to determine wave propagation parameters. Our source arrays are defined as any earthquake in our catalog that falls within 3 km of the medium magnitude earthquake that we are trying to locate. The arrays have a radius of 3 km to ensure that there are enough events to produce a reliable estimate of the slowness parameters, but Each station has a slightly different source array, depending on which earthquakes it recorded. We require a minimum of 35 events contributing to the source array to ensure a sound basis for our slowness determination. The majority of the source arrays have much more than 35 events in their source array, and many have more than 100. We only assemble source arrays for stations where a reliable, low-gain recording of the medium magnitude earthquake in question was available (the stations that we used to locate each earthquake are indicated in Table 6.1, see also Figure 6.1).

Table 6.1: List of earthquakes relocated by each station

Station*	Medium Magnitude Earthquakes Relocated
BAV	1,2,3
BSC	2,3
BSG	1,3
BSR	1
CYB	1
HPL	1,3
HQR	2
MHD	1
MPR	1
PHP	1
PJL	1

*Station locations are indicated in Figure 6.1

Prior to beamforming, we bandpass filter the seismograms from 1-6 Hz and normalize the power of the traces to 1 for a 24 s window starting 2 s before the P arrival. Traces where the signal to noise ratio does not exceed 3 and seismograms that are clipped are removed.

Given the source arrays, we then use delay and sum beamforming to determine wave propagation parameters for 20 time windows. For any trial slowness parameters \tilde{p}_{acd} , the source array stack \tilde{S}_{acd} is determined to be:

$$\tilde{S}_{acd}(\tilde{p}_{acd}, t_{ac}) = \sum_{b=1}^N w_{ab}(t_c - \tilde{p}_{acd} \cdot x_b) + n_{abc}$$

with:

- a station number
- b event number in the source array
- c time window
- d bin number for trial slowness
- t time
- w the waveform (assumed constant over the whole array)
- \tilde{p} trial wavefield slowness
- x the relative position of the source
- N the number of events recorded by station i in this source array
- n noise.

Referring back to Figure 6.3, we assume we know our source locations very well (i.e., 1-4), but the propagation velocity and paths leaving the source array (i.e., A-C) we treat as unknowns. The time windows are 2 seconds long, with the first window centered

on the P arrival. The windows are stepped forward at increments of 1 second. We use a gridsearch method to determine the optimum slowness p_{ac} . We, actually, search over velocity, azimuth, and angle of incidence and compute the trial slowness \tilde{p}_{acd} from these parameters. For azimuth and angle of incidence, we use a grid spacing of 5° . We search over two velocities (3175 m/s and 5500 m/s). These are the S and P velocities that *Schaff et al.* (2002) used to locate these earthquakes. The velocities at these depths will not perfectly match these numbers, but they are consistent with the relative locations of the events within our source arrays as originally determined by *Schaff et al.* (2002). The optimum slowness parameters for any station a and time window c , p_{ac} , are selected to be those where the power of our source array stack \tilde{S}_{acd} is maximized.

For there to be constructive interference and our stacking procedure to work, the relative errors in our earthquake locations must be less than $\frac{1}{4}$ of the shortest wavelength that we examine. Thus, given that the P velocities within our source region are believed to be 5500 m/s, the error in the locations cannot exceed 230 m for us to be certain of constructive interference. *Schaff et al.* (2002) cites the relative location error within small regions to be on the order of meters to tens of meters. Based on this criterion, our methodology should work.

Using the above described methodology, we compute the ideal slowness parameters p_{ac} describing the departure velocity and angles of 20 windows of energy leaving the source region for every station/source array pair. Some example results are shown in Figures 6.4-6.6. Figure 6.4 shows that the beamforming is working; when the waveforms are aligned by origin time, there doesn't appear to be any correlation between the waveforms, but taking location and preferred propagation direction into account shows a coherent waveform, the stack of which has much more power than those aligned on origin time. In Figure 6.5 we see that the stack is most powerful in a narrow range of azimuths and departure angles. This is typical, the majority of the energy we examine for both S and P is coming from a very limited range of azimuths and incidence angles that are close the azimuth from the station to the receiver (Figure 6.6). Other studies examining the early coda also identify that the majority of energy appears to be scattered locally (*Scherbaum et al.*, 1991; *Dodge and Beroza*, 1997).

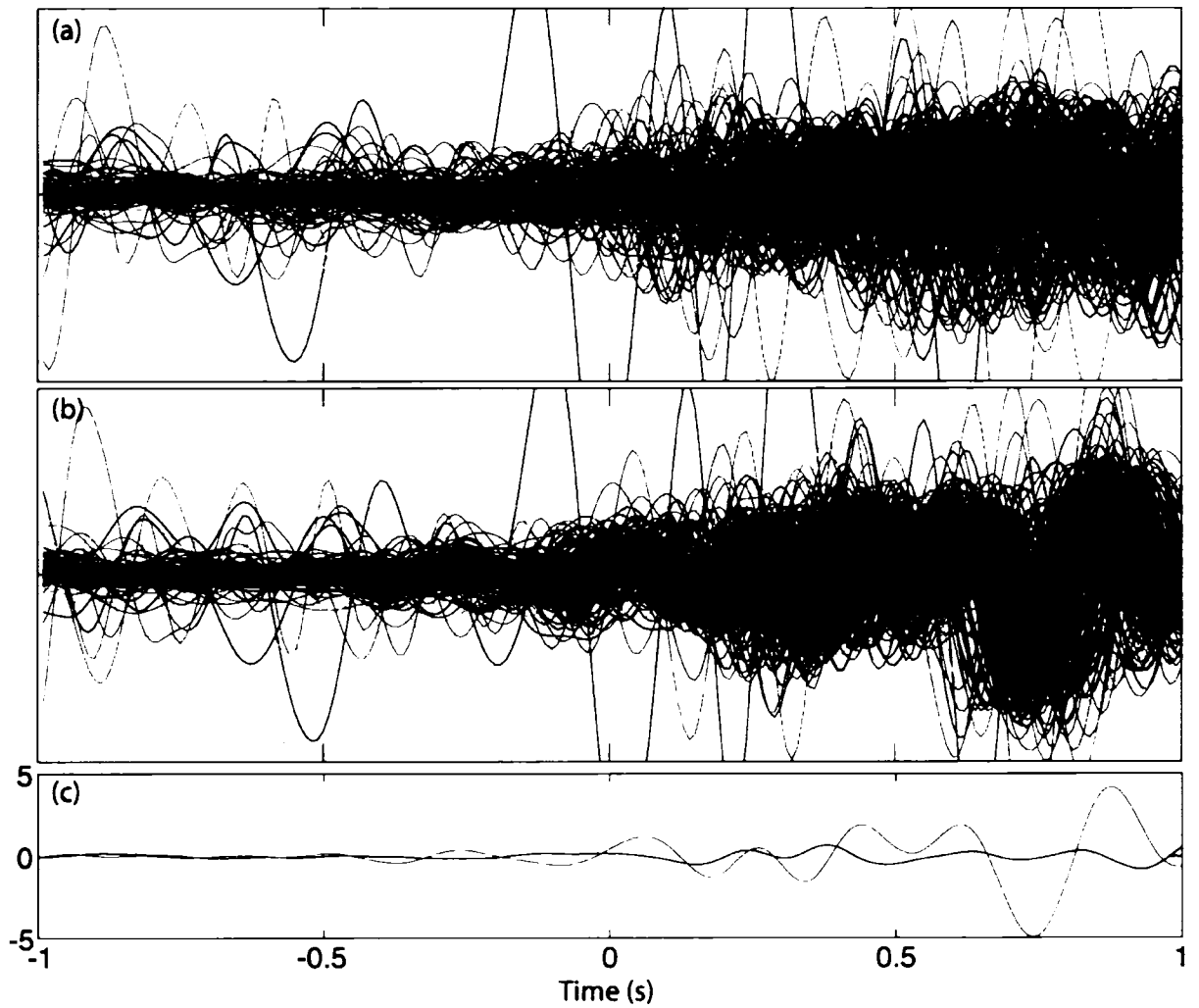


Figure 6.4: Waveforms from the first window for station BAV for medium magnitude earthquake #1. (a) Waveforms aligned based on origin time only. (b) Waveforms aligned using ideal slowness parameters. (c) Stack of all the waveforms aligned based on origin time only (blue) and aligned using ideal slowness parameters (red).

6.3.2 Precise Determination of Earthquake Locations

Once we have computed the slowness descriptions p_{ac} for each window for each source array/station pair, we follow a very similar method to determine the location for the medium magnitude earthquake. We take the preferred slowness parameters p_{ac} determined by the above method for an individual window of one source array at one station, and compute a stack specific to that window, array, station combination. This

stack represents our best approximation of how the waveform should look at a specific station for our earthquake in question. We refer to this as the microearthquake stack, M_{ac} .

$$M_{ac}(p_{ac}, t_{ac}) = \sum_{b=1}^N w_{ab}(t_c - p_{ac} \cdot x_b) + n_{abc}$$

We then search over earthquake location parameters (x , z , and t), shift the trace of our large event accordingly, and sum this with the microearthquake stack. If we refer to Figure 6.3, schematically we could say that we now know our propagation velocities and directions (i.e., A-C), but the earthquake location of our large earthquake is unknown so we search over locations (i.e., 1-4) to identify the ideal earthquake location. This sum of the microearthquake stack and the waveform of the medium magnitude earthquake, we refer to as a location stack \tilde{L}_{acef} , where:

$$\tilde{L}_{acef} = G_{ac} M_{ac} + \tilde{H}_{acef} W_{ac}(t_c - p_{ac} \cdot (X_0 + \tilde{X}_e) + \tilde{t}_{0f}) + n_{ac}^0$$

with:

- W the seismogram of the earthquake that we are relocating
- X_0 the initial, relative position of the earthquake that we are relocating
- G weighting factor of the microearthquake stack
- \tilde{H} weighting factor for the earthquake that we are relocating
- \tilde{X} trial movement of the earthquake that we are locating
- \tilde{t}_0 trial time offset for the centroid time of the earthquake that we are locating
- e bin number for the movement of the earthquake along the fault strike
- f bin number for the centroid time offset
- n^0 noise for the earthquake being located.

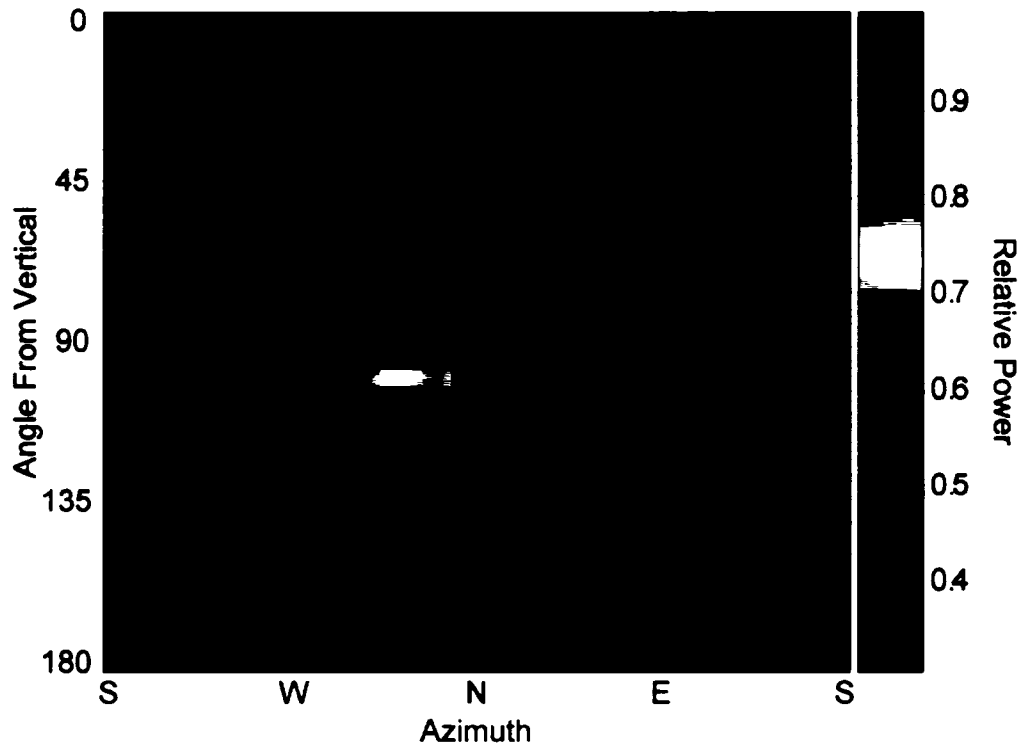


Figure 6.5: Power of the stack of the second window \tilde{S}_{acd} for medium magnitude earthquake #1 at CYB. Angle from the vertical represents the difference from an upgoing wave, i.e., 0° represents an upgoing wave, 90° a horizontal wave, and 180° a downgoing wave. For this figure the power is normalized to the maximum power for this specific window.

The nodes of our grid are separated by 20 m for x and z, and 0.025 s for origin time. We search over a range of ± 1 km in x and z, and ± 1 s in t. The variable x represents distance along the strike of the fault and z represents depth; we do not search for locations of the events that are off the fault, i.e. the y coordinate is fixed *a priori*. We do this for two reasons. First, the Calaveras has been shown to be particularly thin in this region, typically less than 75 m at depth (Schaff *et al.*, 2002) and it is unlikely that the largest ruptures in the vicinity occur off the main fault plane. We also have very little resolution perpendicular to the plane of the fault as the majority of our stations are located at azimuths similar to that of the fault plane. This means that the propagation direction can be approximated to be down the fault, making the plane of uncertainty perpendicular to the fault.

For the location stacking that we do, we note that we normalize the power of the window of both the microearthquake stack and the large earthquake seismogram to 1 using weighting factors G_{ac} and \tilde{H}_{acef} , respectively. This way, the power Q_{acef} of any location stack \tilde{L}_{acef} represents the similarity in phase between the microearthquake stack and the waveform of the large earthquake. It gives secondary importance to amplitudes, but each window has the potential to sum to the same power allowing for easy comparison of different windows. To determine the optimum location predicted by this method at one station, we sum the power of the location stacks Q_{acef} for all 20 time windows. For any individual station a , this produces a matrix describing the power of the location stacks for any x, z, t combination M_{aef} , where:

$$M_{aef} = \sum_{c=1}^{20} Q_{acef}$$

The maximum value of M_{aef} indicates the preferred centroid (x, z, t) of the large earthquake as determined by an individual station. We can further refine this estimate by summing these matrices over all of our stations. The result is a matrix R_{ef} that describes the total power for any location (x, z, t) over all the stations for all 20 time windows

$$R_{ef} = \sum_{a=1}^S M_{aef}$$

where S represents the number of stations used to locate the earthquake in question. The values of M_{aef} should be comparable from station to station as the normalization emphasizes similarity in phase and not relative amplitude. We treat the location determined from this stack as the centroid location. We call it the centroid because the stacking will prefer to put the earthquake in a location where the apparent moment-rate (slip-rate) was largest. An example of the product of the stacking is shown in Figure 6.7. From this figure we see that there is a location where the energy appears to focus and

individual stations are consistent with the location predicted by a stack of all the stations. The final centroid locations we determine using this technique are shown in Figure 6.8 and listed in Table 6.2.

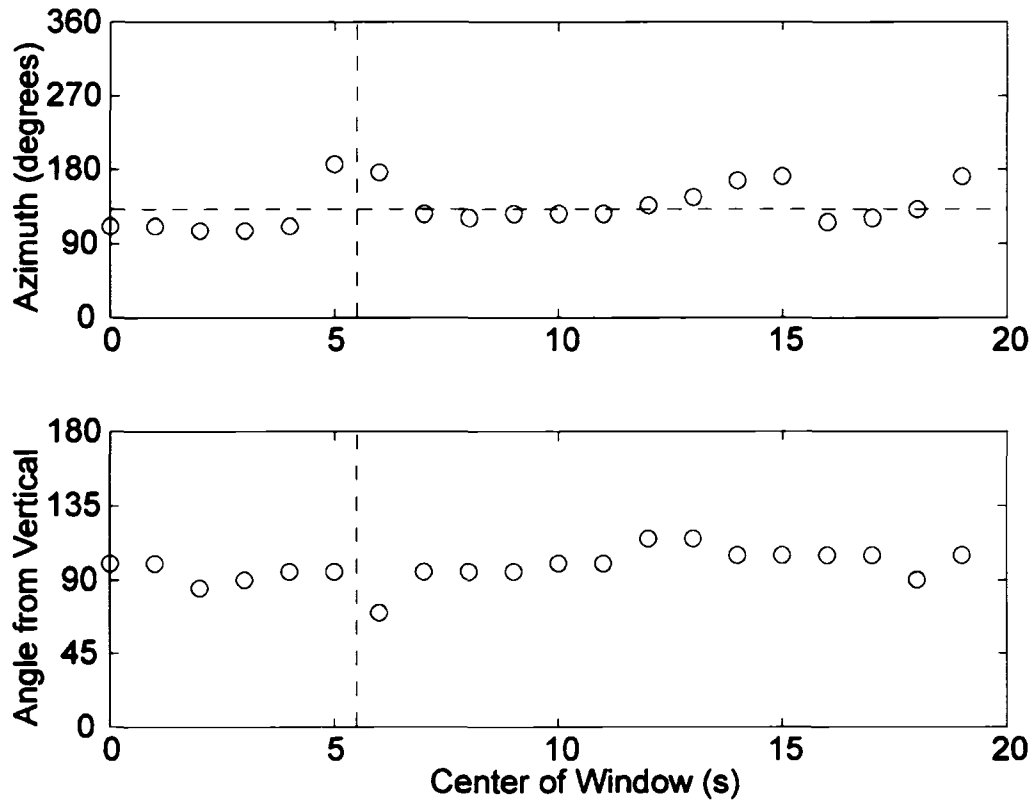


Figure 6.6: Plots showing the optimal propagation azimuth (a) and angle from the vertical (b) for all 20 time windows at station HPL for medium magnitude earthquake 1. The vertical dashed lines approximate the S arrival. The horizontal dashed line in (a) indicates the approximate azimuth of the source arrays to HPL.

6.3.3 Error Analysis

We are interested in the knowing the approximate uncertainty in the locations of the three medium magnitude events that we've relocated. To get a sense of the uncertainties in these locations, we apply the same method we used to locate the medium magnitude earthquakes to relocate 15 microearthquakes, the locations of which we know very well from the cross-correlation/double-difference locations computed by *Schaff et al.* (2002). Any deviation of our relocations from our starting locations, which are

believed to have uncertainty on the order of tens of meters (Schaff *et al.*, 2002), can be considered an estimate of the location uncertainty of the larger events.

For each of our three medium magnitude events, we relocate 5 nearby “trial events”. For medium magnitude earthquakes 2 and 3, we choose the 5 earthquakes closest to the catalog hypocenter of the large event that were recorded by all the stations that located the larger event. For medium magnitude earthquake #1 it is much more difficult to find earthquakes that were recorded by all 9 stations used to locate it. For this event we choose the 5 events closest to medium magnitude event #1 that were recorded by at least 5 of the 9 candidate stations. We also required that each station be used for at least one error estimate. We use the events believed to be closest to the center of our source arrays for error estimation because the waveforms for these events will be better approximated by our source array than those on the extremities. The average distance of our “trial events” to the catalog hypocenter for each source array is approximately 500m, approximately the same distance as our relocations. This suggests that the error estimates from the trial events will be reasonable.

Event	X offset (m)	Z offset (m)	t offset (s)
1	-340	-520	0.55
2	-260	160	0.30
3	-420	-320	0.55

Table 6.2: Movement of each of the medium magnitude events predicted by the repeated source array analysis. Negative offset in X means movement to the NW. Negative offset in Z means movement up. Positive offset in time implies that the earthquake centroid time was later than that predicted by the initial location.

It is important to note that for the locations that we compute for error estimation, we use the same slowness parameters used to determine the locations of the medium magnitude earthquakes. This is a bit circular in that the waveforms of the earthquakes that we relocate for error estimation are also used to determine the slowness parameters used for their relocation. However, the influence of any one earthquake should be relatively negligible in the slowness estimates, as we require a minimum of 35 waveforms for the slowness estimates.

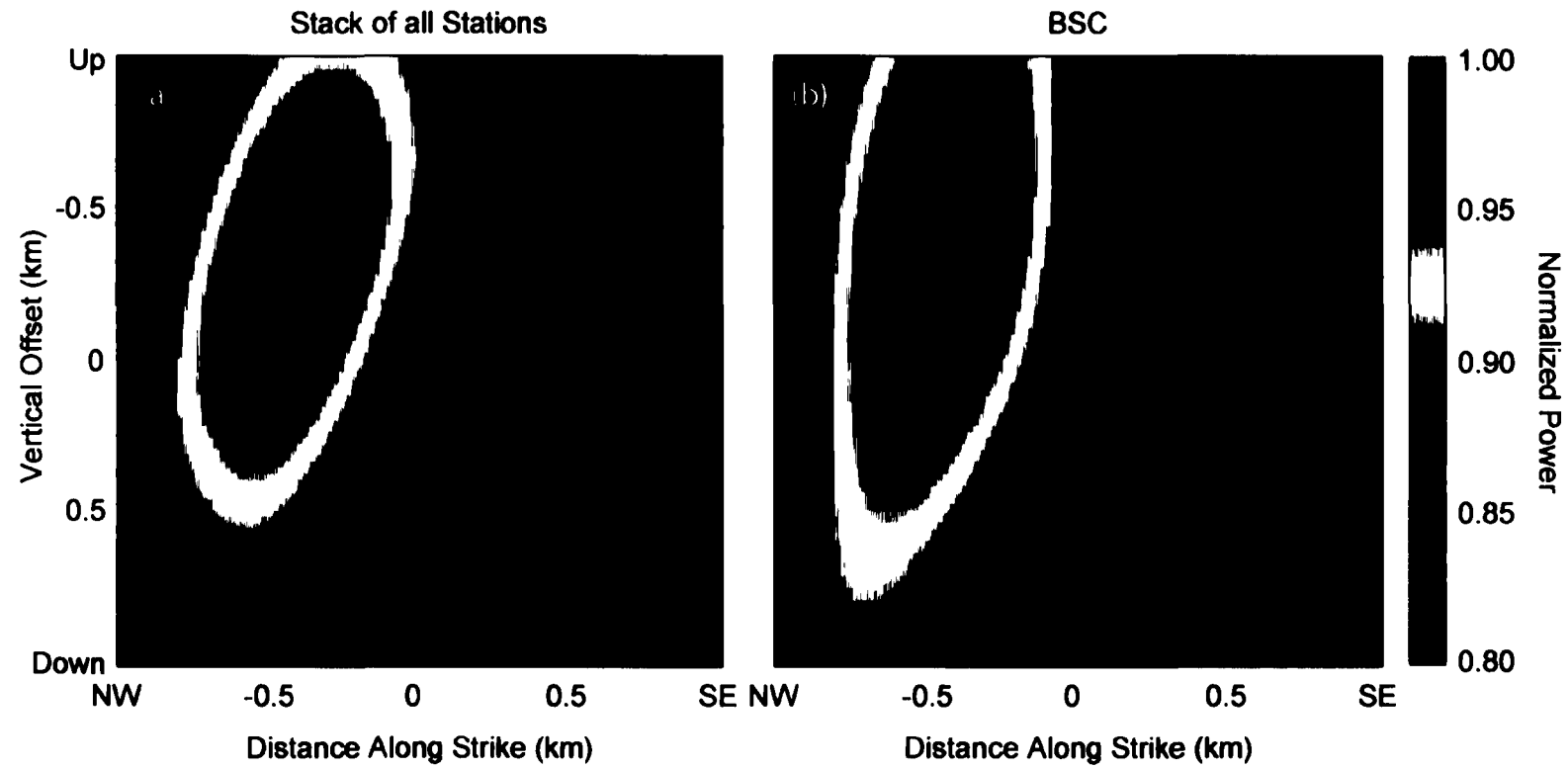


Figure 6.7: Location of earthquake #3 as determined by (a) a stack of all our stations, and (b) a stack of station BSC. (a) represents R_{ef} . (b) represent M_{def} . We note that time is also a variable in our location stacking. Here we show cross sections using the preferred time offset, as identified by the maximum power of the stack, thus fixing f .

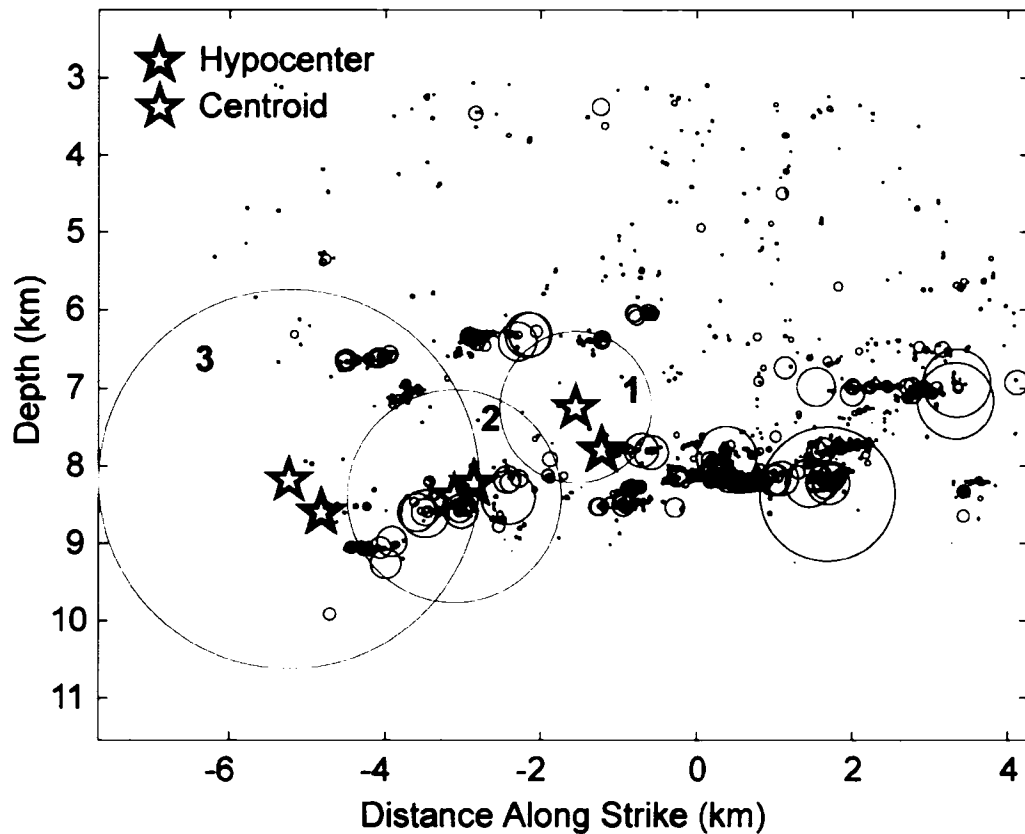


Figure 6.8: Relocations of the 3 medium magnitude earthquakes. Black stars indicate the hypocenters as determined by *Schaff et al. (2002)*. Red stars indicate centroid relocations. Circles represent an approximate rupture dimension assuming circular rupture and uniform 30 bar stress drop. The red circles show approximate rupture location given the new centroid locations. Numbers indicate the earthquake number referred to in this paper.

We find that the error estimates to be relatively consistent, both for all the test events for any medium magnitude event and from medium magnitude event to medium magnitude event (Table 6.3). Because the estimates are relatively consistent for all the test events of any individual medium magnitude earthquake we take the mean of their values and treat that as the uncertainty in their centroid locations. These errors (approximately 100-150 m in x and z, and 0.025 s) are substantially smaller than the movements of the medium magnitude earthquakes (approximately 300 m in x and z, and 0.4 s) found from our relocations (Table 6.2). Uncertainties in the centroid locations are not shown in our cross-section showing the earthquake locations (Figure 6.8), as the size

of the stars representing the centroids are approximately 500m across, such that location uncertainty for all three earthquakes falls within the star representing their centroid.

We note that there does appear to be a bias in our locations, in that all the trial locations for each source array are located systematically in the same direction relative to their double-difference determined locations (Table 6.3). For example, the locations of all the trial events for source array 1 are all to the southeast and above the locations

Test Event #	X error (m)	Z error (m)	T Error (s)
		Source Array 1	
1	40	-80	0.050
2	100	-40	0.025
3	300	-400	0.050
4	180	-80	0.025
5	120	-100	0.000
Mean	148	-140	0.030
		Source Array 2	
1	-200	260	0.025
2	-200	160	0.000
3	-140	60	0.050
4	-100	40	0.050
5	-60	40	0.000
Mean	-140	112	0.025
		Source Array 3	
1	60	-20	0.000
2	60	-20	0.000
3	100	-20	0.000
4	140	0	0.000
5	160	-20	0.025
Mean	104	-16	0.005

Table 6.3: Error estimates from relocations of previously well-located earthquakes. Positive x indicates that the earthquake location that we determine is located to the southeast of the actual location. Positive z indicates that the earthquake location that we determine is below the actual depth. Positive t indicates that the origin time we determine is later than the actual time.

determined by *Schaff et al.* (2002). While the consistent mislocation of our trial events shows a bias, the errors introduced by this bias are small. As noted above, the approximate error in any parameter is much less than the movement of our medium

magnitude earthquakes, and the bias is not strong enough to undermine our interpretation. There are a number of potential sources for this bias. The bias may result from the unfavorable station geometry; the majority of our stations are located at azimuths to the earthquake similar to that of the fault. This stems from the local network geometry, which has the majority of seismometers, in particular the low-gain stations, placed near the most-active faults. The bias also may arise from the unfavorable geometry of our source arrays. The highly organized nature of streak seismicity creates an “array-response”, which results in a large uncertainty in the determination of slowness parameters and potentially influences the locations determined by our method. Another alternative explanation, which we find unlikely, is that the earthquake locations determined by *Schaff et al.* (2002) have an internal bias. We discount this explanation because the bias in our test locations is not consistent from source array to source array.

6.4 Interpretation

The earthquake relocations that we have computed for our three medium magnitude earthquakes suggest that streaks represent a rheologic boundary between creeping and locked (or partially locked) portions of a fault. Others have also argued that the interplay between creeping and locked sections of faults may be responsible for the generation of streaks (Waldhauser *et al.*, 1999; 2004). The hypocenters of events 1 and 3, as determined by *Schaff et al.* (2002), are located on a streak and the centroids are located updip of the hypocenters, suggesting that the rupture propagated updip (Figure 6.8). Others have seen a predominance of updip rupture propagation in this same region (Boatwright and Seekins, 2004). The centroid locations of the medium magnitude earthquakes places them directly between two streaks in a region that is relatively devoid of seismicity. The lack of microseismicity and the presence of larger events that appear to rupture into and across the width of the region between the two streaks, suggests that it is a locked zone, where the bulk of the local slip rate is accommodated through seismic slip. This behavior (moderate earthquakes occurring in regions devoid of microseismicity) has been observed for the Calaveras Fault before (Oppenheimer *et al.*, 1990; Manaker *et al.*, 2003). We argue that the region above the upper streak and below the lower streak accommodate much of their slip through creep processes. This is

supported by the fact that the lower streak marks the bottom of the seismogenic zone on the Calaveras fault, suggesting that ductile processes accommodate slip on the fault below the lower streak. Moreover, *Schaff et al.* (1998) found that the recurrence intervals of repeating earthquakes on the Calaveras fault following the 1984 Morgan Hill earthquake was consistent with them being driven by post-seismic creep under steady-state velocity strengthening friction. There is also significant evidence for surface creep in this region (Galehouse and Lienkaemper, 2003), which is consistent with the notion that the region above the upper streak accommodates much of its slip in creep. This suggests that streaks mark the boundary between regions that slip aseismically and regions that accommodate their slip seismically. Similar observations have been made for streaks on the San Andreas Fault in the Parkfield region, where medium magnitude earthquake nucleate on a deeper streak and rupture into a region devoid of microseismicity (Waldhauser *et al.*, 2004).

The location of medium magnitude earthquake 2 does not fit the above model. Unlike events 1 and 3, the interpretation of rupture propagation for event 2 is less clear. One possibility is that the location of the centroid very close to the hypocenter indicates bilateral rupture. This event appears to nucleate and propagate in a section of the lower streak that is dominated by seismicity that is larger than the majority of events near the hypocenters of events 1 and 3. This difference in the local seismicity may explain the difference in the rupture propagation. It is possible that the boundary between creeping and locked portions of the fault here is less distinct.

We also note that all three earthquakes had a centroid time that was significantly later than their origin times (Table 6.2). We consider this further evidence that our method is working. As argued above, the locations we determine approximate earthquake centroids, the timing of which should be significantly later than the hypocenter, to allow for rupture propagation. Based on the centroid time shift, event 2 appears to be less unilateral than events 1 and 3 (which are certainly not completely unilateral). This parallels our observations of the distance between the hypocenters and centroids of these events.

6.5 Locating Earthquakes Without Direct Arrivals

In this section we demonstrate that it is possible to locate earthquakes using the coda alone, i.e. no direct arrivals. *Snieder and Vrijlandt (2005)* demonstrated that the coda can be used to determine the relative positions of earthquakes, but did not use that information to compute relative locations. In that study, they show that using a moving window cross-correlation one can approximate the distance between two earthquakes.

To compute earthquake locations using only the coda, we remove those windows that include the direct arrivals. As a conservative estimate, we decide that the first 2 seconds of both the P and S arrivals represent directly propagating waves. We remove our first 3 windows (the first window is centered on the P arrival) and the first 3 windows that we determine to be dominated by S energy. To compute the earthquake locations, we follow the same method as before and sum all of our windows at every station (now we only have 14 windows to work with, instead of 20 when we included the direct arrivals). For each earthquake, we then sum over all of our stations. These locations are remarkably similar to those that we determined using both the coda and the direct arrivals (Table 6.2, 6.4, Figure 6.9). This is sensible in that the majority of the windows that we used in our full-waveform locations are still included. It does, however, demonstrate that the coda alone can be used for earthquake location. We also compute error estimates for the coda-only based locations. They behave similarly to those that used both the direct arrivals and the coda, so we only report the average error for each earthquake located in Table 6.4. We do see that the width of the high power area of the location is slightly less when we include direct arrivals than when we use coda alone. This implies that the energy in the direct arrivals is helping to refine the estimate of our locations, however, clearly the coda alone clearly provides enough information to locate the earthquakes.

	X (m)	Z (m)	T (m)
Event 1	-360 +/- 132	-480 +/- 128	0.55 +/- 0.035
Event 2	-260 +/- 096	100 +/- 100	0.30 +/- 0.030
Event 3	-320 +/- 124	-440 +/- 008	0.55 +/- 0.005

Table 6.4: Offset of earthquakes determined using coda only. Errors computed as the mean of the errors determined using the test events.

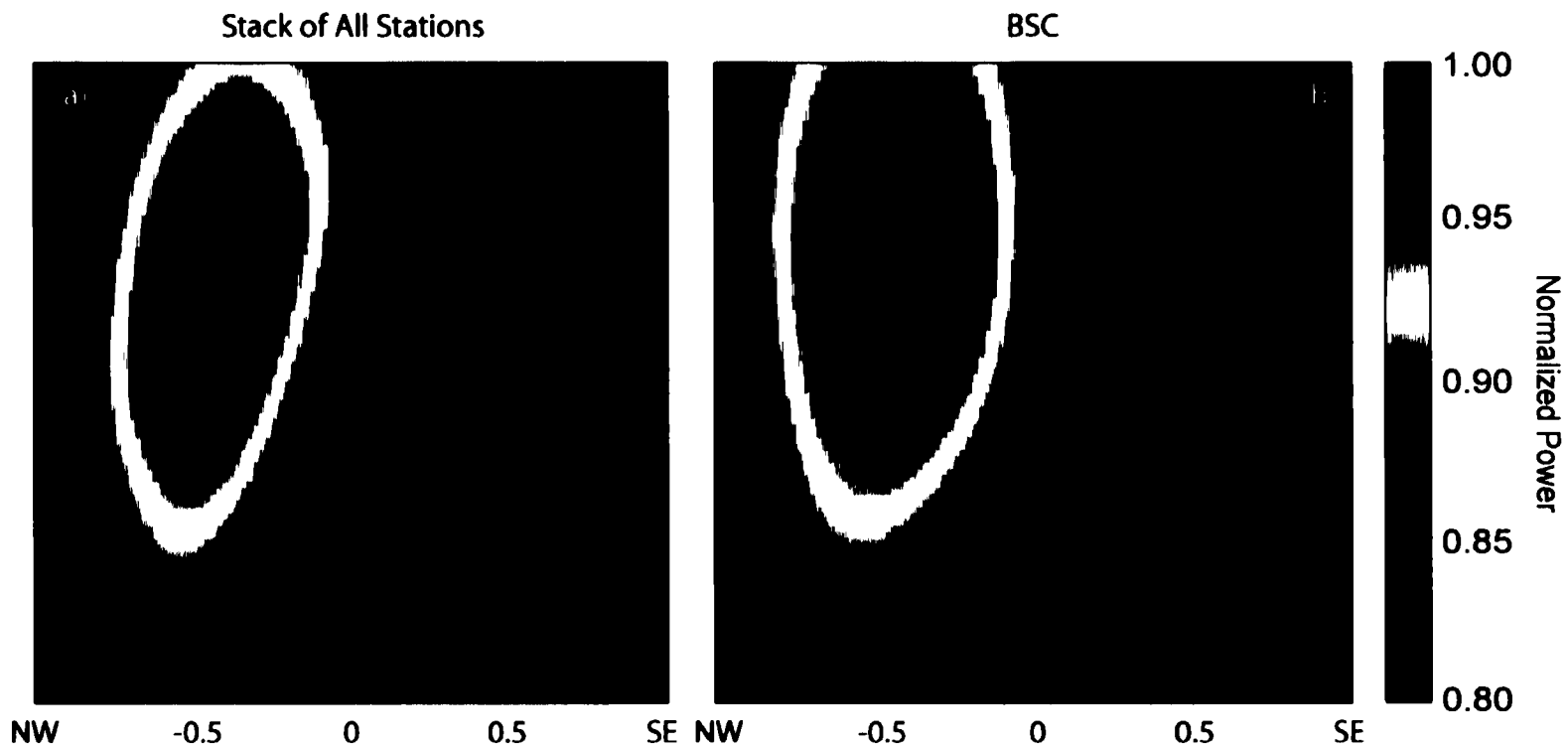


Figure 6.9: Location of earthquake #3 as determined using only the coda for (a) a stack of all our stations, and (b) a stack of station BSC. This is the same Figure as 6.7, only with the direct arrivals removed. The figures are remarkably similar, showing that the coda is controlling the location. We note that time is also a variable in our location stacking. Here we show cross sections using the preferred time offset, as identified by the maximum power of the stack.

6.6 Conclusions

In this paper we presented a technique based upon source-array analysis to locate earthquakes reliably with data from only a few stations at a limited range of azimuths. Our results prove very useful in showing the rupture propagation of medium magnitude earthquakes near streaks on the Calaveras Fault. We determine that these events nucleated on streaks and ruptured into a region relatively devoid of seismicity that we infer to be locked. Because we believe the regions above and below this region that lacks seismicity to be accommodating slip through creep, we argue that the streaks delineate the boundary between creeping and locked sections of a fault. The interplay between creeping and locked sections is likely what drives the lineation in seismicity.

With our method we are able to locate earthquakes reliably when other methods cannot. We take advantage of the information contained within both the P and S codas, which is neglected by standard methods, to compute precise earthquake locations. We demonstrate the power of the information contained within the coda, as we are able to locate earthquakes using only the coda. The uncertainties in the locations determined using the coda alone, are similar to those where we used both the coda and direct arrivals. In principle, the extra information in the coda might be further exploited to locate earthquakes using only 1 station, given a strongly scattering medium. With our current dataset, this is not possible as the large majority of energy is forward scattered, but if we extend the technique to longer times, it might work as later portions of the coda have been shown to be composed of more strongly scattered energy (Scherbaum *et al.*, 1991).

Acknowledgements

We thank Jack Boatwright for many useful and spirited conversations. We acknowledge David Schaff for publicly sharing all his relocation results. All the data used in this study came were made available through the NCEDC. The data were provided by the NCSN, via the USGS Menlo Park. J.R. was partially supported by the William K. Whiteford Fellowship.

References

- Boatwright, J., and L. C. Seekins (2004), Inverting peak ground motions for rupture directivity in moderate and large earthquakes, *Eos Trans. AGU*, **85**, Fall Meet. Suppl., Abstract S24A-05.
- Dodge, D. A., and G. C. Beroza (1997), Source array analysis of coda waves near the 1989 Loma Prieta, California, mainshock: Implications for the mechanism of coseismic velocity changes, *J. Geophys. Res.*, **102**, 24,437-424,458.
- Fletcher, J. B., P. Spudich, and L. M. Baker, Rupture propagation of the 2004 Parkfield, CA, earthquake from observations at the UPSAR array, article *submitted to Bull. Seism. Soc. Am.*,
- Galehouse, J.S. and J.J. Lienkaemper (2003). Inferences draw from two decades of alinement array measurements of creep on faults in the San Francisco Bay Region, *Bull. Seism. Soc. Am.*, **93**, 2415-2433.
- Gillard, D., A. M. Rubin, and P. Okubo (1996), Highly concentrated seismicity caused by deformation of Kilauea's deep magma system, *Nature*, **384**, 343-346.
- Ishii, M., P. M. Shearer, H. Houston, and J. E. Vidale (2005), Extent, duration and speed of the 2004 Sumatra-Andaman earthquake imaged by the Hi-Net array, *Nature*, **435**, doi: 10.1038/nature03675.
- Kao, H., and S.-J. Shan (2004), The Source-Scanning Algorithm: mapping the distribution of seismic sources in time and space, *Geophys. J. Intl.*, **157**, doi: 10.1111/j.1365-246X.2004.02276.x.
- Kao, H., S.-J. Shan, H. Dragert, G. Rogers, J. F. Cassidy, and K. Ramachandran (2005), A wide depth distribution of seismic tremors along the northern Cascadia region, *Nature*, **436**, doi:10.1038/nature03903.
- Krüger, F., and M. Ohrnberger (2005a), Spatio-temporal source characteristics of the 26 December 2004 Sumatra earthquake as imaged by teleseismic broadband arrays, *Geophys. Res. Lett.*, **32**, L24312, doi:10.1029/2005GL023939.
- Krüger, F., and M. Ohrnberger (2005b), Tracking the rupture of the Mw=9.3 Sumatra earthquake over 1,150 km at teleseismic distance, *Nature*, **435**, doi:10.1038/nature03696.

- Krüger, F., M. Weber, F. Scherbaum, and J. Schlittenhardt (1993), Double beam analysis of anomalies the core-mantle boundary region, *Geophys. Res. Lett.*, **20**, 1475-1478.
- Manaker, D.M., R. Bürgmann, W.H. Prescott, J. Langbein (2003), Distribution of interseismic slip rates and the potential for significant earthquakes on the Calaveras fault, central California, *J. Geophys. Res.*, **108**, doi:10.1029/2002JB001749.
- Niazi, M. (1969), Use of source arrays in studies of regional structure, *Bull. Seism. Soc. Am.*, **59**, 1631-1643.
- Oppenheimer, D. H., W. H. Bakun, and L. A. G (1990), Slip partitioning of the Calaveras Fault, California, and prospects for future earthquakes, *J. Geophys. Res.*, **95**, 8483-8498.
- Poupinet, G., W. L. Ellsworth, and J. Fréchet (1984), Monitoring velocity variations in the crust using earthquake doublets: an application to the Calaveras Fault, California, *J. Geophys. Res.*, **89**, 5719-5731.
- Rost, S., and C. Thomas (2002), Array seismology: Methods and applications, *Reviews of Geophysics*, **40**, doi:10.1029/2000RG000100.
- Rubin, A. M., D. Gillard, and J.-L. Got (1999), Streaks of microearthquakes along creeping faults, *Nature*, **400**, 635-641.
- Schaff, D. P., G. C. Beroza, and B. E. Shaw (1998), Postseismic response of repeating aftershocks, *Geophys. Res. Lett.*, **25**, 4549-4552.
- Schaff, D. P., G. H. R. Bokelmann, G. C. Beroza, F. Waldhauser, and W. L. Ellsworth (2002), High-resolution image of Calaveras Fault seismicity, *J. Geophys. Res.*, **107**, doi: 10.1029/2001JB000633.
- Schaff, D. P., G. H. R. Bokelmann, W. L. Ellsworth, E. Zankerka, F. Waldhauser, and G. C. Beroza (2004), Optimizing correlation techniques for improved earthquake location, *Bull. Seism. Soc. Am.*, **94**, 705-721.
- Scherbaum, F., D. Gillard, and N. Deichmann (1991), Slowness power spectrum analysis of the coda composition of two microearthquake clusters in northern Switzerland, *Physics of the Earth and Planetary Interiors*, **67**, 137-161j.

- Scherbaum, F., F. Krüger, and M. Weber (1997), Double beam imaging: Mapping lower mantle heterogeneities using combinations of source and receiver arrays, *J. Geophys. Res.*, **102**, 507-522.
- Snieder, R., and M. Vrijlandt (2005), Constraining the source separation with coda wave interferometry: Theory and application to earthquake doublets in the Hayward fault, California, *J. Geophys. Res.*, **110**, B04301, doi: 10.1029/2004JB003317.
- Spudich, P., and T. Bostwick (1987), Studies of the seismic coda using an earthquake cluster as a deeply buried seismograph array, *J. Geophys. Res.*, **92**, 526-510,546.
- Waldhauser, F., W. L. Ellsworth, and A. Cole (1999), Slip-Parallel Seismic Lineations on the Northern Hayward Fault, California, *Geophys. Res. Lett.*, **26**, 3525-3528.
- Waldhauser, F., and W. L. Ellsworth (2000), A Double-Difference earthquake location algorithm: Method and application to the Northern Hayward Fault, California, *Bull. Seism. Soc. Am.*, **90**, 1353-1368.
- Waldhauser, F., and W. L. Ellsworth (2002), Fault Structure and mechanics of the Hayward Fault, California, from double-difference earthquake locations, *J. Geophys. Res.*, **107**, doi: 10.1029/2000JB000084.
- Waldhauser, F., W. L. Ellsworth, D. P. Schaff, and A. Cole (2004), Streaks, multiplets, and holes: High-resolution spatio-temporal behavior of Parkfield seismicity, *Geophys. Res. Lett.*, **31**, L18608, doi:10.1029/2004GL020649.
- Walker, K. T., M. Ishii, and P. M. Shearer (2005), Rupture details of the 28 March 2005 Sumatra Mw 8.6 earthquake imaged with teleseismic P waves, *Geophys. Res. Lett.*, **32**, L23303, doi: 10.1029/2005GL024395.
- Zhang, H., and C. Thurber (2003), Double-Difference Tomography: The method and Its application to the Hayward Fault, California, *Bull. Seism. Soc. Am.*, **93**, 1875-1889.